Investigation into the Influence of Temperature on the Cryopreservation of Mesenchymal Stem Cells

Mindaugas Norkus B.Eng, B.Sc

A Thesis Submitted for

Doctor of Philosophy Degree

Work Carried Out at

Bioelectronics Research Cluster,
National Centre for Biomedical Engineering Science,
National University of Ireland Galway,
Ireland

And

Electrical & Electronic Engineering,
College of Engineering and Informatics,
National University of Ireland Galway,
Ireland

Supervisors

Mr. Liam Kilmartin

Professor Gearóid Ó Laighin

Submitted to the National University of Ireland Galway,

September 2012

Table of Contents

Table of Contents ..... **i**

List of Figures ..... **v**

List of Tables ..... **xi**

List of Appendices ..... **xiii**

Acknowledgements ..... **xiv**

Abstract ..... **xvi**

Chapter 1 Introduction **1**

1.1 Background and motivation 2

1.2 Thesis structure 5

1.3 References 6

Chapter 2 Literature Review **9**

2.1 Stem cells – A review of scientific progress 10

2.1.1 Bone marrow-derived stem cells *10*

2.1.2 Mesenchymal stem cells *12*

2.1.3 Clinical applications of mesenchymal stem cells *13*

2.2 Cryopreservation of stem cells 16

2.2.1 Fundamentals of cryobiology *16*

2.2.2 The mechanisms of cryoinjury *17*

2.2.3 The role of cryoprotective agents *22*

2.2.4 Preventing cryoinjury by vitrification: alternative cryopreservation approach *25*

2.2.5 Stem cell recovery from cryopreservation *26*

2.2.6 Optimal cryopreservation protocols *26*

2.2.7 Long term storage of stem cells *27*

2.2.8 Transportation of stem cells *30*

2.3 References 31

Chapter 3 External Parameter Impact on the Temperature Profile during Stem Cell Shipment 44

3.1 Introduction 45

3.2 Study design and methods 47

3.2.1 The sensors *47*

3.2.2 Shipping protocol and data acquisition *47*

3.2.3 Data set structure *48*

3.3 Results 49

3.3.1 Thermal conditions during shipping *49*

3.3.2 Classification of transport modes *52*

3.3.3 Transportation activities and their influence on thermal fluctuations *58*

3.4 Discussion 63

3.5 References 64

Chapter 4 Precision Thermoelectric Temperature Control System 67

4.1 Introduction 68

4.2 System overview 69

4.2.1 System functionality *69*

4.2.2 Hardware implementation *70*

4.2.3 Enclosure *72*

4.2.4 Virtual PID controller *73*

4.3 System performance 76

4.4 Discussion 77

4.5 References 77

Chapter 5 The Effect of Temperature Elevation on Cryopreserved Mesenchymal Stem Cells 79

5.1 Introduction 80

5.2 Materials and methods 80

5.2.1 Primary culture of rMSCs *80*

5.2.2 Cryopreservation procedure *81*

5.2.3 Cell cytometric analysis *81*

5.2.4 Experimental procedure *82*

5.2.5 Modelling approach *83*

5.3 Results 85

5.3.1 Model optimisation *85*

5.3.2 Practical application of the model *92*

5.4 Discussion 93

5.5 References 95

Chapter 6 Application of Active Learning and Gaussian Process in Post-Cryopreservation Cell Membrane Integrity Experiments 96

6.1 Introduction 97

6.2 Materials and methods 98

6.2.1 Experimental design *98*

6.2.2 Cell source *99*

6.2.3 Cryopreservation procedure *100*

6.2.4 Thawing procedure *101*

6.2.5 Cytometric assay *101*

6.3 Active learning 102

6.3.1 Data model *103*

6.3.2 Infill function *108*

6.4 Results 111

6.4.1 Data sampling with active learning *111*

6.4.2 Measurement variance *116*

6.4.3 The advantage of the active learning strategy *118*

6.5 Discussion of results 120

6.6 Conclusions 123

6.7 References 125

Chapter 7 Discussion and Conclusions 128

7.1 Temperature elevation during transportation with dry ice 130

7.2 The effects of temperature elevation on cryopreserved rMSCs 131

7.3 Application of active learning for the investigation of temperature elevation effects on cryopreserved hMSCs 132

Appendix 134

List of Figures

Figure 2.1: Schematic view of the bone marrow stem cell compartments. Adapted from (16) 11

Figure 2.2: Human bone marrow derived MSCs adherent to plastic tissue culture flask and showing fibroblast-like morphology. 12

Figure 2.3: Schematic representation of the physical events occuring in cells during freezing. Adapted from (82)..... 21

Figure 2.4: Relationship between the cooling rate and survival of hypothetical cells. At slow cooling rates “solution effects” are the dominant factor in cell damage. These effects are minimised at fast cooling rates due to decreasing exposure time. On the other hand, fast cooling rates promote IIF, which becomes a dominant factor in cell damage, while slow cooling reduces the likelihood of IIF. The combination of these two factors produces the characteristic inverted “U” shape survival curve. The optimal cooling rate minimises both the “solution effects” and the likelihood of IIF. Adapted from (100, 101)..... 22

Figure 2.5: Osmotic excursions when cells are (A) introduced into a solution containing penetrating CPA and (B) removed from the CPA solution. V/V_0 represents the ratio of cell volume to its original volume. Adapted from (105)..... 24

Figure 3.1: Temperature as a function of time inside the shipping containers. The shaded area represents the intervals where temperature exceeds -70°C..... 50

Figure 3.2: Thermal profiles inside the shipping container filled with approximately 5 kg of dry ice pellets when sensor is completely covered under dry ice (s-1) and placed on the surface of dry ice layer (s-2). The third profile (s-3) is the ambient temperature of the container exterior. These profiles were recorded during a separate experiment under static conditions (i.e. the container was maintained stationary for the duration of the experiment). 51

Figure 3.3: Barometric pressure as a function of time recorded during transportation of stem cell specimens. Shaded areas indicate the intervals of air transportation as determined by low pressure area corresponding to typical internal pressure of a transport aircraft at cruising altitude. This low pressure area is bounded by steep gradients of pressure change associated with ascent after takeoff and descent before landing of an aircraft. 54

Figure 3.4: Left panel represents a data set of three different activities used for the training and validation of MLP while the right panel shows the classification boundaries of the best perfoming MLP. 56

Figure 3.5: Magnitude of dynamic acceleration as a function of time recorded during the transportation of 5 stem cell shipments. Colour shaded areas indicate different transportation activities as determined using the MLP classifier (grey represents stationary, yellow-vehicle transport, green-manual handling intervals). Note, the air transportation intervals (shaded in blue) were determined in the first stage of the classification algorithm from the barometric data. The triangular symbols are used to mark the spikes where the total acceleration vector exceeds the scale plotted in the graphs. 57

Figure 3.6: Shipping activities taking place when the flux of temperature occurred. '*w*' represents a window the turn point falls in while *w±i* represent a range of windows *(w-i; w+i)* around the turning point. 59

Figure 3.7: A time window from the shipment No. 2 transportation history where the fluctuation of temperature occurred. The start of the fluctuation and the end of it corresponds to the change in orientation of the shipping container suggesting that this was the cause of the temperature fluctuation. A relative orientation from the upright position of the container at various time points of interest is illustrated in the figure. 61

Figure 3.8: A time window from the shipment No. 3 transportation history showing multiple temperature fluxes. It is evident that the turning points of the temperature profile correspond to the change of container orientation (ϕ, θ). 62

Figure 3.9: Histogram representation of thermal fluctuations caused by the change of container orientation where $\Delta\phi$, $\Delta\theta$>15°. 63

Figure 4.1: Block diagram of the system 70

Figure 4.2: Chamber temperature as a function of voltage applied to the TE unit throughout the operational range. The system exhibits approximately linear gains in both heating and cooling modes. The maximum achievable temperature range in the cooling mode and the heating mode is approximately 44°C and 32°C respectively. 71

Figure 4.3: Enclosure and TE module assembly. Left panel: side view of the assembly. The assembly is elevated on the stand to ensure sufficient air circulation at the heat sink which is attached to the bottom of the enclosure. The lid on the top allows convenient access to the insulated chamber. Right panel: top view of the enclosure with the lid removed. An insulated chamber is seen which is divided into

20 cylinder-shaped compartments. Each compartment can accommodate a standard cryogenic vial (1.8 ml). 72

Figure 4.4: Closed-loop step switch response of the system in cooling and heating modes. The tangent lines to the curves at the points of rising inflection correspond to the maximum slopes. 74

Figure 5.1: Experimental data set of rMSC viability observations (mean and standard deviation) and their projections to the X-Y plane. 86

Figure 5.2: Distributions of model residuals after cross-validation 89

Figure 5.3: Optimised rMSC viability response model. 90

Figure 5.4: Cross-sectional representation of the rMSC viability model. Each section is drawn at fixed temperature (°C) and their corresponding values are labeled individually. 93

Figure 6.1: Matern kernel derived from the $\boldsymbol{t}$-distribution with prior parameters θ= 0.3 and υ= 0.3. 105

Figure 6.2: The infill function and location points for a synthetic example. The X-Y plane represents the points at which the function has already been sampled (represented by 'x') and those at which the constrained optimisation proposes to sample (represented by '.'). The Y-Z plane shows the expected return if a vector of samples is taken at that temperature level. 111

Figure 6.3: Gaussian process model mean estimate based on the initial sample vectors. 112

Figure 6.4: An estimate of the Gaussian process variance 112

Figure 6.5: The infill function (shown on the X-Z plane) and the location points of the candidate sample vectors (shown as dots on the X-Y plane). The highest peak of the infill function (x^*_{max}) is the optimal sampling location for the next sample vector. 112

Figure 6.6: Gaussian process model mean estimate in the last active learning iteration (i=5). 115

Figure 6.7: An estimate of the Gaussian process variance. Note, that the highest variance is on the boundary at x_1= 20. 115

Figure 6.8: The new infill function peaks at x_1=18 avoiding the boundary of the search space despite the highest variance associated with this location. 115

Figure 6.9: Approximate distribution of variance $\sigma^{2*}(x)$, associated with the MSC membrane integrity assays at the test points across the sampling space. This approximation was generated from the linear interpolation between the observed variance values, $\sigma^*(x)$, from the repeated measurements n=4 at each of the test locations. The variance appears to be unevenly distributed across the sampling space hence indicating heterogenous nature of associated noise. 117

Figure 6.10: The distribution of the deviations from the active learning, equally spaced grid and random sampling approaches obtained from the Monte Carlo simulations. 120

Figure 6.11: Gaussian process model mean estimate based on the complete data set. 121

Figure 6.12: An associated estimate of the Gaussian process variance. 121

Figure 6.13: Cross-sectional representation of the Gaussian approximation from the whole data set. These sections were drawn at 4 hour intervals; their corresponding time points (hours passed) are labeled individually. 122

List of Tables

Table 3.1: Summary of the shipments included in the investigation. The duration in transit includes time interval from the moment the specimens were placed into the shipping container until they were removed at the final destination. *The shipment was despatched to Dublin, Ireland and returned back to Galway, Ireland.....48

Table 3.2: Summary of thermal conditions inside the container during shipping, where T_{mean}, T_{min} and T_{max} are mean, minimum and maximum temperatures recorded respectively. The last column represents the combined time interval where temperature exceeded -70°C. 52

Table 3.3 Class discrimination accuracy achieved by MLP as determined by cross-validation (k=100) 55

Table 3.4: Combined intervals of different transportation activities during shipment of stem cell specimens. 58

Table 4.1: Switch step response parameters of the system, where R is the slope of the tangent and L is the smooth moving time constant. 75

Table 4.2: PID controller parameters. K_p = proportional gain; T_i = integral time; T_d = derivative time.....75

Table 4.3: Summary of the system performance. The experiments were carried out in a room temperature environment of approximately 22°C, therefore set temperatures of -20°C, 0°C, and 20°C required system to be operated in a cooling mode while the set temperature of 37°C required heating mode.....76

Table 5.1: Composition of the data set 86

Table 5.2: Composition of data sets used for the repeated random sub-sampling validation..... 88

Table 5.3: Summary of time series normalisation factors, model parameter estimates and residual PDF statistics. 91

Table 6.1: Composition of the dataset 98

Table 6.2: Summary of ANOVA statistics 118

List of Appendices

Appendix – Journal Publications arising from this Research

M. Norkus, D. Fay, M.J. Murphy, Frank Barry, G. ÓLaighin, L. Kilmartin, *On the application of active learning and Gaussian process in post-cryopreservation cell membrane integrity experiments*, IEEE Transactions on Computational Biology and Bioinformatics 2012;9(3):846-855.

M. Norkus, L. Kilmartin, D. Fay, M.J. Murphy, G ÓLaighin, F. Barry, *The effect of temperature elevation on cryopreserved mesenchymal stem cells*, CryoLetters (*In Press*).

Acknowledgements

First and foremost, I would like to extend my gratitude to my supervisor, Mr. Liam Kilmartin for his mentoring, advice and support over the last number of years. Thanks for inspiring me during the times I was struggling and for keeping me grounded when I was aiming too high.

Special thanks to Professor Gearóid Ó Laighin for providing me with an academic home and research 'hub' for the last number of years and for his invaluable advice and assistance in facilitating collaboration with other groups and individuals throughout the course of my PhD.

I would also like to sincerely thank the following collaborators: Professor Frank Barry and Dr. Mary Murphy of the Regenerative Medicine Institute (REMEDI), NUI Galway, for facilitating my research into the biological side of this thesis. The opportunity to work within REMEDI and guidance and support offered to me has instilled me with a respect for the research carried out in this facility. I am grateful for the extension of your invaluable time in assisting the completion of my work. A special mention must also be given to Dr. Damien Fay for providing his statistical expertise in this thesis and for introducing me to the concepts of Active Learning and the Gaussian Process and, of course, the warm welcome of Cork! Surprising what can be achieved in a few days with hard work and the reward of the Cork social scene, many thanks for that!

Many thanks to Georgina Shaw (REMEDI) and Gemma Rooney (REMEDI) for providing training and support in cell culture and cryopreservation, without which I could not have completed my work to the standard achieved. Much obliged for your time and expertise. Thanks are also extended to Aleksandra Leszczynska for keeping my cell cultures alive while I was overseas! And to my good colleague and friend, Mieszko Wilk, for keeping me grounded in REMEDI.

Sincere thank you to the technical staff of the Electrical & Electronic Engineering, NUI Galway – Myles Meehan and Martin Burke - for providing me with the equipment and technical expertise when I needed it.

To everyone in the Bioelectronics Research Cluster; thanks guys, it has been a long road but some good experience!

Big thanks go to my girlfriend, Laura, for endless support and love.

Special thanks to my parents, Irena and Leonardas for allowing me to follow my own path in life and pursue my dreams. Also, big thanks to my aunt Birutė, brother Donatas, cousins Eglė and Vaidotas - you have been a constant support and source of encouragement, without which I would not be here.

Finally I would like to thank Mr. Fergal O'Malley whom offered me the opportunity to embark on my PhD journey and for guiding me through the initial years of my work.

Abstract

Mesenchymal Stem Cells (MSCs) are utilised in regenerative medicine due to their multilineage differentiation potential, ease of isolation, capacity for *in vitro* expansion and wide-spread availability in the adult tissues. Their therapeutic applications have been widely demonstrated. In order to facilitate their transition from a bench to bedside therapeutic, on-demand availability of cells is required. Cryopreservation is thus a crucial element in achieving this goal as it permits the long term stabilisation of biological cells. For successful cryopreservation, ultra-low temperatures are needed. However, uncontrolled elevated temperatures cannot be avoided in certain situations. The work presented in this thesis focuses on the investigation of the influence of temperature elevation on the cryopreservation of MSCs. This thesis comprises of three separate components. The first section examines the temperature variations of cryopreserved stem cells during transportation, using conventional solid CO_2 as the cryogenic agent. It was observed that significant temperature variations can occur using this method of transportation. The second study investigates the effects of temperature elevations of cryopreserved MSCs derived from rats. A multiple regression model composed of two exponentials is proposed to approximate the detrimental effects on cell viability. It demonstrates that temperature elevations have an imminent detrimental effect on cell viability. The topic is further elaborated in a subsequent study which uses human-derived MSCs as well as a larger sample set. In addition, an active learning sampling strategy in conjunction with Gaussian process data model is presented which attempts to maximise the information return from the experiments. This study demonstrates the existence of a “lethal” region causing the highest detrimental effect to cell viability.

Chapter 1 Introduction

1.1 Background and motivation

The discovery of stem cells and their remarkable capacity to self-replicate and differentiate into any tissue in the body has generated intense scientific interest, giving rise to a new concept in healthcare – regenerative medicine. Stem cells are now considered a universal tool with applications in a wide range of therapies. Moreover, they are self-derived and pre-engineered to recognise and integrate fully with the body's complex signal transduction network and cellular microenvironment without the risk of rejection; a feat not yet simulated in any other field of medicine. Mesenchymal Stem Cells (MSCs) constitute one of the stem cell populations in the body. MSCs are unique in their capacity as a cellular therapy due to their multilineage differentiation potential, widespread presence in various tissues, ease of isolation and *in vitro* expansion capabilities. Consequently, a wide spectrum of therapeutic applications has been extensively researched with great success, leading to a number of clinical trials currently underway to assess the effectiveness of MSC treatment for conditions including spinal cord injury (1, 2), osteoarthritis (3, 4), Parkinson's disease (5), multiple sclerosis (6, 7) and many more.

Long term stabilisation of stem cells is vital for the progression of stem cell research and the successful translation of stem cell based therapies to a clinical setting. Despite the fact that adult stem cells, including MSCs, are renewable, their availability can be affected by trauma, disease or treatment of pathophysiological conditions. It has also been shown that aging is a factor leading to a lower density, reduced proliferation and differentiation potential of MSCs in the adult tissue (8-11). Besides the conventional source of MSCs – bone marrow – some alternative sources including umbilical cord, placenta and cord blood (12) are only available during

birth. Due to these reasons, it is becoming a wide spread practice to harvest stem cells from patients during the early phases of treatment or even from healthy individuals and new born babies with no immediate intention to perform cell transplantation but rather for having stem cells readily available if needed for therapy in the future. The ability to preserve cells permits completion of quality and safety testing before use as well as transportation of the cells between the sites of collection, processing and administration (13). The emergence of this 'biobanking' necessitates the need to achieve long term stabilisation of stem cells for research applications in order to have different cell lines promptly available on demand.

Cryopreservation and dehydration are the main methods permitting long term stabilisation of biological cells, with the former being the standard practice used with stem cells. At ultra-low temperatures all cellular bioprocesses become suppressed, effectively pausing the biological clock. However, before this stabilised state can be reached, cells have to survive an intermediate stage where the critical physical, chemical and physiological alterations take place. It is this intermediate stage that is primarily associated with cell injury. The early work in the area of understanding freezing injury manifested in the publication of "Life and death at low temperature" (14) and has been elaborated extensively thereafter. A number of hypotheses have emerged over the years and contributed towards a deeper understanding of the mechanisms of freezing injury. The development of penetrating cryoprotectants has overcome the fundamental problems of low temperature preservation associated with the phase change of water and enabled the progression of applied cryopreservation. This science is built almost solely on an empirical basis as a functional understanding of the exact mechanisms behind cryopreservation-related processes remains a focus of discussion.

While an ultra-low temperature is a fundamental requirement in order to achieve successful long term stabilisation of biological cells, elevation of temperature may occur during the storage of cryopreserved cells in real life applications. For example, it can be caused by the breakdown of a cryostorage system. In addition, a higher risk of temperature elevation is associated with the transportation of frozen cells. The common stem cell transportation practice of using solid CO_2 as a cooling agent is another potential cause of temperature elevation primarily because solid CO_2 sublimates at relatively high temperature marginally close to the acceptable limit necessary to ensure safe cryopreservation.

The effects of temperature elevation have not been studied sufficiently in the context of stem cell preservation. MSCs in particular have not been studied in this regard. In response to this, the work presented in this thesis focuses on examining these effects and determining the underlying relationship in order to model the process using mathematical methods. The first part of the work presented here includes a study carried out to determine the actual thermal conditions during transportation of cryopreserved MSCs with solid CO_2. This method is routinely used for transfer of cryopreserved stem cell specimens as a cost effective alternative to liquid nitrogen shippers, however it involves a higher risk of temperature elevation. The aim of this study was to evaluate the risk and severity of temperature elevation associated with this transportation practice. However, the main focus of this thesis is to investigate the effects on MSC survival caused by the exposure to elevated temperatures. The implicit objective is to develop a model relating the elevated temperature and exposure time with the survival of MSCs. Temperatures ranging from -20°C to 37°C and -40°C to 20°C were investigated in two separate studies including MSCs from rat and human bone marrow. The temperature ranges investigated refer to a complete

breakdown of the temperature control system in the context of stem cell storage or near complete and complete sublimation of CO_2 in the context of frozen stem cell transportation. The work presented in this thesis provides new information of how cryopreserved MSCs respond to elevated temperatures.

1.2 Thesis structure

The structure of the thesis is as follows:

Chapter 2 – provides a detailed review of relevant literature. It includes an overview of advances in stem cell research and their therapeutic applications, with the main focus on bone marrow-derived MSC. The importance of long term stabilisation by cryopreservation is discussed as well as the fundamentals of stem cell cryopreservation and issues relating to this process are described. An outline of the optimal cryopreservation protocols and current practices follows, along with the currently published information on the effects of higher-than-optimal cryopreservation temperature.

Chapter 3 – investigates the risk of temperature elevation associated with the transportation of cryopreserved stem cells using solid CO_2. An implicit objective was to determine shipping conditions and shipment handling activities which present this risk. It was found that considerable temperature elevations are common when using this method and are primarily associated with handling activities; specifically due to changes in the spatial orientation of the transport container closure system.

Chapter 4 – presents a system designed and built to allow laboratory simulation of temperature elevation conditions in order to investigate the effect of such elevated temperatures on the cryopreserved MSCs.

Chapter 5 – describes a study designed to investigate the effect of temperature elevation in the range between -20°C and 37°C on the cryopreserved MSCs derived from rat bone marrow (rMSC). The data collected in this study was used to develop an approximating model of rMSC membrane integrity response to the aforementioned temperature elevation conditions. This chapter has been accepted to the journal of Cryo-Letters.

Chapter 6 – outlines a study designed to investigate the effect of temperature elevation in the range between -40°C and 20°C on the cryopreserved MSCs derived from the human bone marrow. In addition to the different temperature range and use of human MSCs instead of rat MSCs, this study employed an active learning methodology in combination with the Gaussian process data model for selecting the optimal sampling locations and therefore increasing the information from the limited size sample set. This chapter has been published in the IEEE Transactions on Computational Biology and Bioinformatics (2012, 9(3), 846-856).

Chapter 7 – presents a summary of the work completed and also details the conclusions drawn from the work.

1.3 References

1. Transfer of bone marrow derived stem cells for the treatment of spinal cord injury [database on the Internet]. ClinicalTrials.gov: National Librabry of Medicine (US). 2010. Available from: http://clinicaltrials.gov/ct2/show/NCT01162915.

2. Safety and efficacy of autologous mesenchymal stem cells in chronic spinal cord injury [database on the Internet]. ClinicalTrials.gov: National Librabry of Medicine (US). 2012. Available from: http://clinicaltrials.gov/ct2/show/NCT01676441.

3. Intra-articular autologous bone marrow mesenchymal stem cells transplantation to treat mild to moderate osteoarthritis [database on the Internet]. ClinicalTrials.gov: National Librabry of Medicine (US). 2011. Available from: http://clinicaltrials.gov/ct2/show/NCT01459640.

4. The effects of intra-articular injection of mesenchymal stem cells in knee joint osteoarthritis [database on the Internet]. ClinicalTrials.gov: National Librabry of Medicine (US). 2012. Available from: http://clinicaltrials.gov/ct2/show/NCT01504464.

5. Autologous mesenchymal stem cell transplant for Parkinson's disease [database on the Internet]. ClinicalTrials.gov: National Librabry of Medicine (US). 2009. Available from: http://clinicaltrials.gov/ct2/show/NCT00976430.

6. Mesenchymal stem cell transplantation in MS (CMM-EM) [database on the Internet]. ClinicalTrials.gov: National Librabry of Medicine (US). 2010. Available from: http://clinicaltrials.gov/ct2/show/NCT01228266.

7. Evaluation of autologous mesenchymal stem cell transplantation (effects and side effects) in multiple sclerosis [database on the Internet]. ClinicalTrials.gov: National Librabry of Medicine (US). 2011. Available from: http://clinicaltrials.gov/ct2/show/NCT01377870.

8. Bergman RJ, Gazit D, Kahn AJ, Gruber H, McDougall S, Hahn TJ. Age-related changes in osteogenic stem cells in mice. Journal of Bone and Mineral Research. 1996;11(5):568-77.

9. Mendes SC, Tibbe JM, Veenhof M, Bakker K, Both S, Platenburg PP, et al. Bone tissue-engineered implants using human bone marrow stromal cells: Effect of culture conditions and donor age. Tissue Engineering. 2002;8(6):911-20.

10. Bertram H, Mayer H, Schliephake H. Effect of donor characteristics, technique of harvesting and in vitro processing on culturing of human marrow

stroma cells for tissue engineered growth of bone. Clinical Oral Implants Research. 2005;16(5):524-31.

11. Sabatino M, Ren J, David-Ocampo V, England L, McGann M, Tran M, et al. The establishment of a bank of stored clinical bone marrow stromal cell products. Translational Medicine. 2012;10(23):1-12.

12. Mariane Seccoa, Eder Zucconia, Natassia M. Vieiraa, Luciana L.Q. Fogaçaa, Antonia Cerqueiraa, Maria Denise F. Carvalhoa, et al. Mesenchymal stem cells from umbilical cord: Do not discard the cord! Neuromuscular Disorders. 2008;18(1):17-8.

13. Hanna J, Hubel A. Preservation of stem cells. Organogenesis. 2009;5(3):134-7.

14. Luyet BJ, Gehenio PM. Life and death at low temperatures. Normandy, MI: Biodynamica; 1940.

Chapter 2 Literature Review

2.1 Stem cells – A review of scientific progress

A stem cell is a remarkable biological entity that has the unique capacity to renew itself, as well as give rise to other specialised cell types. Stem cells originate as undifferentiated cells lacking tissue-specific characteristics and possess the ability to become a differentiated cell completely distinct from its precursor, have the capacity for extensive self renewal and the facility to maintain itself throughout the entire lifespan of an organism (15).

It is important to distinguish that stem cells, by their origin, are defined as Embryonic Stem Cells (ESCs) or Adult Stem Cells (ASCs). While the source of ESCs is the inner mass of the embryo, ASCs have been identified in most adult tissues including bone marrow, peripheral blood, brain, spinal cord, dental pulp, blood vessels, skeletal muscle, epithelia of the skin and digestive system, cornea, retina, liver, and pancreas. This stem cell population is also present in umbilical cord blood (16). The ability to manipulate lineage-specific commitment of adult stem cells, *in vitro* or *in vivo*, to become a variety of cell types useful for transplantation in cell-based therapy of genetic and degenerative diseases, is evident from the vast amount of published literature.

2.1.1 Bone marrow-derived stem cells

Bone marrow contains a number of stem cells which form less than 0.1% of nucleated cells in the marrow (16). One of the earliest discovered and most well characterised populations of bone marrow stem cells are hematopoietic stem cells (HSCs) (17, 18). HSCs give rise to all types of blood cells in the body. Shortly after the discovery of HSCs, another cell population was identified in the bone marrow –

Mesenchymal Stem Cells (MSCs) (19, 20). This stem cell population has also been referred to as skeletal stem cells, bone marrow stromal cells and multipotent mesenchymal stromal cells, however, these terms are less frequent in the scientific literature. There is also a level of uncertainty as to whether bone marrow stromal cells and MSCs are in fact the same population (21). The MSC population generates non-hematopietic tissue including bone, cartilage, fat, tendon, muscle, and marrow stroma (22). The bone marrow also contains a population of progenitor cells that differentiate into endothelial cells, a type of cell that lines the blood vessel, however, there is still some controversy surrounding this cell population (23). A schematic view of bone marrow stem cell compartments is represented in Figure 2.1.

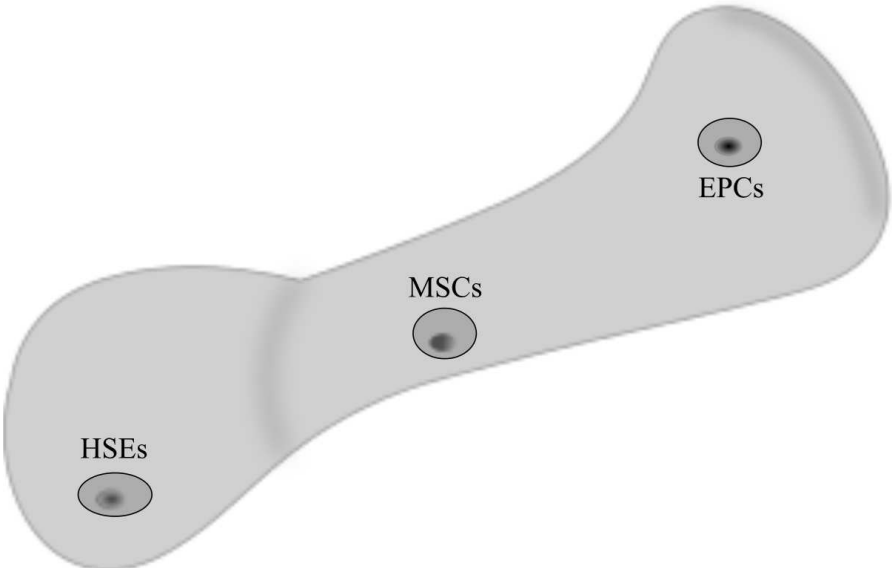

Figure 2.1: Schematic view of the bone marrow stem cell compartments. Adapted from (16)

2.1.2 Mesenchymal stem cells

MSCs which reside in the cavity of bone have been identified and characterised through the pioneering work of Friedenstein et al. (1966) (19) and later elaborated by Owen et al. (1988) in the UK (20), followed by other scientists around the world. The precise definition of MSCs remains a matter of debate due to the fact that they lack a unique marker. For human MSCs, the minimal criteria proposed by the Mesenchymal and Tissue Stem Cell Committee of the International Society for Cellular Therapy is defined as: (i) MSCs must be plastic–adherent when maintained in standard culture conditions and develop Colony-Forming Unit-Fibroblasts (CFU-Fs) as represented in Figure 2.2; (ii) MSCs must express CD105, CD73 and CD 90 and lack expression of CD45, CD34, CD14 or CD11b, CD79alpha or CD19 and HLA-DR surface molecules and; (iii) MSCs must also demonstrate tri-lineage differentiation into osteocytes, adipocytes and chondrocytes *in vitro* (24).

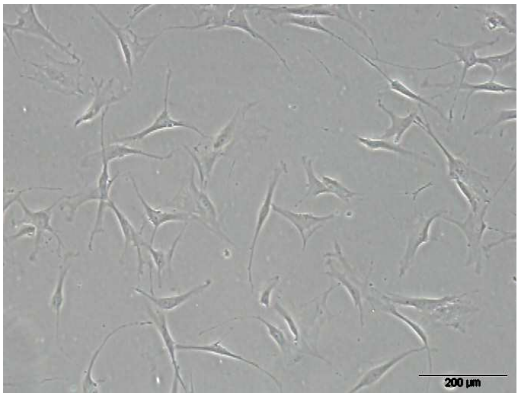

Figure 2.2: Human bone marrow derived MSCs adherent to plastic tissue culture flask and showing fibroblast-like morphology.

MSCs represent only a very small fraction of the total nucleated cell population in the marrow – 0.001 – 0.01% (22). Nevertheless, this population of stem cells plays a vital role in the survival of an organism. It has been reported that the population of MSCs decreases with age or infirmity (8, 25-28) and that their relative presence can control the outcome of reparative events of skeletal tissue. In summary, the complement and performance of

MSCs can have a dramatic impact on mortality by controlling the body's capacity to naturally remodel, repair and rejuvenate various tissues on demand (29).

A considerable effort has also been made to gain a deeper understanding of the differentiation potential of MSCs. It has been demonstrated that MSCs have the capacity to differentiate into chondrocytes, adipocytes and osteoblasts (22, 30), vascular smooth muscle cells (31), skeletal myoblasts (32) and cardiomyocytes (33).

In recent years it has been reported that in addition to the bone marrow, multipotent MSCs can be isolated from a variety of other tissues including the umbilical cord blood (34, 35), adipose tissue (36, 37), skeletal muscle (38), human placenta (39), dermal tissue (40), intervertebral disc (41), synovial membrane (42), amniotic fluid (43) and various dental tissues (44).

2.1.3 Clinical applications of mesenchymal stem cells

MSCs have generated huge interest regarding their use as a cellular therapy in regenerative medicine and tissue engineering. Due to their ease of isolation, expansion, broad differentiation potential and their widespread presence in various tissues, these cells have become attractive candidates for a diversity of disease conditions in need of tissue repair and regeneration.

At present, bone marrow is the most elaborated source of MSCs. These cells can be readily isolated via aspiration from the bone marrow, specifically the superior iliac crest and cultured with high efficiency *in vitro*. The technique for isolating, purifying and culture expanding MSCs from bone marrow specimens *in vitro* has been optimised over the years. With an expansion potential exceeding one billion-fold in culture (45), these cells promise a universal 'raw material' for clinical applications.

There have been a number of exciting clinical applications of MSCs reported in the literature and these address a broad spectrum of conditions. Skeletal tissue regeneration is the primary focus in the clinical use of MSCs. Numerous studies have attempted to demonstrate the feasibility of MSC-mediated bone regeneration in conditions where complete spontaneous healing could not be achieved due to extensive loss of bone tissue. In general, MSCs can either be systemically administered using intravenous (IV) injection or directly implanted in the bone defect site. The systemic approach relies on the capacity of MSCs to migrate across the endothelium and home to injured tissues in a manner similar to the migration of leukocytes to sites of inflammation (46). Several studies have shown that MSCs home to sites of bone fractures (47-51) or to bones with impaired development (52). Although the systematic approach is attractive, the direct implantation approach aims at concentrating a higher number of MSCs at the site of injury thereby attempting to reduce the risk of cell migration to other sites in the body (46). A clinical study conducted in 2001 has also demonstrated the success of locally injected *ex vivo* expanded autologus MSCs for the treatment of large bone defects in patients with defective fracture healing (53).

In addition to bone regeneration, MSCs are targeted for the regeneration of *cartilage*. Due to its avascular, hypocellular nature; articular cartilage has a very limited capacity of effective repair. Degradation of cartilage is characteristic to degenerative joint disease or *osteoarthritis* (OA) (54, 55). The capacity of adult MSCs to differentiate into chondrocytes makes them ideal candidates for cartilage tissue repair. Direct intra-articular injection of MSCs has proven beneficial against degenerative changes in trauma-induced OA in animal studies (55). MSCs have also been found to have limited success in forming long-lasting cartilage tissue (46) in

human studies (56, 57). Other studies in which animal models were used have demonstrated the feasibility of using biodegradable scaffolds seeded with MSCs for articular cartilage repair (58, 59).

There is also a growing interest in the area of non-skeletal tissue regeneration by MSCs including heart, nerve, liver, kidney, lungs and pancreas (46). The potential of MSCs in cardiovascular disease therapy has been demonstrated in animal models; namely in the study conducted by Makino et al. (2003) and has shown that cardiomyocytes generated from MSCs remained differentiated after transplantation to the heart (60). Magini et al. (2008) also demonstrated that transplantation of MSCs improved cardiac function (61). Other promising research findings have led to a number of pre-clinical studies in large animals resulting in further encouragement of MSC potential for the treatment of heart disease (62-64). Small scale clinical studies have also been undertaken and report excellent results (65, 66). MSCs have also shown beneficial effects in animals with lung injury (67). These results have broad implications in the area of lung disease associated with environmental damage (68).

MSCs have also proven lucrative in the area of tissue engineering. MSCs are candidates for use in tissue engineering because of the relative ease of expansion *in vitro* and their differentiation potential (69). Tissue engineering methods using MSC loaded scaffolds have also been demonstrated in a number of animal models to repair segmental defects in long bones (70-73) and spinal fusion (74). Other examples of clinical applications include MSC-seeded scaffolds in engineered craniofacial bone (75). Several studies have demonstrated that locally implanted MSCs are effective in the treatment of bone defects (76, 77).

2.2 Cryopreservation of stem cells

Long term stabilisation of stem cells is at the core of stem cell research and stem cell-based therapies primarily because it is vital to have stocks of cells readily available on demand (78). If cells are maintained in a liquid milieu, they undergo age-related processes that cause progressive loss of viability. To prevent such degradation, cells need to be placed in conditions that essentially stop all chemical reactions for the duration of the time of storage (79). The standard method for long-term stabilisation of biological cells is freezing at ultra-low temperatures (typically using *liquid nitrogen*). This process in known as *cryopreservation*.

The freezing behaviour of stem cells has been described as early as 1955 (80) and was extensively researched thereafter, mostly involving HSCs. There has been considerably less research on the freezing behaviour of MSCs up until recently, with more comprehensive studies appearing as late as 1996 (81).

2.2.1 Fundamentals of cryobiology

Long term stabilisation of a stem cell population is achieved through suppression of cellular bioprocesses. The biological metabolism in living cells dramatically diminishes at low temperatures - this is the fundamental factor that permits cryopreservation of living cells (82). At temperatures below the *normothermic* range (32-37°C for mammalian species), the loss of heat to the environment causes the reduction of *kinetic* energy necessary to support chemical reactions and this in turn disrupts metabolic activity of living cells. However, before this stable cryopreserved state can be reached, a transition through the intermediate state is necessary. Within this range (0°C to -70°C), the critical physical, chemical and physiological

alterations take place which are associated with cell injury and this is known as *freezing injury* or *cryoinjury*. Some hypotheses have emerged over the years that have led to a functional understanding of freezing injury – these include the two-factor hypothesis (83), minimum volume (84, 85), salt concentration (86, 87) and several others. The advent of penetrating *cryoprotective agents* (CPAs), most notably *glycerol* and *dimethyl-sulfoxide* (DMSO) and their successful use in the cryopreservation of a variety of living cells have formed the basis of applied cryopreservation as used today for the long-term storage of stem cells.

Gao et al. (2000) (82) summarised the major steps crucial in the process of cryopreservation as follows:

i. Addition of CPAs to cells before cooling,
ii. Controlled cooling of cells towards ultra-low temperatures followed by a storage period in cryogenic environment (e.g. liquid nitrogen),
iii. Thawing of cells,
iv. Removal of CPAs from the cells after thawing.

Unfortunately, cryoinjury is a complex process and can be caused by individual or any combination of the above steps.

2.2.2 The mechanisms of cryoinjury

Cryoinjury of living cells is primarily associated with the events arising from the phase change of water in both extra and intracellular environments (82). Such phase changes occurs in the intermediate temperature zone from approximately 0°C to -70°C, but this range may vary depending on the composition of the preservation solution. During transition through this intermediate temperature zone, water

transport between intracellular and extracellular solutions is one of the major factors determining cell fate.

The kinetics of the water exchange process during cell freezing was first described by Mazur (88) and relates the amount of water in a cell with temperature. A chain of events related to water transport between intracellular and extracellular solutions governs the fate of cells during transition through the intermediate temperature zone. As cells are cooled to approximately -5°C, both the cells and the surrounding medium remains unfrozen and super-cooled. Between -5°C and approximately -15°C, ice forms in the external medium; however, the intra-cellular solution remains unfrozen and super-cooled. The super-cooled water in the cells has a greater chemical potential than that of the water in the partially frozen extracellular solution and water thus flows out of the cells osmotically and freezes externally (82). The total amount of water that can be transported during this transition period depends on the cooling rate.

Mazur described two cases of cryoinjury caused by water transport at slow and fast cooling rates in his “two-factor” hypothesis (83), with other researchers further elaborating in this field. The mechanisms of injury during fast and slow cooling can be summarised as follows:

i. In the event of rapid cooling, intracellular water cannot be transferred through the cell membrane fast enough because the chemical potential in the extracellular solution is being lowered at a greater rate than the rate at which water can escape out of the cell to maintain equilibrium. Therefore cells become increasingly super-cooled, eventually attaining equilibrium by

freezing intracellulary (89). This effect is also known as *Intracellular Ice Formation* (IIF) and it usually associated with lethal damage to the cells (90, 91). For most cell types, there is a fairly narrow range of cooling rates over which the percentage of cells with IIF increases from 0% to 100% (78).

ii. In the event of slow cooling, the cells will lose water rapidly enough to concentrate the intracellular solutes sufficiently to eliminate super-cooling. However, they will experience a collection of damage mechanisms falling under the general classification of "solution effects" (92) which include:

   a. Dehydration damage to lipid vesicles and cell membranes. There are several proposed mechanisms for the loss of membrane integrity due to dehydration including phase separation, membrane fusion, phase transition, lipid desorption/dissolution, formation of non-lamellar phases and partitioning of amphiphilic molecules into the membrane (92).

   b. Severe volume shrinkage and the resulting physical compression forces in the cell membrane (84, 85, 93). This injury mechanism is known as the "minimum volume hypothesis". Cell shrinkage has also been implicated in the loss of cell membrane area due to vesiculation (94).

   c. Long term exposure to high solute concentrations (composed mainly of electrolytes) before they reach the point at which all of the components in the solution are solidified. Exposure to elevated salt concentrations has been shown to cause damage due to denaturation of lipoproteins in the cell membrane (95).

d. Mechanical damage due to formation of channels between adjacent ice crystals, in which cells are sequestered. As the temperature decreases, the size of the channels decreases too (78) hence the compression and shear forces affected by this process on the cells may result in membrane damage (96-98).
e. Damage due to eutectic formations (99) - postulated to be due to two possible mechanisms: (i) mechanical damage by eutectic crystals or (ii) formation of intracellular eutectic crystals (92).

It is evident from the published literature that the mechanisms of injury are clearly defined for the case of fast cooling. However, due to various phenomena occurring simultaneously during slow freezing it has been difficult to ascertain the exact damage mechanism to cells (92).

Figure 2.3 illustrates the effects of different freezing rates on water transport and phase change.

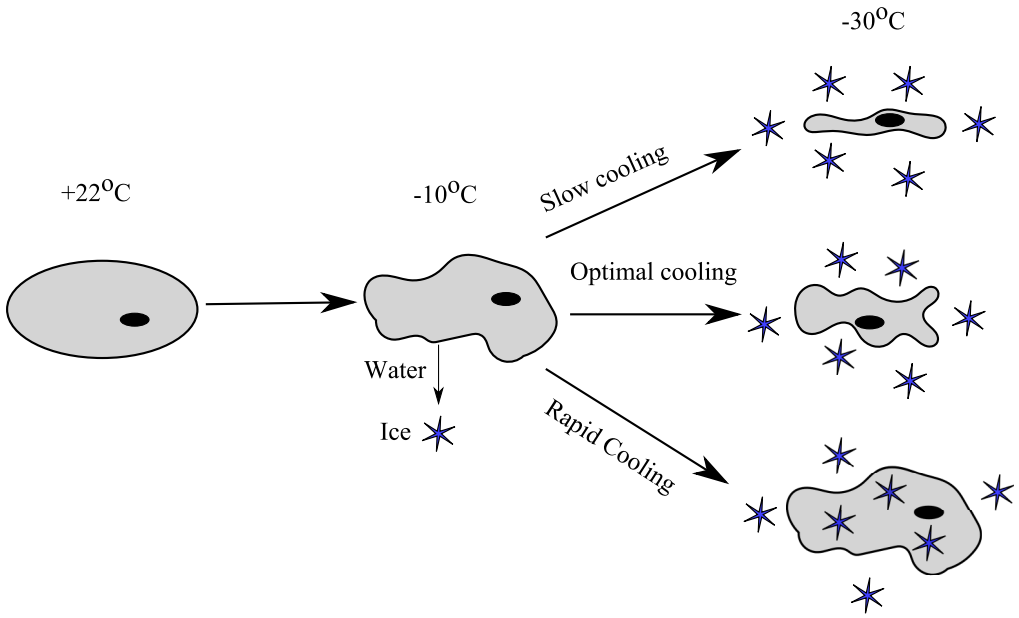

Figure 2.3: Schematic representation of the physical events occuring in cells during freezing. Adapted from (82).

Regardless of the injury mechanism, both scenarios constitute lethal effects on biological cells. The ideal cooling rate, where the survival of cells is optimal, is slow enough that the intracellular ice cannot form and rapid enough that the cells are not damaged by "solution effects". For many of the cell types, the survival curve in respect to the freezing rate has an inverted 'U' shape and the peak of this curve corresponds to the optimal cooling rate as illustrated in Figure 2.4.

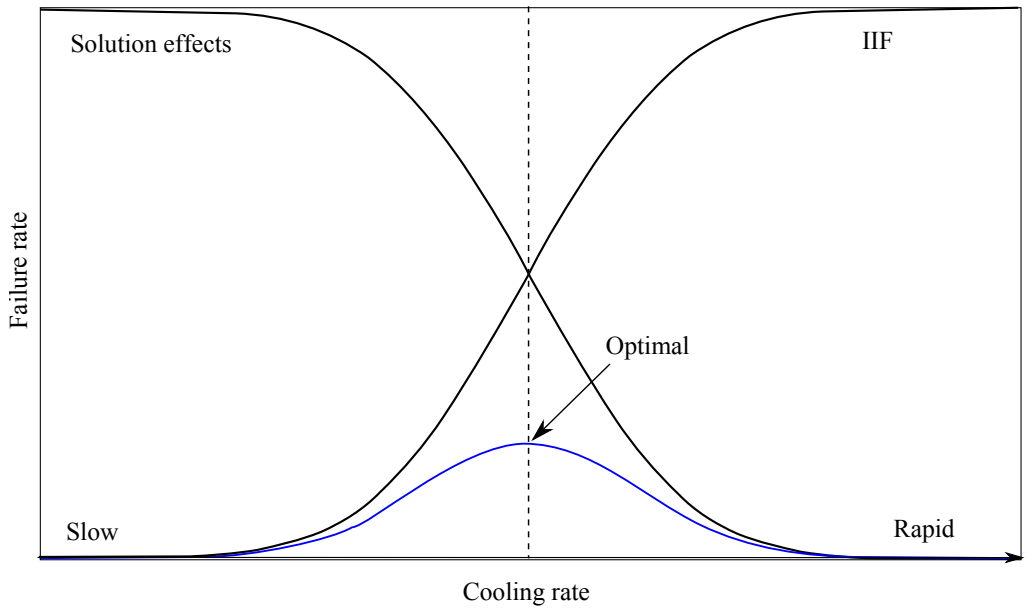

Figure 2.4: Relationship between the cooling rate and survival of hypothetical cells. At slow cooling rates "solution effects" are the dominant factor in cell damage. These effects are minimised at fast cooling rates due to decreasing exposure time. On the other hand, fast cooling rates promote IIF, which becomes a dominant factor in cell damage, while slow cooling reduces the likelihood of IIF. The combination of these two factors produces the characteristic inverted "U" shape survival curve. The optimal cooling rate minimises both the "solution effects" and the likelihood of IIF. Adapted from (100, 101).

2.2.3 The role of cryoprotective agents

Cryoprotective agents, CPAs, are used to promote cell survival during freezing. The two most commonly used CPAs are glycerol and DMSO (78) and are categorised as 'penetrating cryoprotectants'. Penetrating cryoprotectants are small molecules that easily penetrate cell membranes. Other (non-penetrating) substances used include sugars, polymers and alcohols (102). The exact mechanisms of cryoprotection are still a matter of debate. However, studies have demonstrated that cryoprotectants contribute towards the reduction of solution effects during slow freezing (103). The addition of a CPA changes the phase diagram for solution. For a given subzero temperature, the net concentration of ionic solutes that are known to be damaging is

reduced when CPA is present (78). The extent of protection depends primarily on the molar ratio of the CPA to endogenous solutes inside and outside the cells and the general protective mechanism of action is thus colligative (i.e. dependent only on the concentration of dissolved substances and not on their nature) (82). CPAs that penetrate the cell membrane also provide a dilution effect for the cytoplasm and therefore help to decrease the extent of osmotic shrinkage (82, 104). Non penetrating CPAs only provide a dilution effect in the extracellular space (78). In most cases these solutes will not protect in the absence of a penetrating CPA but will often substantially augment the effectiveness of a permeating CPA or permit the use of a lower concentration of permeating CPA (82).

Despite the effectiveness of the penetrating cryoprotectants, their use raises a number of new issues. Any penetrating CPA (principally glycerol and DMSO) can exert osmotic stress on cells during introduction and removal (78). During addition of a permeating CPA, cells shrink transiently due to dehydration and then return to near-normal volume as the CPA permeates. Removal of the CPA causes the cells to undergo temporary volume expansion, the magnitude of which depends on how the removal is effected and on the inherent permeability of the cell to water and CPA (82). Figure 2.5 provides a schematic representation of osmotic excursions during introduction and removal of penetrating CPA.

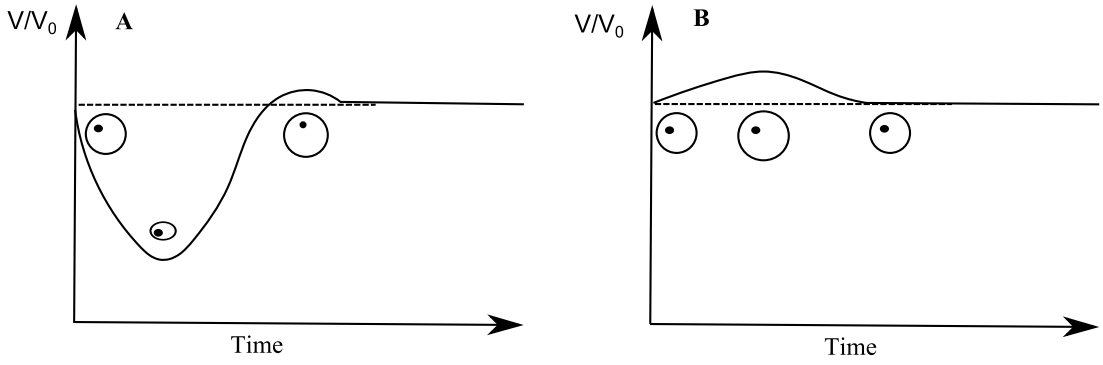

Figure 2.5: Osmotic excursions when cells are (A) introduced into a solution containing penetrating CPA and (B) removed from the CPA solution. V/V_0 represents the ratio of cell volume to its original volume. Adapted from (105).

Glycerol penetrates cells slowly and in some cases will not traverse the cell membrane at all, therefore cells can experience major osmotic excursions (102). Nevertheless, glycerol is regarded as being a non-toxic macromolecular stabiliser (106) and consequently assists in the maintenance of critical macromolecular interactions at subzero temperatures. DMSO, in contrast, has better penetrating properties to glycerol. However, it is also recognised as a macromolecular destabiliser with demonstrated toxicity (107). Not only are large step changes in osmolarity potentially damaging, but long-term exposure to even low concentrations of CPAs at room temperature (specifically DMSO) can be lethal to a variety of mammalian cells (78, 108). Although a number of mechanisms have been proposed, the exact method by which DMSO is toxic to stem cells has not been determined (78). Fahy et al. (1990) have explored the possible molecular/biochemical mechanisms of DMSO toxicity for a variety of biological systems (108). Exposure of cells to DMSO has also been found to produce alterations in the cytoskeleton, epigenetic events and crosslinking of nuclear proteins (78). Arakawa et al. (1990) proposed a hypothesis that certain CPAs, including DMSO, interact hydrophobically

with proteins and thus act as protein destabilisers or denaturants at higher temperatures (107). Due to this reason, both pre-freeze processing and thawing protocols are designed to minimise the DMSO exposure.

2.2.4 Preventing cryoinjury by vitrification: alternative cryopreservation approach

Another approach to cryopreservation is to use either high concentrations of certain CPAs or ultra-rapid cooling rates to induce the cell cytoplasm to form amorphous glass (i.e. to vitrify cells) rather than to crystallise (82, 109). Unfortunately, ultra-rapid cooling rates required to achieve vitrification of isotonic saline (in the order of 10^5-10^6 °C/min) are technically difficult to achieve (101). In order to facilitate ultra-rapid cooling rates, the surface area to volume ratio of the cell suspension must be very high. This has been achieved using a "cryo-loop"(110) and very thin straws (111). The alternative relies on the ability of highly concentrated aqueous solutions of CPAs to supercool to very low temperatures. At sufficiently low temperatures, these solutions become so viscous that they solidify without the formation of ice. At higher concentrations traditional CPA solutions become vitrifiable at cooling rates on the order of 10^3 °C/min (101). However, this approach is not without its challenges given that penetrating CPAs are too toxic for the cells at the concentrations needed to achieve successful vitrification. New and non-toxic penetrating CPAs are therefore needed for the successful implementation of this method. Substantial research has been conducted in developing vitrification protocols for the cryopreservation of embryos and embryonic stem cells (112-114). Some examples of successful MSC cryopreservation by vitrification have been demonstrated in the recent studies (115, 116).

2.2.5 Stem cell recovery from cryopreservation

Cell recovery from cryopreservation can exert effects on survival comparable with those of cooling (82, 90). These effects depend on whether the prior rate of cooling has induced intracellular freezing or cell dehydration. In the former case, rapid thawing can rescue many cells, likely due to the prevention of the growth of small intracellular ice crystals into harmful large ice crystals (i.e. so-called *recrystallisation*). Even when cells are cooled slowly enough to preclude intracellular freezing, the response to warming rate is often highly dependent on the freezing conditions and cell type and is difficult to predict *a priori* (82).

Removal of the CPA gives rise to osmotic challenges that need to be overcome for successful cell recovery. Cells are much more sensitive to lysis upon expansion (versus dehydration) therefore post-thaw removal protocols are critical for preventing cell death (105).

Minimising post-thaw exposure to concentrated CPA solutions (especially those containing DMSO) is another important aspect in recovery of cells. Exposure to DMSO has been shown to produce a number of changes ultimately responsible for loss of stem cell viability (107, 108).

2.2.6 Optimal cryopreservation protocols

Optimised cryopreservation protocols are available for most of the stem cell types, which permit minimal cell loss during this process. For a number of stem cell types, the same protocol, sometimes with minor alternations, is generally applied. The conventional cryopreservation protocol typically uses 10% DMSO in the freezing solution with a freezing rate of 1°C/min, which is optimal for most cell types. Rapid

thawing is typically employed for the recovery of cells in the conventional protocol. In order to reduce the risk of osmotic damage during the removal of DMSO, gradual dilution of the cell suspension is advised (117).

For MSCs, it has been shown that they can be effectively preserved using conventional protocol (10% DMSO) in combination with 1°C/min freezing rate while rapid thaw is optimal for recovery of these cells. A study which used MSCs obtained from human bone marrow has found that conventionally cryopreserved MSCs maintained functionality and the ability to support growth *in vitro* (81). Similar results were demonstrated using proprietary freezing solutions containing DMSO to preserve MSCs from bone marrow. These cells could be preserved and maintain multi-lineage potential upon thawing (118). Comparable published data with the MSCs obtained from the umbilical cord blood echoed the findings of previous study groups (16, 119). Although the conventional cryopreservation protocol is widely used for the cryopreservation of stem cells - different variations of same have been applied with varying levels of success. Surprisingly, even in clinical applications there appears to be a lack of standardisation and apparently no consensus on what should be an optimal cryopreservation protocol (120).

2.2.7 Long term storage of stem cells

Contrary to popular belief, enduring storage at low temperatures is not a major challenge to the cells. It is rather a transition between the metabolic state and the cryopreserved state (82). This is due to the fact that no thermally driven reactions can occur in human-relevant time at cryogenic temperatures. Multiple studies have confirmed that stem cells retain their viability and differentiation potential even after extended periods of storage at cryogenic temperatures. One such study has reported,

that human HSCs retain their viability and engraftment potential after 14 years of storage (121). A recent study has confirmed that HSCs remain viable after 5 years of cryostorage (122). There are also a number of other studies that reported similar results for other types of stem cells.

For the long term storage of stem cells, temperatures below -120°C are considered to be safe (82). The optimal storage temperature is hence below this critical point, typically at -196°C (when a liquid nitrogen storage system is used). In addition to the optimal temperature range, two other intervals can be distinguished:

i. Sub-optimal temperatures ranging from -120°C to approximately -70°C (below the eutectic temperature of the CPA solution), which are associated with cryoinjury during long term storage. These temperatures are however, frequently used for cryopreservation applications as they permit simplification of cryopreservation protocols and the use of mechanical freezers which are more cost-effective than liquid nitrogen cryostorage systems.

ii. The harmful temperature zone above eutectic temperature where significant damage is caused, even over short periods of time. A typical CPA solution is not fully solidified unless it is below the eutectic temperature (123) - this temperature is a function of the solution composition (124). For a solution containing 10% dimethyl sulfoxide (DMSO) the eutectic temperature is approximately -70°C. If stored at or near the eutectic temperature, cells will still be surrounded by the highly concentrated solutions and ice crystals can continue to grow and coalesce (105) causing mechanical injury to the membrane of the cells. The biological activity of cells at these temperatures

is another factor associated with cryoinjury. Many cellular functions are suppressed at temperatures below -50°C (e.g. water transport, metabolism) but enzymatic activity persists at much lower temperatures (105, 125). Temperatures above the eutectic point are not intentionally used for storage, however they often cannot be avoided in the typical sample handling cycle

A number of comparative studies have been published on the effects of sub-optimal versus optimal temperatures for long term storage. To date, the most extensive studies have been conducted on haematopoietic stem cells, with only a limited number of such studies published on MSCs.

A study by Galmes et al. (1999) (126) investigated the effects of storage in mechanical freezers (at -80°C) on haematopoietic progenitor cells (HPC) from bone marrow and peripheral blood cryopreserved with 5% and 10% DMSO respectively. In both cases a progressive decrease of membrane integrity with increasing duration in cryopreservation (from 78.9%/80.0% median to 32.0%/33.0% median after 1-31 months of storage respectively with 5%/10% DMSO) was reported. Similar gradual degradation was observed on the *in vitro* clonogenic potential of those same cells. This study concluded that HPC can be cryopreserved at -80°C for no longer than 6 months. Another study by Sputtek at al. (2005) (127) compared the effects of long term storage where HPC from peripheral blood were cryopreserved with 10% DMSO and initially stored in the vapour phase of liquid nitrogen for 5 to 52 months and then split into two groups, one of which was transferred to a mechanical freezer (at -80°C). The storage of both sample groups was continued for another 13-29 months. This study reported a significantly higher loss of membrane integrity for the sample group stored at -80°C in the mechanical freezer (mean ± standard deviation

of intact cells at the end of storage interval was 52.7±18.2%) compared to the sample group stored at -170°C in the vapour phase of liquid nitrogen (81.4±10.2%). Additional findings of this comparative study included significantly higher losses of *in vitro* clonogenic potential for a sample group stored at -80°C compared to that of a sample group stored at -170°C. Fowke et al. (2000) expanded the scope of their investigation to include storage at -30°C (below eutectic temperature) as well as -70°C and -150°C of whole blood and Peripheral Blood Mononuclear Cells (PBMC) for 10 weeks with 10% DMSO as CPA (128). The authors reported that PBMC showed a dramatic loss of cellular membrane integrity immediately after thawing for those stored at -30°C (20.2±2.5%) relative to those stored at -70°C (86.2±1.6%) and -150°C (86.7±4.1%). Moreover, PBMC showed significantly higher levels of spontaneous and activation-induced *apoptosis* from samples stored at -30°C compared to those stored at -70°C and -150°C. The authors also reported that PBMC, after 10 weeks storage at -30°C, were too severely damaged to even attempt an *in vitro* cell function assay, while PBMC stored at -70°C and -150°C showed normal *in vitro* function.

2.2.8 Transportation of stem cells

Stem cells may be transported from one laboratory to another as living cultures (i.e. in their original culture vessels) or in cryopreserved state. Despite being an accepted practice, transportation of living cultures is frequently not a preferred method due to the difficulty in maintaining cellular homeostasis in transit and consequently, a higher risk of damage. Data published in 1991 by a cell bank in Germany specialising in continuous cell lines indicated based on their practice that only 77% (n=73) cell lines received as live cultures survived (129). This may be due to

exposure to extreme changes in temperature or other environmental conditions during transportation. Shipping in a cryopreserved state is thus the preferred method of transportation. Observations by the same cell bank indicated 100% (n=58) rate of successful recovery of cell line received in cryopreserved state (129).

Standard protocols specify shipment of cryopreserved stem cells in solid CO_2 or *dry ice*, in a thick-walled polystyrene foam container (117). Solid CO_2 has a sublimation temperature of -78.5°C at standard atmospheric pressure and is at the very limit of what is generally considered a safe temperature for cell cryopreservation. Vitrified material requires the use of *Liquid Nitrogen* (LN) shippers to avoid devitrification (or crystallisation) which can result in the disruption of cell integrity and ultimately, cell death. LN shippers are designed to maintain stable, ultra-low temperatures by retaining LN within a molecular sieve-like material, thereby permitting storage at LN temperature for up to 14 days (130). Maintenance of sufficiently low temperature is the main concern associated with transportation of frozen stem cells. While shipping in solid CO_2 is a cheaper method, it is less effective in maintaining sufficiently low temperature.

2.3 References

8. Bergman RJ, Gazit D, Kahn AJ, Gruber H, McDougall S, Hahn TJ. Age-related changes in osteogenic stem cells in mice. Journal of Bone and Mineral Research. 1996;11(5):568-77.

15. Barry FP. Biology and clinical applications of mesenchymal stem cells. Birth Defects Research Part C: Embryo Today. 2003;69:250-6.

16. Lee MW, Choi J, Yang MS, Moon YJ, Park JS, Kim HC, et al. Mesenchymal stem cells from cryopreserved human umbilical cord blood. Biochemical and Biophysical Research Communications. 2004;320(1):273-8.

17. Till JE, McCulloch EA. A direct measurement of the radiation sensitivity of normal mouse bone marrow cells. Radiation Research. 1961;14(2):213-22.

18. Becker AJ, Till JE, McCulloch EA. Cytological demonstration of the clonal nature of spleen colonies derived from transplanted mouse marrow cells. Nature. 1963;197(486):452-4.

19. Friedenstein AJ, Piatetzky-Shapiro II, Petrakova KV. Osteogenesis in transplants of bone marrow cells. Journal of Embryology and Experimental Morphology. 1966;16(3):381-90.

20. Owen M. Marrow stromal stem cells. Journal of cell science Supplement. 1988;10:63-76.

21. Pittenger MF, Marshak, D.R. Mesenchymal atem cells of human adult bone marrow. Marshak DR, Gardner, D. K., Gottlieb, D., editor: Cold Spring Horbor Laboratory Press; 2001.

22. Pittenger MF, Mackay AM, Beck SC, Jaiswal RK, Douglas R, Mosca JD, et al. Multilineage potential of adult human mesenchymal stem cells. Science. 1999;284(5411):143-7.

23. Shi Q, Rafii S, Wu MHD, Wijelath ES, Yu C, Ishida A, et al. Evidence for circulating bone marrow-derived endothelial cells. Blood. 1998;92(2):362-7.

24. Dominici M, Le Blanc K, Mueller I, Slaper-Cortenbach I, Marini FC, Krause DS, et al. Minimal criteria for defining multipotent mesenchymal stromal cells. The International Society for Cellular Therapy position statement. Cytotherapy. 2006;8(4):315-7.

25. Inoue K, Ohgushi H, Yoshikawa T, Okumura M, Sempuku T, Tamai S, et al. The effect of aging on bone formation in porous hydroxyapatite: Biochemical and histological analysis. Journal of Bone and Mineral Research. 1997;12(6):989-94.

26. Kahn A, Gibbons R, Perkins S, Gazit D. Age-related bone loss. A hypothesis and initial assessment in mice. Clinical Orthopaedics and Related Research. 1995(313):69-75.

27. Quarto R, Thomas D, Liang CT. Bone progenitor cell deficits and the age-associated decline in bone repair capacity. Calcified Tissue International. 1995;56(2):123-9.

28. Tsuji T, Hughes FJ, McCulloch CAG, Melcher AH. Effects of donor age on osteogenic cells of rat bone marrow in vitro. Mechanisms of Ageing and Development. 1990;51(2):121-32.

29. Caplan AI, Bruder SP. Mesenchymal stem cells: building blocks for molecular medicine in the 21st century. Trends in Molecular Medicine. 2001;7(6):259-64.

30. Murphy JM, Dixon K, Beck S, Fabian D, Feldman A, Barry F. Reduced chondrogenic and adipogenic activity of mesenchymal stem cells from patients with advanced osteoarthritis. Arthritis and Rheumatism. 2002;46(3):704-13.

31. Minguell JJ, Erices A, Conget P. Mesenchymal stem cells. Experimental Biology and Medicine. 2001;226(6):507-20.

32. Bhagavati S, Xu WM. Isolation and enrichment of skeletal muscle progenitor cells from mouse bone marrow. Biochemical and Biophysical Research Communications. 2004;318(1):119-24.

33. Orlic D, Hill JM, Arai AE. Stem cells for myocardial regeneration. Circulation Research. 2002;91(12):1092-102.

34. Hutson EL, Boyer S, Genever PG. Rapid isolation, expansion, and differentiation of osteoprogenitors from full-term umbilical cord blood. Tissue Engineering. 2005;11(9-10):1407-20.

35. Bieback K, Kern S, Kluter H, Eichler H. Critical parameters for the isolation of mesenchymal stem cells from umbilical cord blood. Stem Cells. 2004;22(4):625-34.

36. Zuk PA, Zhu M, Mizuno H, Huang J, Futrell JW, Katz AJ, et al. Multilineage cells from human adipose tissue: Implications for cell-based therapies. Tissue Engineering. 2001;7(2):211-28.

37. Zuk PA, Zhu M, Ashjian P, De Ugarte DA, Huang JI, Mizuno H, et al. Human adipose tissue is a source of multipotent stem cells. Molecular Biology of the Cell. 2002;13(12):4279-95.

38. Bujan J, Pascual G, Corrales C, Gomez-Gil V, Garcia-Honduvilla N, Bellon JM. Muscle-derived stem cells used to treat skin defects prevent wound contraction and expedite reepithelialization. Wound Repair and Regeneration. 2006;14(2):216-23.

39. Parolini O, Alviano F, Bagnara GP, Bilic G, Buehring H-J, Evangelista M, et al. Concise review: Isolation and characterization of cells from human term placenta: Outcome of the first international workshop on placenta derived stem cells. Stem Cells. 2008;26(2):300-11.

40. Bartsch G, Yoo JJ, De Coppi P, Siddiqui MM, Schuch G, Pohl HG, et al. Propagation, expansion, and multilineage differentiation of human somatic stem cells from dermal progenitors. Stem Cells and Development. 2005;14(3):337-48.

41. Risbud MV, Guttapalli A, Tsai T-T, Lee JY, Danielson KG, Vaccaro AR, et al. Evidence for skeletal progenitor cells in the degenerate human intervertebral disc. Spine. 2007;32(23):2537-44.

42. De Bari C, Dell'Accio F, Tylzanowski P, Luyten FP. Multipotent mesenchymal stem cells from adult human synovial membrane. Arthritis and Rheumatism. 2001;44(8):1928-42.

43. De Coppi P, Bartsch G, Jr., Siddiqui MM, Xu T, Santos CC, Perin L, et al. Isolation of amniotic stem cell lines with potential for therapy. Nature Biotechnology. 2007;25(1):100-6.

44. Huang GTJ, Gronthos S, Shi S. Mesenchymal Stem Cells Derived from Dental Tissues vs. Those from Other Sources: Their Biology and Role in Regenerative Medicine. Journal of Dental Research. 2009;88(9):792-806.

45. Bruder SP, Jaiswal N, Haynesworth SE. Growth kinetics, self-renewal, and the osteogenic potential of purified human mesenchymal stem cells during extensive subcultivation and following cryopreservation. Journal of Cellular Biochemistry. 1997;64(2):278-94.

46. Cells and Tissue Development. In: Atala A, Lanza R, Thomson JA, Nerem R, editors. Principles of Regenerative Medicine. Second edition ed: Elsevier; 2011.

47. Devine MJ, Mierisch CM, Jang E, Anderson PC, Balian G. Transplanted bone marrow cells localize to fracture callus in a mouse model. Journal of Orthopaedic Research. 2002;20(6):1232-9.

48. Shirley D, Marsh D, Jordan G, McQuaid S, Li G. Systemic recruitment of osteoblastic cells in fracture healing. Journal of Orthopaedic Research. 2005;23(5):1013-21.

49. Kumar S, Ponnazhagan S. Bone homing of mesenchymal stem cells by ectopic alpha 4 integrin expression. Faseb Journal. 2007;21(14):3917-27.

50. Kitaori T, Ito H, Schwarz EA, Tsutsumi R, Yoshitomi H, Oishi S, et al. Stromal Cell-Derived Factor 1/CXCR4 Signaling Is Critical for the Recruitment of Mesenchymal Stem Cells to the Fracture Site During Skeletal Repair in a Mouse Model. Arthritis and Rheumatism. 2009;60(3):813-23.

51. Kumar S, Wan C, Ramaswamy G, Clemens TL, Ponnazhagan S. Mesenchymal Stem Cells Expressing Osteogenic and Angiogenic Factors Synergistically Enhance Bone Formation in a Mouse Model of Segmental Bone Defect. Molecular Therapy.18(5):1026-34.

52. Horwitz EM, Gordon PL, Koo WKK, Marx JC, Neel MD, McNall RY, et al. Isolated allogeneic bone marrow-derived mesenchymal cells engraft and stimulate growth in children with osteogenesis imperfecta: Implications for cell therapy of bone. Proceedings of the National Academy of Sciences of the United States of America. 2002;99(13):8932-7.

53. Quarto R, Mastrogiacomo M, Cancedda R, Kutepov SM, Mukhachev V, Lavroukov A, et al. Repair of large bone defects with the use of autologous bone marrow stromal cells. New England Journal of Medicine. 2001;344(5):385-6.

54. Creamer P, Hochberg MC. Osteoarthritis. Lancet. 1997;350(9076):503-9.

55. Murphy JM, Fink DJ, Hunziker EB, Barry FP. Stem cell therapy in a caprine model of osteoarthritis. Arthritis and Rheumatism. 2003;48(12):3464-74.

56. Wakitani S, Imoto K, Yamamoto T, Saito M, Murata N, Yoneda M. Human autologous culture expanded bone marrow mesenchymal cell transplantation for repair of cartilage defects in osteoarthritic knees. Osteoarthritis and Cartilage. 2002;10(3):199-206.

57. Matsumoto T, Okabe T, Ikawa T, Iida T, Yasuda H, Nakamura H, et al. Articular cartilage repair with autologous bone marrow mesenchymal cells. Journal of Cellular Physiology.225(2):291-5.

58. Im GI, Kim DY, Shin JH, Hyun CW, Cho WH. Repair of cartilage defect in the rabbit with cultured mesenchymal stem cells from bone marrow. Journal of Bone and Joint Surgery-British Volume. 2001;83B(2):289-94.

59. Li W-J, Chiang H, Kuo T-F, Lee H-S, Jiang C-C, Tuan RS. Evaluation of articular cartilage repair using biodegradable nanofibrous scaffolds in a swine model: a pilot study. Journal of Tissue Engineering and Regenerative Medicine. 2009;3(1):1-10.

60. Makino S, Fukuda K, Miyoshi S, Konishi F, Kodama H, Pan J, et al. Cardiomyocytes can be generated from marrow stromal cells in vitro. Journal of Clinical Investigation. 1999;103(5):697-705.

61. Mangi AA, Noiseux N, Kong DL, He HM, Rezvani M, Ingwall JS, et al. Mesenchymal stem cells modified with Akt prevent remodeling and restore performance of infarcted hearts. Nature Medicine. 2003;9(9):1195-201.

62. Potapova IA, Doronin SV, Kelly DJ, Rosen AB, Schuldt AJT, Lu Z, et al. Enhanced recovery of mechanical function in the canine heart by seeding an extracellular matrix patch with mesenchymal stem cells committed to a cardiac lineage. American Journal of Physiology-Heart and Circulatory Physiology. 2008;295(6):H2257-H63.

63. Qi C-m, Ma G-s, Liu N-f, Shen C-x, Chen Z, Liu X-j, et al. Identification and differentiation of magnetically labeled mesenchymal stem cells in vivo in swines with myocardial infarction. International Journal of Cardiology. 2009;131(3):417-9.

64. Wolf D, Reinhard A, Seckinger A, Gross L, Katus HA, Hansen A. Regenerative capacity of intravenous autologous, allogeneic and human mesenchymal stem cells in the infarcted pig myocardium - complicated by myocardial tumor formation. Scandinavian Cardiovascular Journal. 2009;43(1):39-45.

65. Joggerst SJ, Hatzopoulos AK. Stem cell therapy for cardiac repair: benefits and barriers. Expert Reviews in Molecular Medicine. 2009;11.

66. Trivedi P, Tray N, Nguyen T, Nigam N, Gallicano GI. Mesenchymal stem cell therapy for treatment of cardiovascular disease: Helping people sooner or later. Stem Cells and Development.19(7):1109-20.

67. Ortiz LA, Gambelli F, McBride C, Gaupp D, Baddoo M, Kaminski N, et al. Mesenchymal stem cell engraftment in lung is enhanced in response to bleomycin exposure and ameliorates its fibrotic effects. Proceedings of the National Academy of Sciences of the United States of America. 2003;100(14):8407-11.

68. Barry FP, Murphy JM. Mesenchymal stem cells: clinical applications and biological characterization. International Journal of Biochemistry & Cell Biology. 2004;36(4):568-84.

69. Bianco P, Robey PG. Stem cells in tissue engineering. Nature. 2001;414(6859):118-21.

70. Bruder SP, Kraus KH, Goldberg VM, Kadiyala S. The effect of implants loaded with autologous mesenchymal stem cells on the healing of canine segmental bone defects. Journal of Bone and Joint Surgery-American Volume. 1998;80A(7):985-96.

71. Bruder SP, Kurth AA, Shea M, Hayes WC, Jaiswal N, Kadiyala S. Bone regeneration by implantation of purified, culture-expanded human mesenchymal stem cells. Journal of Orthopaedic Research. 1998;16(2):155-62.

72. Kon E, Muraglia A, Corsi A, Bianco P, Marcacci M, Martin I, et al. Autologous bone marrow stromal cells loaded onto porous hydroxyapatite ceramic accelerate bone repair in critical-size defects of sheep long bones. Journal of Biomedical Materials Research. 2000;49(3):328-37.

73. Arinzeh TL, Peter SJ, Archambault MP, van den Bos C, Gordon S, Kraus K, et al. Allogeneic mesenchymal stem cells regenerate bone in a critical-sized canine segmental defect. Journal of Bone and Joint Surgery-American Volume. 2003;85A(10):1927-35.

74. Cinotti G, Patti AM, Vulcano A, Della Rocca C, Polveroni G, Giannicola G, et al. Experimental posterolateral spinal fusion with porous ceramics and mesenchymal stem cells. Journal of Bone and Joint Surgery-British Volume. 2004;86B(1):135-42.

75. Robey PG, Bianco P. The use of adult stem cells in rebuilding the human face. Journal of the American Dental Association. 2006;137(7):961-72.

76. Bruder SP, Fink DJ, Caplan AI. Mesenchymal stem-cells in bone-development, bone repair, and skeletal regeneration therapy. Journal of Cellular Biochemistry. 1994;56(3):283-94.

77. Ohgushi H, Goldberg VM, Caplan AI. Repair of bone defects with marrow cells and porous ceramic. Experiments in rats. Acta Orthopaedica Scandinavica. 1989;60(3):334-9.

78. Hubel A. Parameters of cell freezing: Implications for the cryopreservation of stem cells. Transfusion Medicine Reviews. 1997;11(3):224-33.

79. Katkov II, Kim MS, Karpova NS, Lulat AGM, Cao C, Levine F, et al. 6. Cryobiology for stem cell therapy: Research overview. Cryobiology. 2006;53(3):369-70.

80. Barnes DWH, Loutit JF. The radiation recovery factor: preservation by the Polge-Smith-Parkes technique. Journal of the National Cancer Institute. 1955;15(4):901-5.

81. Nicol A, Nieda M, Donaldson C, DenningKendall P, Truman C, Bradley B, et al. Cryopreserved human bone marrow stroma is fully functional in vitro. British Journal of Haematology. 1996;94(2):258-65.

82. Gao D, Critser JK. Mechanisms of cryoinjury in living cells. ILAR. 2000;41(4):187-96.

83. Mazur P, Leibo SP, Chu EHY. A two-factor hypothesis of freezing injury: Evidence from Chinese hamster tissue-culture cells. Experimental Cell Research. 1972;71(2):345-55.

84. Meryman HT. A model of freezing injury based on osmotic stress. Cryobiology. 1971;8(4):382-3.

85. Meryman HT. The attainment of a minimum cell volume is the fundamental cause of slow-freezing injury: A position for. Cryobiology. 1985;22(6):628-9.

86. Lovelock JE. The mechanism of the protective action of glycerol against haemolysis by freezing and thawing. Biochimica Et Biophysica Acta. 1953;11(1):28-36.

87. Lovelock JE. The protective action of neutral solutes against haemolysis by freezing and thawing. Biochemical Journal. 1954;56(2):265-70.

88. Mazur P. Kinetics of water loss from cells at subzero temperatures and likelihood of intracellular freezing. Journal of General Physiology. 1963;47(2):347-69.

89. Mazur P. Equilibrium, quasi-equilibrium, and nonequilibrium freezing of mammalian embryos. Cell Biophysics. 1990;17(1):53-92.

90. Mazur P. Freezing of living cells - mechanisms and implications. American Journal of Physiology. 1984;247(3):C125-C42.

91. Toner M. Nucleation of ice crystals inside biological cells. Steponkus PL, editor: JAI Press Ltd.; JAI Press Inc.; 1993. 1-51 p.

92. Ragoonanan V. Mechanisms and models of dehydration and slow freezing damage to cell membranes: University of Minnesota; 2010.

93. Meryman HT. Osmotic stress as a mechanism of freezing injury. Cryobiology. 1971;8(5):489-500.

94. Steponkus PL. Behaviour of the plasma membrane during osmotic excursions. In: Hawes CR, Coleman JOD, Evans DE, editors. Endocytosis, exocytosis, and vesicle traffic in plants. London, UK: Society for Experimental Biology; 1991.

95. Lovelock J. The denaturation of lipid-protein complexes as a cause of damage by freezing. Proceedings of the Royal Society of London Series B - Biological Sciences. 1957;147:427-33.

96. Mazur P, Cole KW. Roles of unfrozen fraction, salt concentration, and changes in cell volume in the survival of frozen human erythrocytes. Cryobiology. 1989;26(1):1-29.

97. Hubel A, Cravalho EG, Nunner B, Körber C. Survival of directionally solidified B-lymphoblasts under various crystal growth conditions. Cryobiology. 1992;29(2):183-98.

98. Ishiguro H, Rubinsky B. Mechanical interactions between ice crystals and red blood cells during directional solidification. Cryoviology. 1994;31(5):483-500.

99. Han B, Bischof JC. Direct cell injury associated with eutectic crystallization during freezing. Cryobiology. 2004;48(1):8-21.

100. Muldrew K, Acker JP, Elliot JA, McGann LE. The water to ice transition: Implications for living cells. In: Fuller B, Lane N, Benson E, editors. Life in the frozen state. New York: CRC Press; 2004.

101. Benson JD. Mathematical problems from cryobiology: University of Missouri; 2009.

102. McGrath JJ. Membrane transport properties. In: McGrath JJ, Diller KR, editors. Low temperature biotechnology. New York, NY: ASME; 1988.

103. Fahy GM. Analysis of "solution effects" injury. Equations for calculating phase-diagram information for the ternary-systems NaCl-dimethylsulfoxide-water and NaCl-glycerol-water. Biophysical Journal. 1980;32(2):837-50.

104. Woods EJ, Zieger MA, Gao DY, Critser JK. Equations for obtaining melting points for the ternary system ethylene glycol/sodium chloride/water and their application to cryopreservation. Cryobiology. 1999;38(4):403-7.

105. Fleming KK, Hubel A. Cryopreservation of hematopoietic stem cells: Emerging science, technology and issues. Transfusion Medicine and Hemotherapy. 2007;34(4):268-75.

106. Advances in biopreservation. Baust JG, Baust JM, editors. Boca Raton, FL: CRC Press; 2006.

107. Arakawa T, Carpenter JF, Kita YA, Crowe JH. The basis for toxicity of certain cryoprotectants: A hypothesis. Cryobiology. 1990;27(4):401-15.

108. Fahy GM, Lilley TH, Linsdell H, Douglas MS, Meryman HT. Cryoprotectant toxicity and cryoprotectant toxicity reduction - in search of molecular mechanisms. Cryobiology. 1990;27(3):247-68.

109. Rall WF, Fahy GM. Ice-free cryopreservation of mouse embryos at -196 degrees C by vitrification. Nature. 1985;313(6003):573-5.

110. Lane M, Schoolcraft W, Gardner D. Vitrification of mouse and human blastocysts using a novel cryoloop container-less technique. Fertility and Sterility. 1999;72(6):1073-8.

111. Ramezani M, Valojerdi MR, Parivar K. Effect of three vitrification methods on development of two-cell mouse embryos. Cryo Letters. 2005;26(2):85-92.

112. Kasai M, Mukaida T. Cryopreservation of animal and human embryos by vitrification. Reproductive Biomedicine. 2004;9(2):164-70.

113. Hunt CJ, Timmons PM. Cryopreservation of human embryonic stem cell lines. Methods in molecular biology. 2007;368:261-70.

114. Heng BC, Kuleshova LL, Bested SM, Liu H, Cao T. The cryopreservation of human embryonic stem cells. Biotechnology and applied biochemistry. 2005;41:97-104.

115. Bahadori MH, Soltani B, Mirzajani E, Babaei P, Ansar MM, Moghaddam MAJ. Cryopreservation of rat bone marrow derived mesenchymal stem cells by two conventional and open-pulled straw vitrification methods. Yakhteh medical journal. 2009;11(3):317-26.

116. Wang HY, Lun ZR, Lu SS. Cryopreservation of umbilical cord blood-derived mesenchymal stem cells without dimethyl sulfoxide. Cryo Letters. 2011;32(1):81-8.

117. Freshney RI. Cryopreservation. Culture of animal cells. 6th ed. Hoboken, NJ: Willey & Sons; 2010. p. 317-33.

118. Kotobuki N, Hirose M, Takakura Y, Ohgushi H. Cultured autologous human cells for hard tissue regeneration: Preparation and characterization of mesenchymal stem cells from bone marrow. Artificial Organs. 2004;28(1):33-9.

119. Lee MW, Yang MS, Park JS, Kim HC, Kim YJ, Choi J. Isolation of mesenchymal stem cells from cryopreserved human umbilical cord blood. International Journal of Hematology. 2005;81(2):126-30.

120. Windrum P, Morris TCM, Drake MB, Niederwieser D, Ruutu T, Par ECLW. Variation in dimethyl sulfoxide use in stem cell transplantation: a survey of EBMT centres. Bone Marrow Transplantation. 2005;36(7):601-3.

121. Spurr EE, Wiggins NE, Marsden KA, Lowenthal RM, Ragg SJ. Cryopreserved human heamatopoietic stem cells retain engraftment potential after extended (5-14 years) cryostorage. Cryobiology. 2002;44:210-7.

122. Liseth K, Ersvoer E, Abrahamsen JF, Nesthus I, Ryningen A, Bruserud O. Long-term cryopreservation of autologous stem cell grafts: a clinical and experimental study of hematopoietic and immunocompetent cells. Transfusion. 2009;49(8):1709-19.

123. Cocks FH, Brower WE. Pase-diagram relationships in cryobiology. Cryobiology. 1974;11(4):340-58.

124. Pegg D. Equations for obtaining melting-points and eutectic temperatures for the ternary-system dimethylsulfoxide sodium-chloride water. Cryo-letters. 1986;7(6):387-94.

125. Tappel AL. Effects of low temperature and freezing on enzymes and enzyme systems. In: Meryman HT, editor. Cryobiology. New York: Acadamic Press; 1966. p. 163-7.

126. Galmes A, Besalduch J, Bargay J, Novo A, Morey M, Guerra JM, et al. Long-term storage at -80 degrees C of hematopoietic progenitor cells with 5-percent dimethyl sulfoxide as the sole cryoprotectant. Transfusion. 1999;39(1):70-3.

127. Sputtek A, Nowicki B, Rowe A, Kuhnl P. Temperatures lower than-80 degrees C are required for the long-term storage of human peripheral blood progenitor cells. Trasfusions. 2005;45(3):9A.

128. Fowke K, Behnke J, Hanson C, Shea K, Cosentino M. Apoptosis: a method for evaluating the cryopreservation of whole blood and peripheral blood mononuclear cells. Journal of Immunological Methods. 2000;244:139-44.

129. Drexler HG, Gignac SM, Brauer S, Quentmeier H. Different survival of continuous cell lines transported in live or frozen form. In Vitro Cellular & Developmental Biology - Animal. 1991;11:841-2.

130. Hunt CJ. Cryopreservation of human stem cells for clinical application: A review. Transfusion Medicine and Hemotherapy. 2011;38(2):107-23.

Chapter 3 External Parameter Impact on the Temperature Profile during Stem Cell Shipment

3.1 Introduction

One major benefit gained from the cryopreservation of stem cells is the relative ease of transportation between storage, research and clinical facilities. Efficient cryopreservation dictates the rate at which recovered stem cells proliferate and differentiate to facilitate the expansion and production of the cell line of choice (131). The key requirement to be met for the successful transportation of cryopreserved specimens is the sufficiently low temperature for the duration of transit. *Liquid Nitrogen* (LN) shippers are currently considered the 'gold standard' for cryogenic transportation. LN shippers are designed to maintain stable, ultra-low temperatures by retaining LN within a molecular sieve-like material, thereby permitting storage at LN temperature for up to 14 days (130). Shippers are available in a range of sizes from those suitable for use internally within a laboratory or cell bank, to those utilised for shipping the cells over long distances. Although being the best practice, the use of LN shippers is typically limited for *vitrified* or cryopreserved Good Manufacturing Practice (GMP)-compliant material due to high transportation costs. For conventionally cryopreserved material, transportation on pellets of solid *carbon dioxide* (CO_2) (commonly referred to as *dry ice*) is the accepted practice (130).

Conventional cryopreservative solutions containing 10% DMSO have a *eutectic* temperature of approximately -70°C - this is the threshold temperature at which the intracellular and extracellular solutions are completely solidified (123). It is important that the temperature during shipping remains below this critical point to avoid damaging effects to the specimens. Dry ice has a sublimation temperature of -78.5°C at standard atmospheric pressure and is at the very limit of what is generally

considered a safe temperature for cell cryopreservation. Shipping of cryopreserved stem cells with dry ice is mostly used in research applications and is specified by individual laboratory in-house Standard Operating Procedures (SOPs). For a typical research application, cells are transported in vials placed within an insulated container which is filled with dry ice and shipped by a courier. When in transportation, the shipment is exposed to a dynamic environment which can affect the internal temperature and hence the specimens being transported.

In order to understand the actual environmental conditions that could lead to thermal variations during the transportation of cryopreserved stem cell specimens maintained on the pallets of dry ice, we carried out a study using sensors to record relevant environmental conditions during the transit of stem cell shipments. Specifically, we used a cryogenic temperature sensor to record the internal temperature at which the transported specimens were maintained, a tri-axial accelerometer for recording both dynamic and static forces and a barometric pressure sensor to establish when the shipment was transported by air.

The objective of the present study was to gain insight into typical thermal conditions experienced by the specimens during transportation with dry ice. In addition we aimed to examine the external physical activities which were applied on the shipment and their effect on the internal temperature in particular.

3.2 Study design and methods

3.2.1 The sensors

Three sensors were used in this study, specifically: temperature, barometric pressure and acceleration. The temperature sensor was capable of measuring in a range from -86°C to 35°C and was programmed to record temperature at a frequency of two samples per minute. The barometric pressure sensor with a working range of 0 mbar to 2000 mbar was set to take a measurement at a rate of one sample per minute. For the force measurement, a tri-axial accelerometer capable of measuring both static and dynamic forces along three orthogonal axes (x, y and z) was used. The dynamic range of the accelerometer was ±10g. Acceleration data was sampled at a rate of 2Hz and this was primarily limited by the amount of memory available on the data logger to allow recording for a minimum of 72 hours.

3.2.2 Shipping protocol and data acquisition

Packaging and shipping of cryopreserved stem cell specimens was carried out in accordance with the Regenerative Medicine Institute (REMEDI), National University of Ireland, Galway in-house shipment procedures. A styrofoam container was filled with dry ice pellets, typically 4 to 6 kg and the vials of cryopreserved stem cell specimens were placed into the container such that the dry ice pellets covered the vials completely. A temperature logger was placed in close proximity to the vials. The atmospheric pressure and acceleration sensors were attached to the exterior of the container. The study information sheet for the receiving party, along with the instructions for removing and returning the recording devices, was enclosed with the shipment. The styrofoam container was placed into a carton and appropriate mailing markings and hazardous material information labels were attached. The

shipment was then transported via courier. Several different courier services were used to carry out the transportation depending on the destination. Upon receipt of the shipment, the data loggers were removed and returned for data analysis.

3.2.3 Data set structure

Two data sets were generated in this study to facilitate the proposed tests. The first data set contained sensor data including internal temperature, barometric pressure and acceleration of five stem cell shipments as detailed in Table 3.1. Cases included in this data set were regular shipments of Mesenchymal Stem Cell (MSC) lines sent from the Regenerative Medicine Institute (REMEDI), National University of Ireland, Galway to collaborating research institutions world-wide.

Table 3.1: Summary of the shipments included in the investigation. The duration in transit includes time interval from the moment the specimens were placed into the shipping container until they were removed at the final destination. *The shipment was despatched to Dublin, Ireland and returned back to Galway, Ireland.

Shipment No.	Destination	Duration, [hrs]
1	Galway, Ireland*	24
2	York, United Kingdom	24.5
3	Durham, NC, United States	53
4	Barcelona, Spain	20.2
5	Oxford, United Kingdom	25.4

The second data set contained accelerometer traces of three transportation activity classes, namely: stationary, road transport by vehicle and manual handling. The purpose of this database was to facilitate training and validation of the transportation

activity classifier. This data set was collected using the same accelerometer and sampling frequency (2Hz) as used with the shipments. The stationary condition was recorded by placing the accelerometer on a stationary object located in the environments of varying background activities. Vehicle transportation activity was collected with the help of three volunteers by placing the accelerometer in their vehicles and recording the data while driving. This class included slow driving in the city as well as high speed driving on the motorway. Similarly, the manual handling class was recorded with a help of three volunteers who were asked to carry a container of similar size and weight as those used for the stem cell shipments. A visual inspection of the recorded data indicated the presence of non-activity class related artefacts at the start and the end of recordings. These artefacts were introduced by the steps undertaken in order to initiate and terminate the recordings. The artefacts were removed by discarding the first and the last 5 minutes from each of the recordings. The data set contained approximately 5 hours of accelerometer traces for each activity class.

3.3 Results

3.3.1 Thermal conditions during shipping

The thermal history of five shipments included in this investigation from the time samples were placed into the shipping container with dry ice until they were removed at the final destination is presented in Figure 3.1 and summarised in Table 3.2. It can be seen that the mean temperature of all shipments was in the acceptable range (below the eutectic point); however, it is also seen that in four cases (shipments No. 2, 3, 4 and 5) the temperature rose above the eutectic point for some period of time. While shipment No. 5 experienced a relatively short event (lasting

less than 20 minutes) of temperature elevation above the eutectic point, shipments No. 2, 3 and 4 experienced extensive exposure above this critical temperature (combined time of 3 hours, 11.6 hours and 3.5 hours respectively). In all cases the temperature profiles show fluctuations distributed over the entire span of transportation interval.

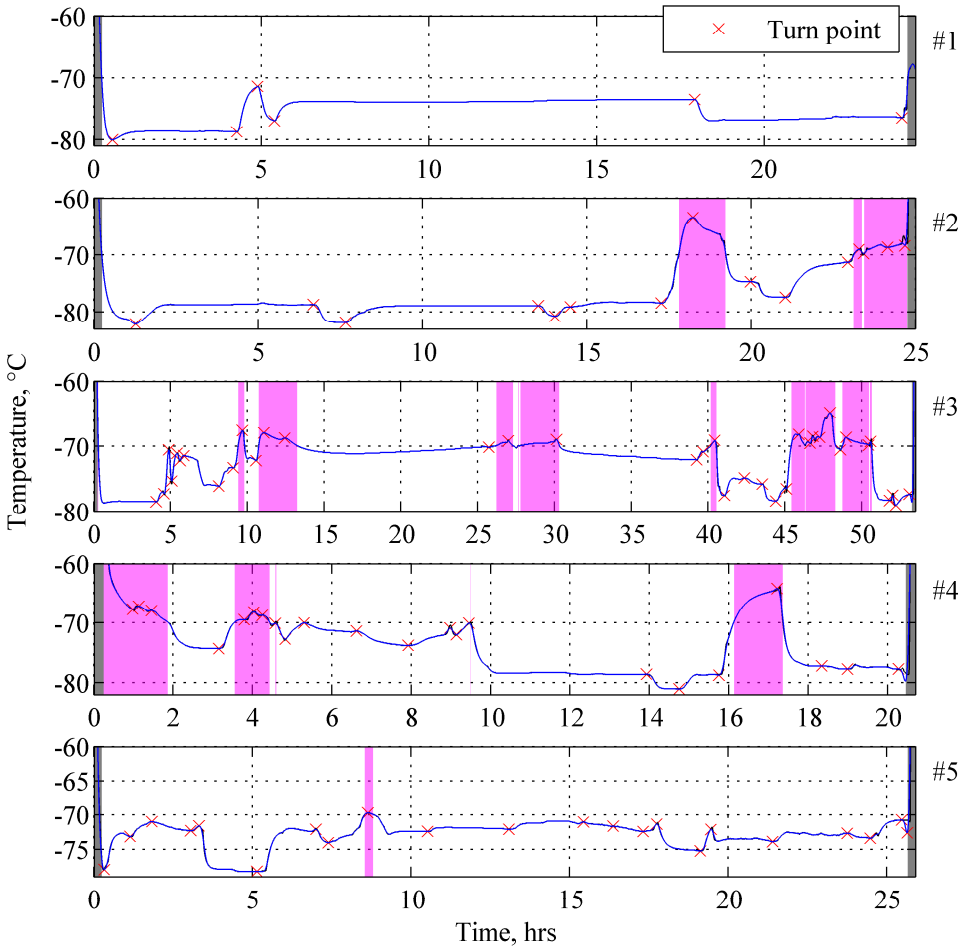

Figure 3.1: Temperature as a function of time inside the shipping containers. The shaded area represents the intervals where temperature exceeds -70°C.

For the purpose of comparison, we carried out a separate experiment with the same setup as used for the shipment of specimens; however, the container was maintained

stationary for the duration of the experiment (see Figure 3.2). It can be seen that under static conditions, the temperature was nearly constant at -78.9°C for approximately 100 hours when the sensor was completely covered under dry ice pellets. The mean temperature on the surface of the dry ice layer was higher (-66.5°C) showing a gradual increase with slight fluctuations. Nevertheless, fluctuations of similar magnitude as observed in actual shipments were not present under static conditions. These observations lead to a conclusion that dynamic activities related to transportation trigger these events of temperature elevation.

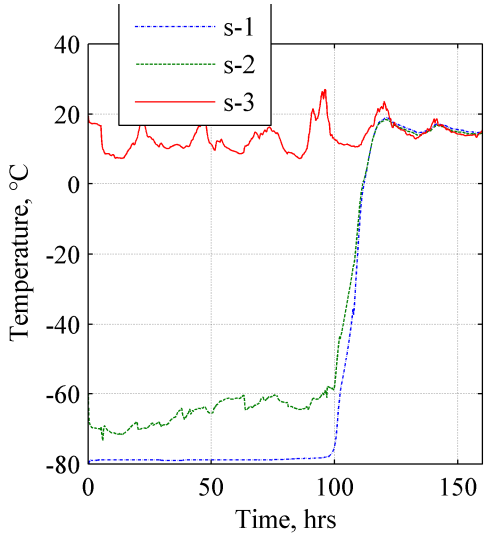

Figure 3.2: Thermal profiles inside the shipping container filled with approximately 5 kg of dry ice pellets when sensor is completely covered under dry ice (s-1) and placed on the surface of dry ice layer (s-2). The third profile (s-3) is the ambient temperature of the container exterior. These profiles were recorded during a separate experiment under static conditions (i.e. the container was maintained stationary for the duration of the experiment).

In order to identify the locations where temperature fluctuations occurred we established the turning points in the shipment temperature profiles. The following procedure was applied to determine this:

i. Temperature data were smoothened using cubic spline interpolation (132); this smoothing step was needed in order to approximate the underlying function.

ii. Turning points were identified by the change of gradient sign around x i.e. $f'(x-\epsilon)$ and $f'(x+\epsilon)$

iii. and a threshold amplitude of ≥0.5°C was set to avoid inclusion of small (<0.5°C) temperature fluctuations.

The identified turning points are represented in Figure 3.1. Our next step was to establish what happened to the shipment at the time these fluctuations occurred in order to identify the root cause of the temperature fluctuations.

Table 3.2: Summary of thermal conditions inside the container during shipping, where T_{mean}, T_{min} and T_{max} are mean, minimum and maximum temperatures recorded respectively. The last column represents the combined time interval where temperature exceeded -70°C.

Shipment	T_{mean}, [°C]	T_{min}, [°C]	T_{max}, [°C]	T>-70°C, [hrs]
#1	-75.3	-80	-70.9	0
#2	-76.8	-82.1	-63.5	3.0
#3	-72.2	-79.1	-64.3	11.6
#4	-74.0	-81.0	-45.0	3.5
#5	-72.9	-78.2	-69.7	0.3

3.3.2 Classification of transport modes

A number of techniques are reported for the classification of transportation modes of individuals. Some are based solely on accelerometer data (133-135) while others use a combination of acceleration and other sensor data (136, 137). In the current investigation we aimed to classify between the three activities related to transportation of a shipment, namely stationary, vehicle transport, and manual

handling. In addition, we aimed to divide the vehicle transportation class into two subclasses, namely ground and air transportation. We applied a two stage algorithm to carry out this classification; firstly, we used the barometric pressure data to discriminate the intervals of air transportation and secondly, we used the accelerometer trace to classify the non air transport intervals into stationary, ground vehicle transport and manual handling.

a) Barometric data

The transport category aircraft are typically pressurised between approximately 840 mbar and 750 mbar at cruising altitude, an equivalent to 1524 m and 2438 m altitudes above the mean sea level respectively (138, 139). The cargo type aircraft are typically pressurised to the same standard (140). The pressure inside an aircraft depends on the altitude (139) therefore steep pressure gradients are characteristic during ascent after takeoff and descent before landing of an aircraft. These features enable identification of air transport intervals from the barometric pressure data with relative ease by visual inspection. It was established that shipments No. 2, 3, 4 and 5 were part-transported by air. The time intervals when air transportation took place are illustrated in Figure 3.3.

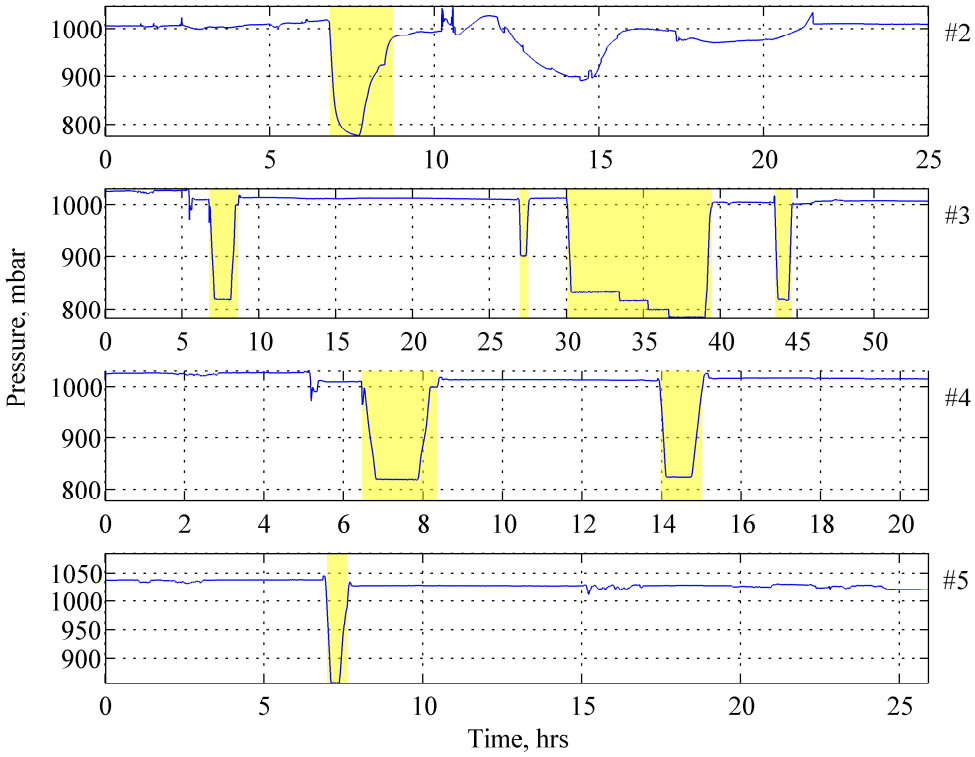

Figure 3.3: Barometric pressure as a function of time recorded during transportation of stem cell specimens. Shaded areas indicate the intervals of air transportation as determined by low pressure area corresponding to typical internal pressure of a transport aircraft at cruising altitude. This low pressure area is bounded by steep gradients of pressure change associated with ascent after takeoff and descent before landing of an aircraft.

b) Acceleration data

A convenient way for classifying the transportation activity from the accelerometer data is by transforming the tri-axial signals into an orientation-invariant signal. Such a signal is the total acceleration vector expressed as the sum of the square value of the force in x, y and z axes (3.1):

$$a = \sqrt{{a_x}^2 + {a_y}^2 + {a_z}^2} \qquad (3.1)$$

From here, the magnitude of the total acceleration vector (with the gravity component subtracted) can be expressed as $|a-1|$. The features used to infer transportation activities were the mean (μ) and the variance (σ^2) of this acceleration vector magnitude over a 1 minute interval (referred to as a *window*). For this investigation a *Multilayer Percepton* (MLP)[1] which is a class of *Artificial Neural Network* (ANN) classifiers was used. Examples of MLP use for activity recognition can be found in (142). We randomly selected 300 windows from each of the three known activity sets and extracted the features (i.e. μ and σ^2 values) to form a data set for training and validation of the classifier. A method of *cross-validation* (143) was employed for this purpose. Specifically, the data set of known activity examples was split into training and validation subsets with a ratio of 2/3 and 1/3 respectively. Both splits contained equal ratios (1/3) of data from the different activity classes in order to minimise issues typically seen in imbalanced training sets (144). MLP training and validation was repeated 100 times with the new training and validation sets obtained using a *random sub-sampling* technique (143). The summary of MLP performance after cross-validation is detailed in Table 3.3. The mean recognition rate of 98.05% and 97.47% was achieved when applied on training and validation data respectively. All classifiers performed similarly with the standard

Table 3.3 Class discrimination accuracy achieved by MLP as determined by cross-validation (*k*=100)

Data sub-set	Accuracy, [%]	
	μ	σ
Training	98.05	0.54
Validation	97.47	1.30

[1] Specifically, a single MLP with 3 output nodes, each representing one of the 3 classes in the system, was used. The MLP was composed of 2 hidden layers with 15 neurons in both layers using hyperbolic tangent sigmoid (141) transfer function for the neurons. The MLP was implemented using the Neural Network Toolbox in Matlab.

deviation of 0.54% and 1.30% from training and validation data respectively. We selected the best performing classifier to be used in the further investigation. The classification boundaries of the selected classifier along with the original data set used for training and validation are represented in Figure 3.4. The trained MLP was then used to classify the transportation activities of the 5 stem cell shipments from the recorder accelerometer data. The results of this classification step are illustrated in Figure 3.5.

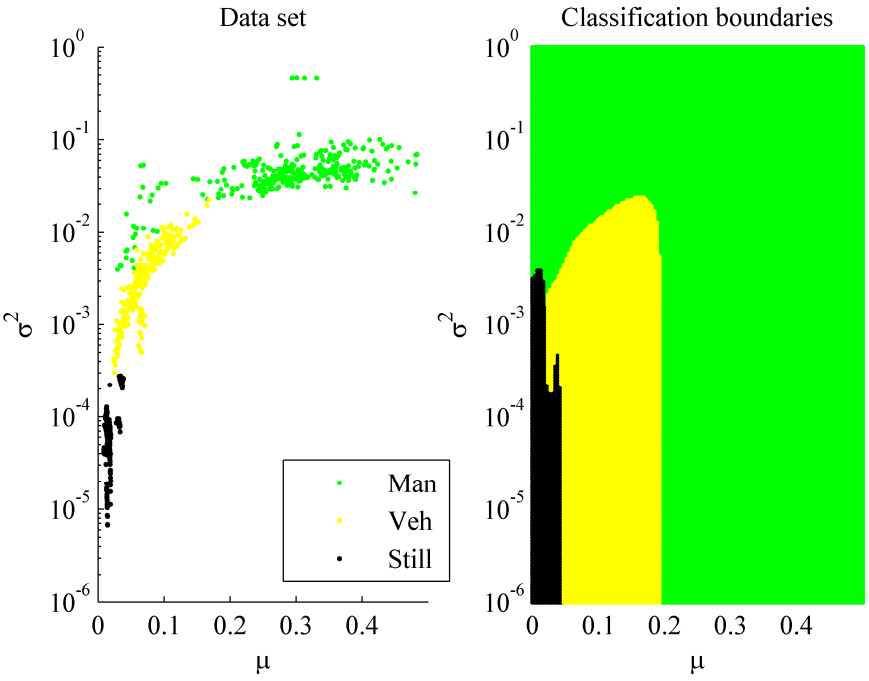

Figure 3.4: Left panel represents a data set of three different activities used for the training and validation of MLP while the right panel shows the classification boundaries of the best perfoming MLP.

The summary of transportation activities used to facilitate transportation of stem cell shipments as determined by the algorithm are summarised in Table 3.4.

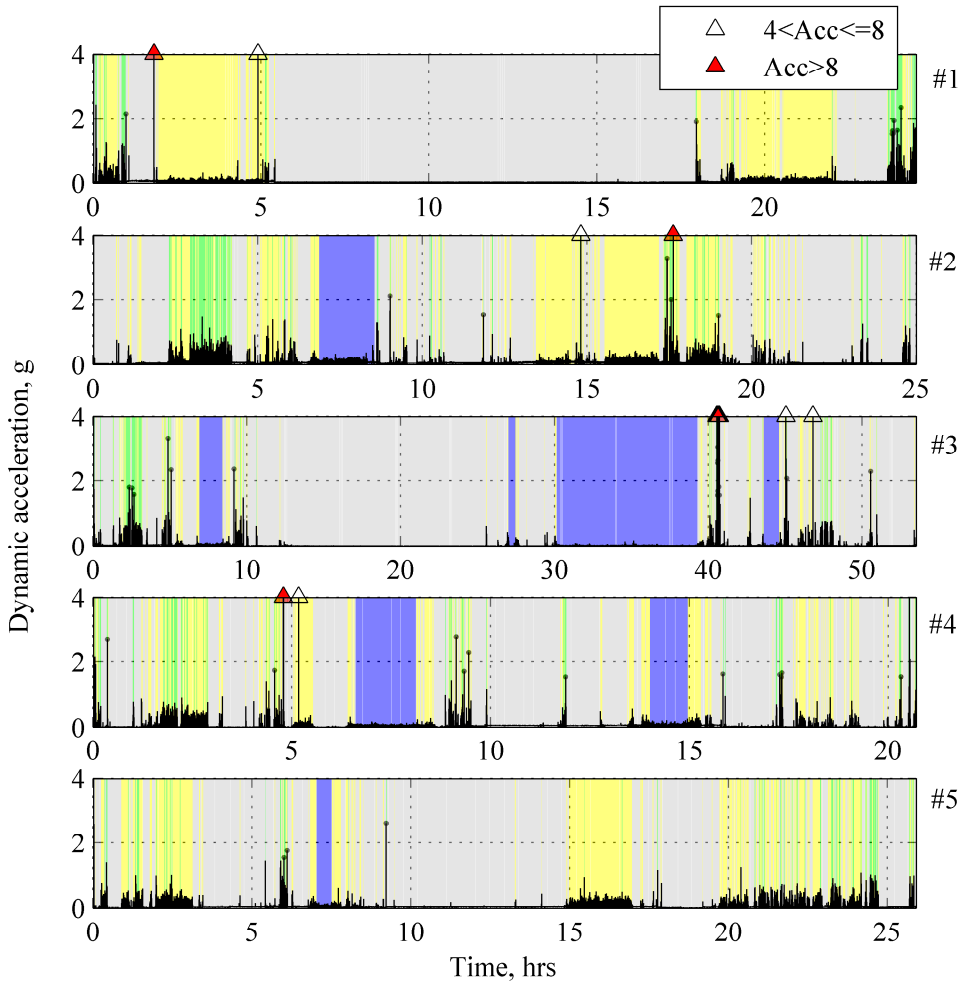

Figure 3.5: Magnitude of dynamic acceleration as a function of time recorded during the transportation of 5 stem cell shipments. Colour shaded areas indicate different transportation activities as determined using the MLP classifier (grey represents stationary, yellow-vehicle transport, green-manual handling intervals). Note, the air transportation intervals (shaded in blue) were determined in the first stage of the classification algorithm from the barometric data. The triangular symbols are used to mark the spikes where the total acceleration vector exceeds the scale plotted in the graphs.

Table 3.4: Combined intervals of different transportation activities during shipment of stem cell specimens.

Shipment	Stationary, [%]	Vehicle (ground), [%]	Air, [%]	Manual, [%]
#1	67.1	29.4	0	3.5
#2	51.0	36.0	6.7	6.3
#3	65.0	8.9	22.6	3.5
#4	57.6	23.8	11.9	6.7
#5	63.2	31.1	1.9	3.8

3.3.3 Transportation activities and their influence on thermal fluctuations

In this section we analyse how different transportation activities contribute to the fluctuations observed in the thermal history of the shipments. We hypothesised earlier that dynamic activities related to transportation may cause the observed temperature fluctuations. In order to examine this hypothesis, we assessed the correlation between transportation modes and temperature fluctuations. This was achieved by the following steps:

i. Using the classification technique described in Section 3.3.2 the time span of shipment transportation was segmented into one minute windows and a mode of transportation was assigned to each of them, and
ii. we assessed which of the transportation activities took place at the time temperature fluctuations occurred.

It is important to consider that temperature is a relatively slowly varying property, therefore due to this time lag, the turning point of a temperature fluctuation may not

occur within the same 1 minute window as the activity which triggered the variation. Moreover, the use of smoothing techniques for the estimation of an underlying temperature function and hence the turning points also inevitably introduce some degree of time shift. Taking these considerations into account we hence assessed a range of time windows around the turning point. The results of this analysis are presented in Figure 3.6.

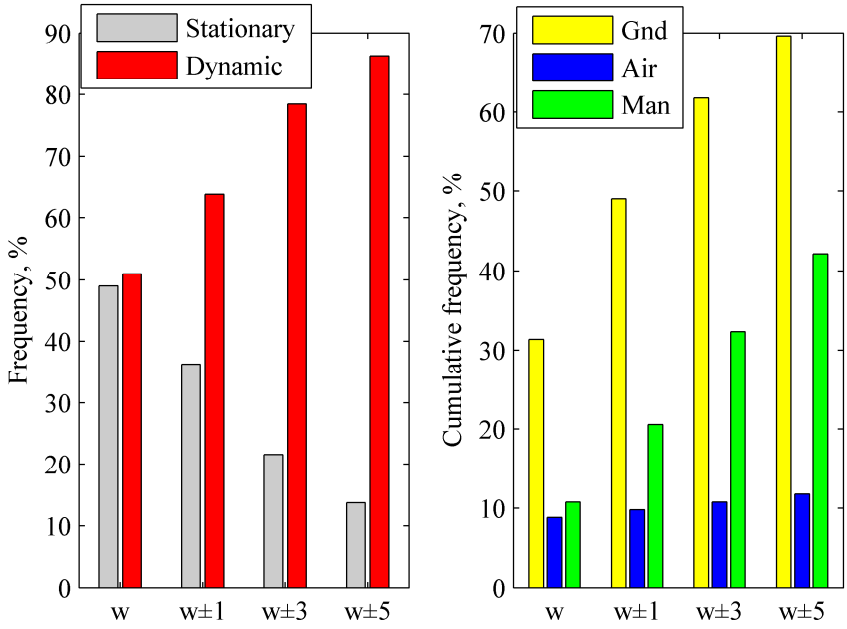

Figure 3.6: Shipping activities taking place when the flux of temperature occurred. '*w*' represents a window the turn point falls in while *w±i* represent a range of windows *(w-i; w+i)* around the turning point.

It is evident that dynamic activities (including ground and air transportation as well as manual handling) were predominantly present in the time intervals around the fluctuations (see Figure 3.6, left panel). Results also suggest that ground transportation by vehicle and manual handling were the most frequent activities in

the interval when thermal fluctuations occurred, while air transportation was least frequent (see Figure 3.6, right panel). The motion associated with dynamic activities is thought to cause the effect of temperature fluctuation. This could be explained by the introduced movement of dry ice pellets whereby specimen vials may become partially exposed to the warmer gas filled part of the container. The opposite effect when the vial becomes covered under the pellets of dry ice can explain the observed drops of temperature.

The change of container orientation would inevitably cause movement of dry ice pellets and therefore may contribute to thermal fluctuations. To confirm this theory we examined the intervals where the fluctuation of temperature occurred and matched these intervals with the orientation of the container as determined from the accelerometer data. This was done by filtering the acceleration data by a low pass FIR filter with a cut-off frequency f_{stop}=250mHz in order to eliminate signal noise and unwanted high frequency components. The remaining signal of the static component due to gravity was used to establish the orientation of the container in spherical coordinate angles, namely: *elevation* (φ) and *azimuth* (θ).

Two examples demonstrating how the change of container orientation corresponds to the temperature fluctuation are illustrated in Figures 3.7 and 3.8. The example in Figure 3.7 taken from shipment No. 2 shows a long fluctuation of temperature above the important eutectic temperature level of -70°C. The start of this fluctuation occurred around the same time (between 17.4 and 17.8 hour time points) as a series of container orientation changes. Another series of orientation change events occurred between approximately 19 and 19.2 hour time points causing a negative fluctuation of temperature.

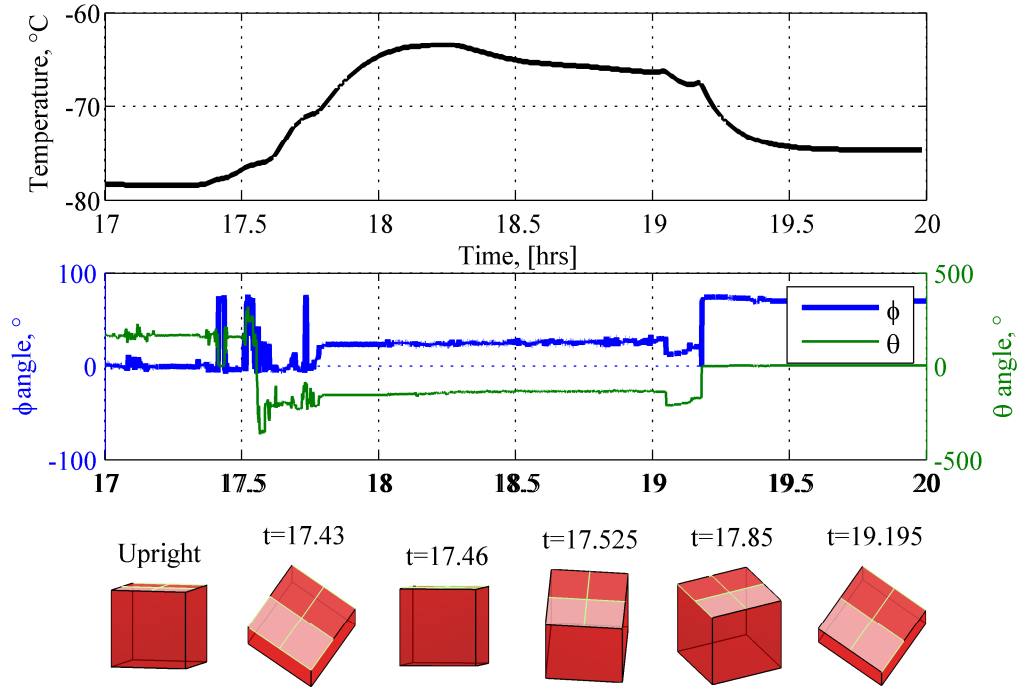

Figure 3.7: A time window from the shipment No. 2 transportation history where the fluctuation of temperature occurred. The start of the fluctuation and the end of it corresponds to the change in orientation of the shipping container suggesting that this was the cause of the temperature fluctuation. A relative orientation from the upright position of the container at various time points of interest is illustrated in the figure.

A second example (shown in Figure 3.8) taken from shipment No. 3 shows multiple temperature fluctuations occurring over a space of 1.6 hours. Under closer inspection it is clear that the turning points of the temperature curve occurring at approximately 4.16, 4.5, 4.62, 4.94, 5.08 and 5.5 hour time points correspond to the change of container orientation represented by angles φ and θ.

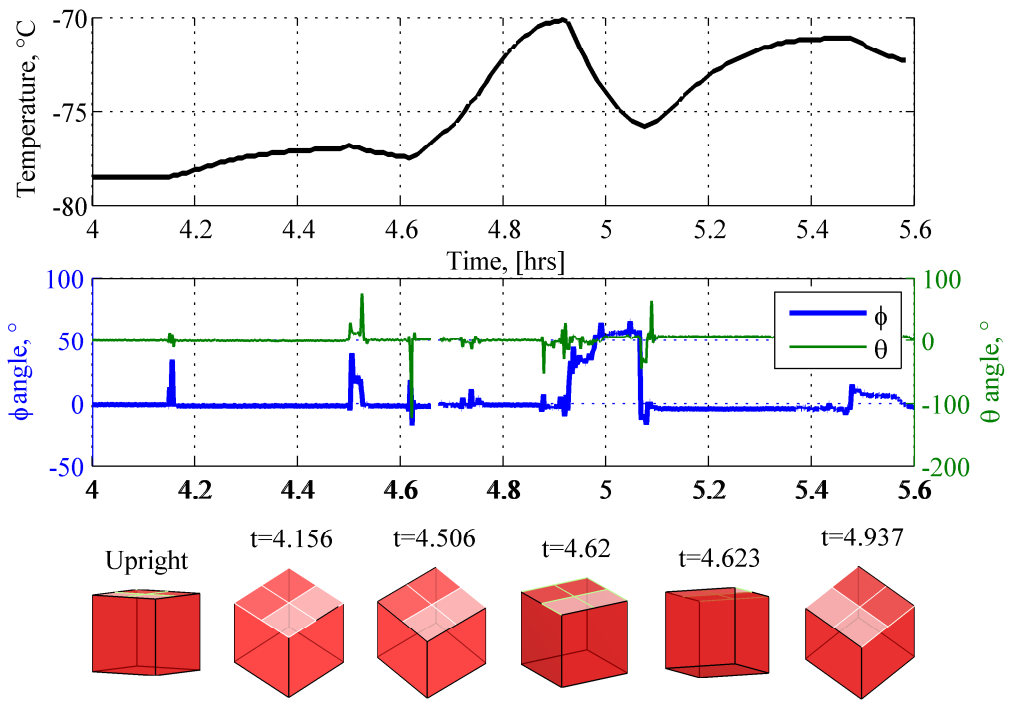

Figure 3.8: A time window from the shipment No. 3 transportation history showing multiple temperature fluxes. It is evident that the turning points of the temperature profile correspond to the change of container orientation (ϕ, θ).

From these examples it is evident that the orientation of the container is a major factor in contributing to the fluctuations of the internal temperature of the shipment container. In order to further assess the significance of orientation change to the fluctuation of internal temperature we applied the following procedure:

i. Classified the fluctuations into 4 groups based on the magnitude of the fluctuation (ΔT_f), namely >0.5°C, >1°C, >3°C and >5°C,

ii. Established the change of orientation in a 5 minute window centred at the location corresponding to the start of the fluctuation. Change of orientation was established as $\Delta\varphi_w=\varphi_{w(max)}-\varphi_{w(min)}$ and $\Delta\theta_w=\theta_{w(max)}-\theta_{w(min)}$.

It was found that $\Delta\varphi$ and $\Delta\theta$ greater than 15° occurred in 43.1% and 57.8% of fluctuations, respectively, in the >0.5°C class, while the larger fluctuations (>5°C) correspond to orientation change criteria in 66.7% and 81% of cases respectively (see Figure 3.9). These results lead to the conclusion that a change of container orientation is the key factor resulting in large thermal fluctuations.

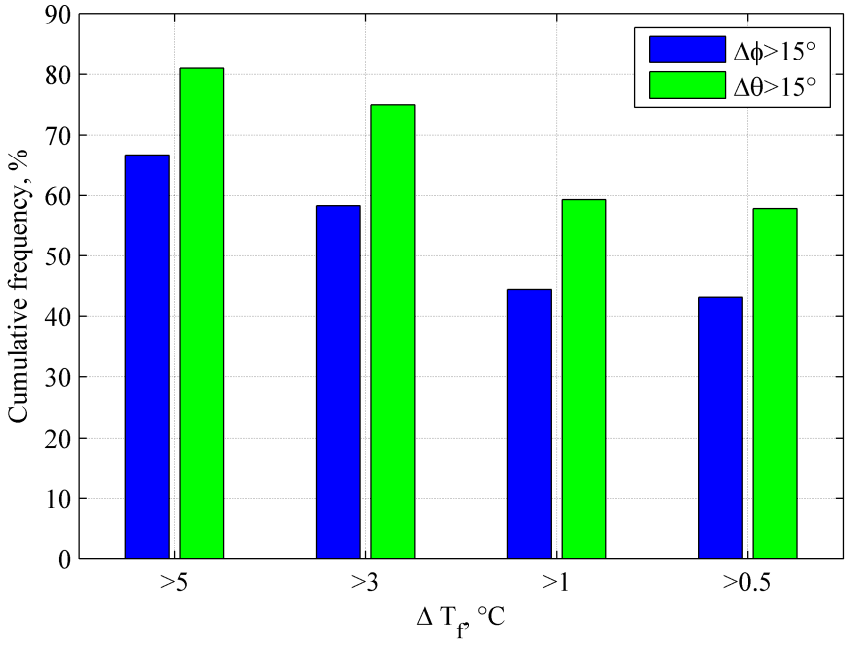

Figure 3.9: Histogram representation of thermal fluctuations caused by the change of container orientation where $\Delta\phi$, $\Delta\theta$>15°.

3.4 Discussion

In this study we assessed thermal fluctuations associated with the shipping of frozen stem cell specimens with dry ice. We used sensory devices to monitor five shipments to world-wide destinations with transportation time varying from 24 to 50 hours.

The thermal history of shipments revealed fluctuations occurring at various stages in transportation. In four cases thermal fluctuations exceeded the eutectic temperature

(-70°C) for some period of time highly increasing the risk of cryoinjury to the specimens. Further investigation revealed that fluctuations were mainly concentrated in the intervals where ground transportation by vehicle and manual handling took place. Furthermore, we found that the change of container orientation was a key factor causing large temperature fluctuations. This can be explained by the movement of dry ice pellets inside the container whereby the specimen vials become partially exposed to the warmer gas filled portion of the container and cause the increase in specimen temperature. The opposite effect when the change of orientation covers the vial under the pellets of dry ice can explain the observed drops of temperature.

This study has provided an insight to the temperature conditions experienced by the specimens during transportation with dry ice and revealed that elevated temperatures are encountered on frequent basis, thus raising some concerns relating to the detrimental effects on the viability of transported specimens.

3.5 References

123. Cocks FH, Brower WE. Pase-diagram relationships in cryobiology. Cryobiology. 1974;11(4):340-58.

130. Hunt CJ. Cryopreservation of human stem cells for clinical application: A review. Transfusion Medicine and Hemotherapy. 2011;38(2):107-23.

131. Haack-Sorensen M, Bindslev L, Mortensen S, Friis T, Kastrup J. The influence of freezing and storage on the characteristics and functions of human mesenchymal stromal cells isolated for clinical use. Cytotherapy. 2007;9(4):328-37.

132. de Bour C. A practical guide to splines: Springer; 2001.

133. Shuangquan W, Canfeng C, Jian M, editors. Accelerometer Based Transportation Mode Recognition on Mobile Phones. Wearable Computing Systems (APWCS), 2010 Asia-Pacific Conference on; 17-18 April 2010.

134. Randell C, Muller H. Context awareness by analysing accelerometer data. Proceedings of the 4th International Symposium on Wearable Computers; Los Alamitos, Ca: IEEE Computer Society Press; 2000. p. 175-6.

135. Miluzzo E, Lane ND, Fodor K, Peterson R, Lu H, Musolesi M, et al. Sensing meets mobile social networks: The design implementation and evaluation of the cenceMe application. Proceedings of the 6th ACM Conference on Embedded Network Sensor Systems; New York: ACM; 2008. p. 337-50.

136. Reddy S, Burke J, Estrin D, Hansen M, Srivastava M, editors. Determining transportation mode on mobile phones. Wearable Computers, 2008 ISWC 2008 12th IEEE International Symposium on; 2008 Sept. 28 2008-Oct. 1 2008.

137. Lester J, Hurvitz P, Chaudhri R, Hartung C, Borriello G. MobileSense - Sensing modes of transportation in studies of the built environment. Proceedings of the International Workshop on Urban, Community, and Social Applications of Networked Sensing Systems; New York: ACM; 2008.

138. Aerospace Medical Association, Aviation Safety Committee, Civil Aviation Subcommittee. Cabin cruising altitudes for regular transport aircraft. Aviation, Space, and Environmental Medicine. 2008;79(4):433-9.

139. Kelly PT, Seccombe LM, Rogers PG, MJ. P. Directly measured cabin pressure conditions during Boeing 747-400 commercial aircraft flights. Respirology. 2007;12(4):511-5.

140. Singh SP, Singh2 J, Stallings J, Burgess G, Saha K. Measurement and analysis of temperature and pressure in high altitude air shipments. Packaging Technology and Science. 2010;23(1):35-46.

141. Vogl TP, Mangis JK, Rigler AK, Zink WT, Alkon DL. Accelerating the convergence of the backpropagation method. Biological Cybernetics. 1988;59:257-63.

142. Kilmartin L, Ibrahim RK, Ambikairajah E, Celler B, editors. Optimising recognition rates for subject independent gait pattern classification. Signals and Systems Conference (ISSC 2009), IET Irish; 2009 10-11 June 2009.

143. Picard RR, Cook RD. Cross-Validation of Regression Models. Journal of the American Statistical Association. 1984;79:575-83.

144. Japkowicz N. The class imbalance problem: Significance and strategies. International Conference on Artificial Intelligence 2000. p. 111-7.

Chapter 4 Precision Thermoelectric Temperature Control System

4.1 Introduction

In the previous chapter we examined the temperature elevations during transportation of cryopreserved stem cell specimens under normal conditions. While the observed fluctuations in temperature raised some concerns regarding their negative impacts on the specimens, it is unlikely that the damage would be significant over the typical duration of shipping. However, in the event of prolonged transportation a near complete or complete thawing of specimen may occur. Such a case was demonstrated by a static experiment where we observed a gradual increase of temperature after approximately 4 days of storage in a dry ice container. In applied cryopreservation, temperatures above -50°C are typically associated with an imminent risk of damage to the specimen (117). The subsequent work presented in this thesis was focused on the viability of stem cells when stored in the temperature range above this critical point; specifically -40°C to 37°C. In order to collect the data on how such temperature elevations impact the viability of cryopreserved MSCs, a series of experiments were proposed. To facilitate the proposed experiments, cryopreserved stem cells had to be exposed to various fixed temperature elevations in order to allow observations on how this affects the viability of cells. However, the limited availability of a precise temperature control system at the time of experimentation and high cost of the commercially available substitutes lead to a development of a specialised temperature control system for the proposed experiments. In the current chapter, we present this purpose built temperature control system. Several design alternatives were considered including use of controlled flow of liquid nitrogen for cooling in combination with a resistance heating element, however a *thermoelectric* (TE) converter was selected for being the most feasible

option. Such converters are frequently used when precise temperature control is required (145-147). The developed TE system can in an experimental setup subject cryopreserved cells to various fixed temperature levels. In order to enable automated precise temperature control, a computer-based application was also developed using the LabVIEW environment. The system presented here has a potential to be used in a wider range of research applications, particularly where there is an absence of suitable commercially available systems.

4.2 System overview

4.2.1 System functionality

TE conversion is based on the phenomenon known as the Peltier effect which creates a temperature gradient in the junction of two dissimilar conductors when direct electric current flows through the junction (148). In a TE conversion cycle, heat is transferred by an electric current from one dissimilar conductor (cold side) to the other (hot side). The direction of the electric current governs the direction of heat transfer, therefore TE devices can be used for both heating and cooling. TE converters allow precise control of the temperature gradient between the cold side and the hot side by controlling the flow of electric current through the junction of the dissimilar conductors.

The architecture of our TE-based computer controlled temperature cycling system is shown in Figure. 4.1.

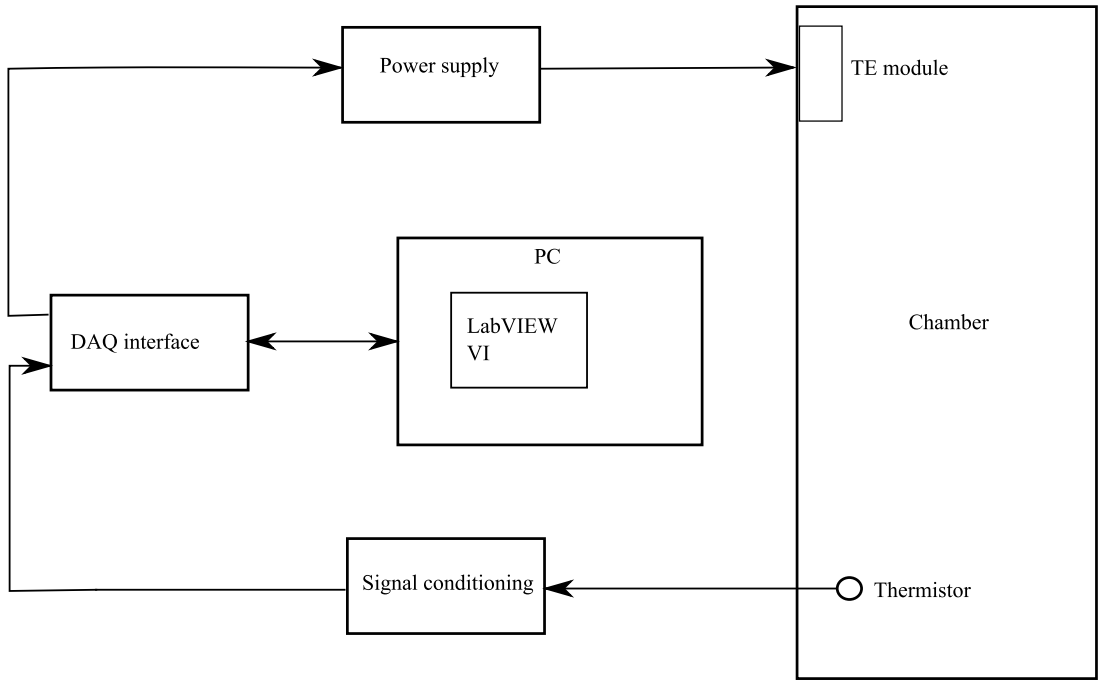

Figure 4.1: Block diagram of the system

4.2.2 Hardware implementation

A medium power TE module (manufactured by TE Technology Inc.) was used for the implementation of the proposed system. The module has an air-cooled heat sink and an external electric fan is used to maintain air circulation at the heat sink. The TE module is powered by a DC power supply unit (manufactured by TE Technology Inc.). The output of the power supply is controlled by a pulse-width modulated (PWM) square wave. The operational range of the TE module in the proposed configuration enabled a maximum temperature difference between the hot and cold sides of approximately 32°C in the heating mode and 44°C in the cooling mode (see Figure 4.2). Therefore, the limits of achievable controlled temperature range were in a range of approximately -22°C to 54°C when the system was operated in typical room temperature environment of 22°C. However, the range of achievable controlled temperature can be extended by operating the system in different ambient temperature environment. For example, by operating the system in a cold room of

4°C, the lowest achievable controlled temperature limit can be extended to approximately -40°C.

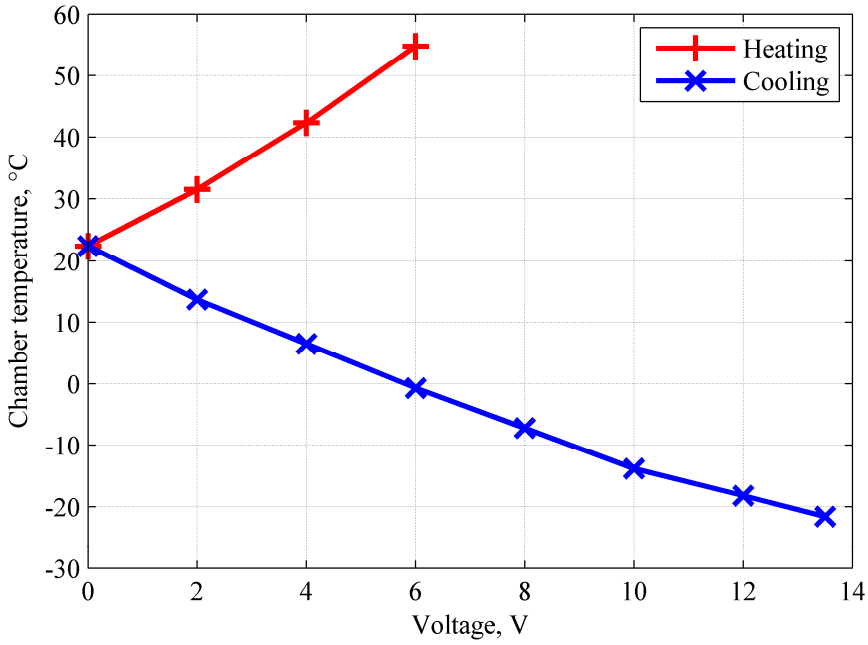

Figure 4.2: Chamber temperature as a function of voltage applied to the TE unit throughout the operational range. The system exhibits approximately linear gains in both heating and cooling modes. The maximum achievable temperature range in the cooling mode and the heating mode is approximately 44°C and 32°C respectively.

The temperature feedback loop consists of a thermistor (Omega Engineering Ltd.) which measures the temperature inside the chamber, a signal conditioning circuitry and a data acquisition (DAQ) module (manufactured by National Instruments Corp.) which provides the temperature measurements to the control computer. The LabVIEW based control instrument allows the output of the power supply to be adjusted in order for the system to achieve a desired set temperature.

4.2.3 Enclosure

A polyester foam enclosure (size 24x24x24cm) was used to create a thermally insulated chamber. The enclosure had an opening made on the bottom to accommodate the TE module while maintaining the heat sink outside the insulating enclosure. A lid on the top of the enclosure allows convenient access to the insulated chamber. The chamber was divided into 20 separate cylinder-shaped compartments of identical size. The base of the chamber was made of aluminium to facilitate efficient heat exchange between the vials and the TE module. A photograph of the enclosure is shown in Figure 4.3.

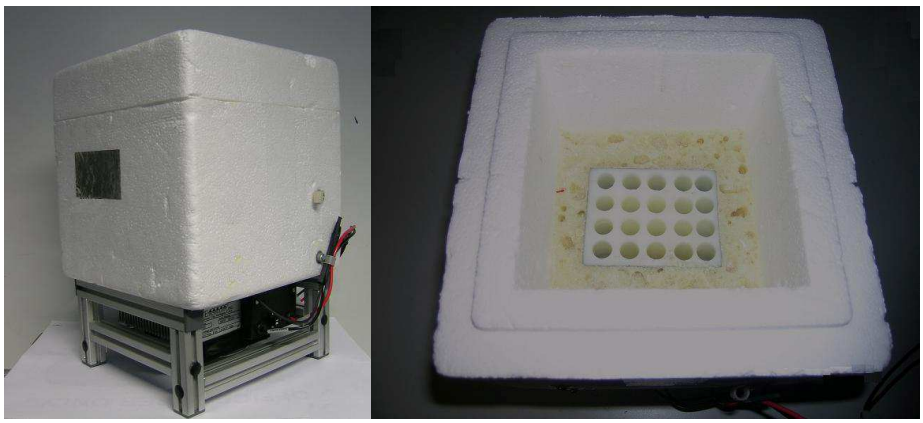

Figure 4.3: Enclosure and TE module assembly. Left panel: side view of the assembly. The assembly is elevated on the stand to ensure sufficient air circulation at the heat sink which is attached to the bottom of the enclosure. The lid on the top allows convenient access to the insulated chamber. Right panel: top view of the enclosure with the lid removed. An insulated chamber is seen which is divided into 20 cylinder-shaped compartments. Each compartment can accommodate a standard cryogenic vial (1.8 ml).

4.2.4 Virtual PID controller

A computer based virtual controller was implemented as a virtual instrument (VI) within National Instrument's LabVIEW platform which is widely used for data acquisition, measurement, control systems etc. (149). The virtual controller employs a Proportional-Integral-Derivative (PID) (150) algorithm to implement automated control of temperature at a desired set value. It uses feedback from the control sensor which measures the temperature in the chamber to calculate and actively adjust the required DC voltage supplied to the TE module thus maintaining the chamber temperature at the user preset level.

The dynamics of the presented system can be approximated by the first order model with time delay as given by Equation 4.1 (151):

$$G(s) = \frac{Ke^{-\tau s}}{Ts+1} \qquad (4.1)$$

where K is the static gain of the process, T is the inertia constant and τ is a time delay. The tuning of the PID parameters is mainly dependant on T and τ. There are a significant number of techniques for identifying these parameters with varying accuracy (152). A closed-loop switch step response method proposed in (151) was used to estimate the process parameters of the presented system as it enables higher accuracy in comparison to the conventional open-loop step response method. The following procedure was applied in order to accomplish the tuning task:

i. The manipulation variable (MV) was set to 100%, which corresponds to 6V and 13.5V in heating and cooling modes, respectively. When the process

variable (PV), temperature in this case, reached the set level (40°C in the heating and 0°C in the cooling modes), the MV was set to 0%.

ii. System response to the step inputs was recorded and used to calculate the process parameters, specifically the maximum slope R and the equivalent time delay L.

System responses to a step input in heating and cooling modes are represented in Figure 4.4, and the associated process parameters are detailed in Table 4.1.

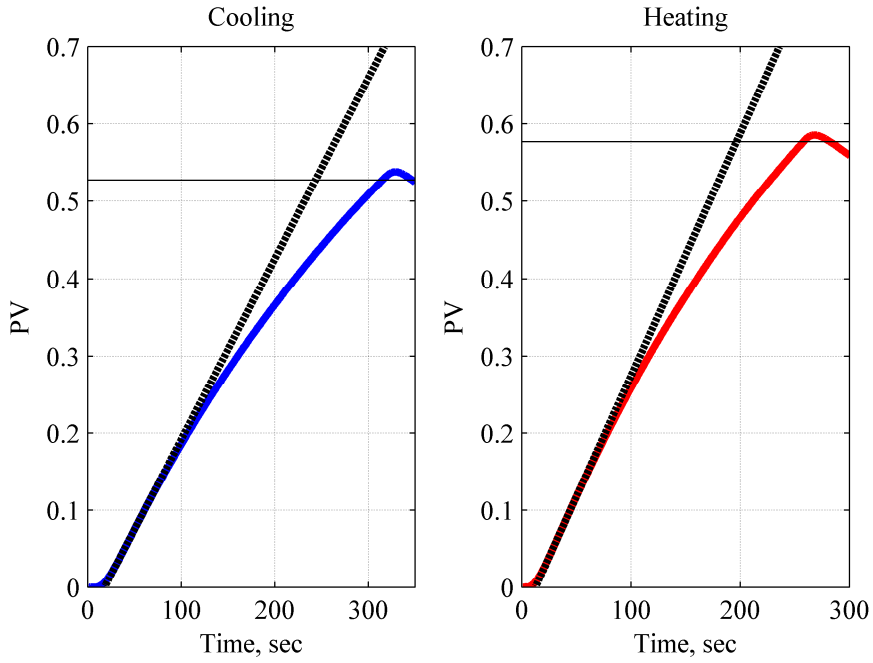

Figure 4.4: Closed-loop step switch response of the system in cooling and heating modes. The tangent lines to the curves at the points of rising inflection correspond to the maximum slopes.

Table 4.1: Switch step response parameters of the system, where *R* is the slope of the tangent and *L* is the smooth moving time constant.

	R	L
Heating	0.0030	18
Cooling	0.0022	24

According to the Ziegler-Nichols tuning rules, a set of controller parameters for the PID type controller can be calculated from the following equations (151):

$$K_p = \frac{1.2}{RL} \qquad (4.2)$$

$$T_i = 2L \qquad (4.3)$$

$$T_d = \frac{L}{2} \qquad (4.4)$$

The calculated values of the process parameters are enumerated in Table 4.2.

Table 4.2: PID controller parameters. K_p = proportional gain; T_i = integral time; T_d = derivative time.

	K_p	T_i, sec	T_d, sec
Heating	16.6	36	9
Cooling	30.3	48	12

4.3 System performance

In order to demonstrate the performance of the designed system in maintaining the specimens at precise temperature, several experiments were carried out. In these experiments, a cryogenic vial containing 1ml of water (this is a typical volume of cell suspension in a vial) was placed in a chamber and a probe was inserted into a vial to measure the internal temperature. The target temperature was set to a specific level and, when the steady state was reached, the internal temperature of the vial was recorded over a 30 minute interval at a sampling rate of 2 samples per minute. These results were processed and are represented by their mean (μ) and standard deviation (σ) in Table 4.3.

Table 4.3: Summary of the system performance. The experiments were carried out in a room temperature environment of approximately 22°C, therefore set temperatures of -20°C, 0°C, and 20°C required system to be operated in a cooling mode while the set temperature of 37°C required heating mode.

Set temperature, °C		-20	0	20	37
Measured temperature, °C	μ	-19.3	0.4	19.4	36.7
	σ	<0.1	0.1	<0.1	<0.1

It was observed that the temperature of the vial was maintained very close to the set temperature with the mean error level of 0.5°C. The system also showed good stability over time with a typical standard deviation of ≤0.1°C. These tests demonstrated that the performance of the system is acceptable for the proposed experiments.

4.4 Discussion

The system was designed specifically to be used in laboratory experiments investigating the effect of elevated temperature on cryopreserved stem cells. A design based on TE conversion proved to be suitable for such mid-scale application primarily due to the possibility of precise temperature control, relatively simple implementation, compact size, low weight and safe operation in a laboratory environment. The LabVIEW VI enabled automatic temperature control employing PID control algorithm. System performance tests have shown that it is capable of maintaining precise temperature levels as required for the proposed experimental studies.

4.5 References

117. Freshney RI. Cryopreservation. Culture of animal cells. 6th ed. Hoboken, NJ: Willey & Sons; 2010. p. 317-33.

145. Riffat SB, Ma X. Thermoelectrics: a review of present and potential applications. Applied Thermal Engineering. 2003;23:913-35.

146. Chu RC, Simons RE. Application of thermoelectrics to cooling electronics: review and prospects. 18th International Conference on Thermoelectrics; 29 August - 2 September; Poughkeepsie, NY: IEEE; 1999. p. 270-9.

147. Watanabe H. Thermoelectric strategy for consumer applications. 17th lntemational Conference on Thermoelectrics; May 24-28; Kanagaawa, Japan: IEEE; 1998. p. 486-90.

148. Rowe DM. CRC Handbook of Thermoelectronics. 1 ed: CRC Press LLC; 1995. 702 p.

149. Gary W. Johnson RJ. LabVIEW Graphical Programming. 4 ed: McGraw-Hill Professional; 2006.

150. Datta A, Ho M-T, Bhattacharyya SP. Structure and synthesis of PID controllers: Springer; 2000. 233 p.

151. Yang Zhi WJ. Auto-Tuning of PID Parameters Based on Switch Step Response. lnternational Conference on Intelligent Processing Systems; Beijing, China: lEEE; 1997.

152. Aström KJ, Hägglund T. PID controllers: Theory, design and tuning. 2nd ed: Instrument Society of America; 1995.

Chapter 5 The Effect of Temperature Elevation on Cryopreserved Mesenchymal Stem Cells

5.1 Introduction

This chapter presents a study focusing on the effect of temperature elevation on the membrane integrity of cryopreserved rat MSCs (rMSCs). The study includes a series of experiments in which the elevation of temperature was simulated in the laboratory environment. The scope of this study includes a near complete and complete thaw of cryopreserved cells (temperatures ranging from -20°C to 37°C). This temperature range recapitulates the total breakdown of a temperature control system with regard to stem cell storage or transportation. The data collected during the study enabled us to find a relationship between the aforementioned range of temperature elevation conditions and the death of rMSC due to damage to the cellular membrane.

5.2 Materials and methods

5.2.1 Primary culture of rMSCs

Bone marrow-derived rMSCs were prepared as reported previously (153). Briefly, bone marrow was obtained from the femurs and tibiae of 8-12 week old male Sprague Dawley rats (Harlan, UK) and washed with medium (Gibco). Marrow mononuclear cells were resuspended in α-MEM/F12 containing 10% foetal bovine serum and 1% (v/v) antibiotic/antimycotic solution (Gibco) and plated at density of 1.2×10^8 cells/cm^2. Non-adherent cells were removed by routine media changes. After 8 days or when the culture was confluent, the adherent spindle-shaped MSCs were detached with 0.25% trypsin-EDTA, re-plated at 5.5×10^3 cells/cm^2 and passaged every 5-7 days at ~80% confluency. The cells were cultured at 37°C at 21% O_2, 5% CO_2 until passage number 5 (P5) when over 80×10^6 cells were harvested.

5.2.2 Cryopreservation procedure

rMSCs were prepared for freezing following the conventional cryopreservation protocol (154) on days 5 and 6 of the last passage (P5). Cell freezing was carried out in batches to ensure timely processing; 3 batches were frozen on each of the days. Briefly, cells were suspended in the freezing medium consisting of Fetal Bovine Serum (FBS) and 10% DMSO at a density of $1.12\times10^{6}\pm5.42\times10^{4}$ cells/ml. The cell suspension was then transferred to cryogenic tubes (1ml/tube) and the samples were cooled to -80°C at a rate of 1°C/min using a Nalgene 5100 Cryo 1°C freezing container (NALGENE, Thermo Fisher Scientific Inc.). The frozen cells were then transferred to liquid-nitrogen and stored for 7-52 days (mean 28.8±16.2) until used in the experiments.

5.2.3 Cell cytometric analysis

Trypan-blue exclusion test was used throughout the study for rMSC viability assessment (154). Trypan-blue is used routinely as a standard cell membrane integrity assay in research. However, it should be noted that this method is prone to a higher measurement error compared to automated assessment methods as reported by Brinkmann et al. (155). Briefly, after trypsinising cell suspension was neutralised with 5ml of medium containing FBS, centrifuged and the cell pellet resuspended in 1ml of medium. A 20µl volume of cell suspension was stained with equal volume of trypan-blue solution giving 0.2% (w/v) final dye concentration. Total cell (stained plus unstained cells) and dead cell counts (stained membrane-damaged cells) were obtained by visual inspection under an inverted light microscope with the aid of a haemocytometer. In all cases, cytometric assays were performed in triplicate by the

same investigator and cell counts were expressed as a mean (μ) and standard deviation (σ).

5.2.4 Experimental procedure

The overall approach for the experimental investigation was to collect time series data (note: we refer to them as *data vectors*) corresponding to rMSC viability at different levels of temperature elevation. The temperature interval of interest was divided into six discrete levels, namely -20°C, -10°C, 0°C, 10°C, 20°C and 37°C, and separate experiments were carried out for each of the aforementioned temperature elevation conditions. The temperature in the test chamber was monitored continuously using a temperature logger (Omega Engineering Ltd.) and it was observed that the temperature deviation in the chamber did not exceed ±1°C during the experiments. Thaw rate of the specimens was not a controlled condition in this study; however, thawing profiles were recorded in order to determine the rates at which specimens defrosted when subjected to the experimental temperature conditions. This was achieved by placing a thermocouple probe (Omega Engineering Ltd.) into one of the specimen vials from the sample set. This vial was used only for temperature reference and excluded from cytometric assessment due to the intervention. It was observed that the specimens thawed at a rate of 8.4±3.2°C/min when subjected to the experimental conditions.

As described in Section 5.2.2 cells were cryopreserved in 6 batches (also referred to as *sample sets*) and 1 sample set was used in each of the experiments. The sample sets originated from the same starting material and were cryopreserved at the same cell cycle state. However, as cells were frozen in independent batches some variation in the base-line viability was inevitable and unavoidable. At the start of the

experiment, a single randomly selected vial from a sample set unaffected by the experimental condition was assessed as detailed in Section 5.2.3 in order to establish a base-line cell viability of the given sample set. The sample set was only accepted to undergo further experimental study if the base-line cell viability was determined to be 80% or higher.

Over the course of the experiment, a single rMSC sample was taken per time point for the assessment to establish the viability level at a given time. The rate of sampling was 1/2-1 samples/hour when rMSCs were subjected to -20°C, -10°C, 0°C and 10°C conditions and 2-4 samples/hour when rMSCs were subjected to 20°C and 37°C conditions. The sampling rate was differentiated due to the observed trend of lower rMSC metabolic responses at lower temperatures. In order to facilitate homogenous mixing of samples at lower temperatures where ice was present in the solution, vials were dipped into a 37°C water bath for several seconds prior to the assessment.

5.2.5 Modelling approach

For the purpose of modelling rMSC membrane integrity in response to temperature elevation, we proposed a parametric regression model composed of two exponentials (Equation 5.1), according to the trends exhibited by the experimental data set.

$$\hat{z}(x, y) = z_0 e^{(-\alpha x)e^{(\beta y)}} \qquad (5.1)$$

where $\hat{z}$ is an estimate of viable cell percentage, x and y are time and temperature variables respectively, z_0 is base-line cell viability, α and β are model parameters. A strong trend resembling an exponential decay along the time axis was observed in

the experimental data towards the higher temperatures. Similarly, the dependency along the temperature axis appeared to have a trend corresponding to exponential. An exponential model was also convenient because it offers a direct physical interpretation of the associated parameters. Specifically, the two model parameters α and β define the decay rate of the regression along the time and temperature axes respectively. In order to estimate the model parameters and assess the generalisation properties of the proposed model, we applied a method of *cross-validation* (143) by repeated random sub-sampling. Specifically, the experimental data points ($N=59$) were randomly split into two groups; first group G_1 ($n=39$) points was used to determine regression model parameters by nonlinear least-squares method and the second group G_2 ($n=20$) to determine prediction ability of the model i.e. model validation[2]. We performed 10^4 iteration cycles of G_1 and G_2 re-sampling of the experimental data and used each of the subsets for model fitting and validation respectively[3].

The variance in base-line cell viability between sample sets (see Section 5.2.4 for details) used in experiments was accounted for by the use of normalisation factors $n_1, n_2, \ldots, n_k$; thereby, all experimental time series were normalised to a uniform base-line level. This data normalisation step was considered necessary in order to eliminate the bias towards the model due to associated base-line variance in the original observations.

[2] The optimal split of data for cross-validation depends on two competing factors; the larger the training set the better the parameter estimates while the larger the validation set the better the estimate of the generalisation properties of the model. In (143) the difficulty of assessing an optimal split is discussed and a matched split is recommended. In our current case it was felt that 39:20 (i.e. 2:1 of the data) provided a good trade-off.

[3] In (143) it is recommended that the number of sub-sampling iterations should be as high as possible. In our current case it was felt that 10^4 iterations were sufficient for rigorous cross-validation.

Since we want to be robust to measurement error associated with the experimental data, we applied the following criteria for model parameter estimation:

$$r' = \begin{cases} r, & r < 1.96\sigma_r \\ 1.96\sigma_r, & r \geq 1.96\sigma_r \end{cases} \qquad (5.2)$$

where r denotes residual between the observation and the estimate and r' denotes the weighted residual. This last step reduces the weight of residuals which are outside the 95% confidence interval assuming independent and identically distributed (i.i.d) additive noise.

5.3 Results

5.3.1 Model optimisation

The composition of the data set acquired during the experimental investigation is detailed in Table 5.1. The dataset contains 6 vectors of time series data points at different levels of temperature elevation, 59 data points in total. We used the following annotations for the data set:

$$S = \{s_1, \dots, s_6\} = \{Z_1, \dots, Z_{59}\} \qquad (5.3)$$

where S denotes the data set, s_k is a vector of time series observations and Z_i denotes the raw data points which constitute these vectors.

Table 5.1: Composition of the data set

Data vector index (*k*)	Set temperature, °C	# data points in the vector	Total data points (*N*)
1	-20	10	59
2	-10	7	
3	0	10	
4	10	7	
5	20	10	
6	37	15	

A 3-D representation of the data set in the bounded model space is shown in Figure 5.1.

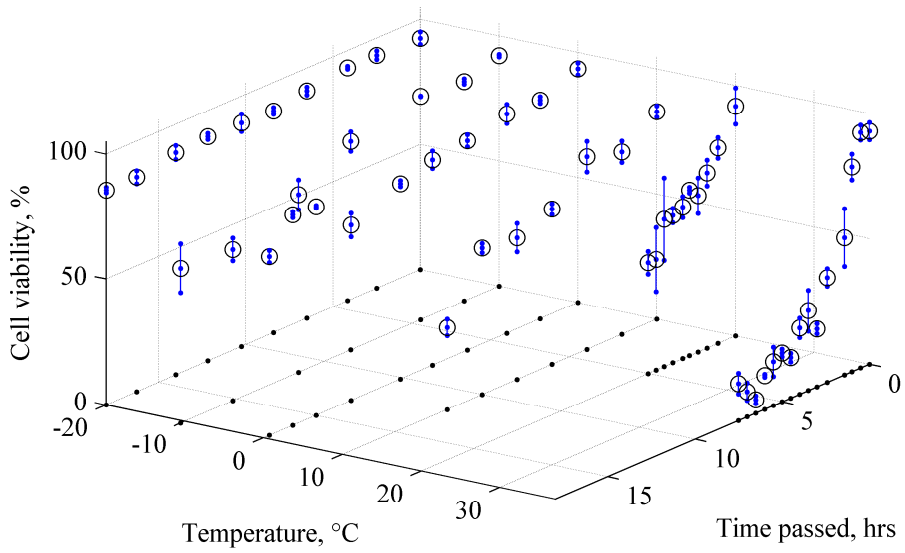

Figure 5.1: Experimental data set of rMSC viability observations (mean and standard deviation) and their projections to the X-Y plane.

Applying the proposed regression model (Equation 5.1) and assuming the presence of i.i.d additive noise, the experimental observations can be expressed as:

$$Z_i(x,y) = z_0 e^{(-\alpha x)e^{(\beta y)}} + \varepsilon(x,y) \qquad (5.4)$$

where $\varepsilon(x,y)$ is i.i.d additive noise.

Each of the six experimental time series was normalised individually (the need for normalisation is discussed in Section 5.2.5) to give a percentage baseline viability as:

$$S' = \{n_1 s_1, \dots, n_6 s_6\} \qquad (5.5)$$

where S' denotes a normalised data set and $n_1, \dots, n_6$ are the normalisation factors. A simple approach to normalisation relying on a single data point (the first data point from each of the data point vectors) proved to be inaccurate as it is susceptible to the measurement noise at a single point. Two alternative approaches are therefore proposed:

i. Two stage approach in which data normalisation factors and model parameters were estimated separately:

$$\psi(n_1, \dots, n_6, \alpha, \beta) = \varphi(n_1, \dots, n_6)\zeta(\alpha, \beta \backslash n_1, \dots, n_6) \qquad (5.6)$$

where ψ is the distribution of parameters, φ is the marginal distribution of normalisation factors and ζ is the conditional distribution of model parameters. In this case, the data vectors are first fitted with a 1-D exponential regression model given by Equation 5.7:

$$f_k(x) = n_k e^{-\alpha_k x}, k = 1, \dots, 6 \qquad (5.7)$$

where k is data vector index and α_k are nuisance parameters. The intercept of this function (n_k) is then used as a normalisation factor; the parameters α and β are optimised given these normalisation factors.

ii. One stage approach in which data normalisation factors and model parameters were estimated jointly. In this approach, the normalisation factors are considered unknown and fed into the model optimisation algorithm as an additional set of parameters. The optimisation is then performed given:

$$\phi(n_1, \dots, n_6, \alpha, \beta) \qquad (5.8)$$

where ϕ is the distribution of model parameters.

By applying the aforementioned normalisation approaches, the base-line cell viability was normalised to 100%, thus, z_0=100. Repeated random sub-sampling validation of 10^4 iterations was then carried out first by using the two stage approach producing Model 1, and then the one stage approach which produced Model 2. The splits of data used for model training and validation are summarised in Table 5.2. Optimisation of model parameters from the training sets was achieved by employing the Nelder-Mead (156) algorithm[4].

Table 5.2: Composition of data sets used for the repeated random sub-sampling validation

Full data set (*N*)	G_1 (training)	G_2 (validation)
59	39	20

[4] Specifically the fminsearch function in Matlab was used.

Figure 5.2 shows the distribution of residuals after cross-validation for the two alternative models. The data appears to be drawn from a bimodal distribution - most

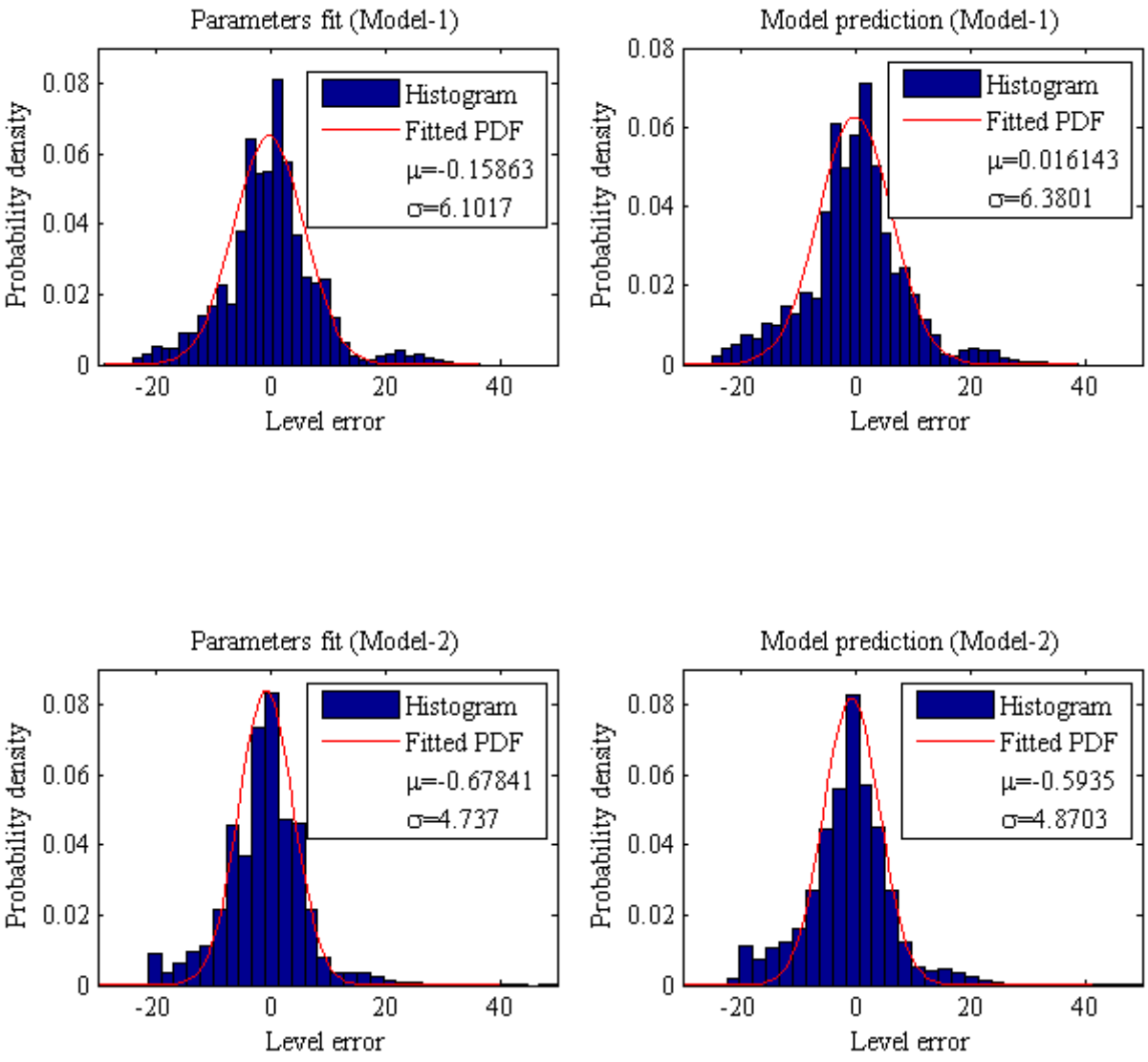

Figure 5.2: Distributions of model residuals after cross-validation

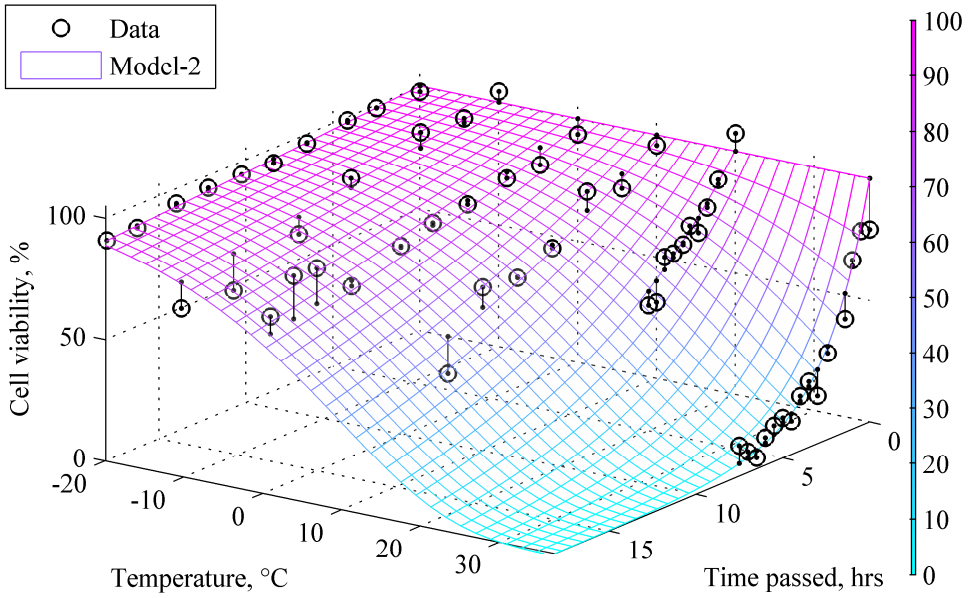

Figure 5.3: Optimised rMSC viability response model.

of the residuals are distributed approximately normal (outlined by the fitted PDF). However, an additional mode appears on the tails of this distribution. Larger sample sets are needed to conclusively determine if this is a genuinely different mode in the distribution or the effect of experimental error. In the current investigation, we applied robust techniques as described in Section 5.2.5 to counter the effect of this additional mode. In comparing the residual PDFs of two models shown in Figure 5.2, it is seen empirically that Model 2 with σ_{G1}=4.737 and σ_{G2}=4.8703 has an advantage over Model 1 with σ_{G1}=6.1017 and σ_{G2}=6.3801; thus Model 2 provides a better fit to the experimental data. A 3-D representation of the Model 2 with the original experimental data set is shown in Figure 5.3 and model parameters are summarized in Table 5.3.

Table 5.3: Summary of time series normalisation factors, model parameter estimates and residual PDF statistics.

Result	Model 1		Model 2	
Data vector normalisation factors				
n1	93.7319		94.6197	
n2	94.7962		88.3014	
n3	90.5658		99.8832	
n4	85.6014		86.7521	
n5	89.9558		85.5891	
n6	101.2587		117.6702	
Model parameter estimates				
α^{*}	0.02406		0.02508	
β^{**}	0.0745		0.0747	
Residual PDF statistics				
	Parameter fit	Model prediction	Parameter fit	Model prediction
μ	-0.15863	0.016143	-0.67841	-0.5935
σ	6.1017	6.3801	4.737	4.8703
MSE	67.0283	77.0139	50.4869	59.7366

* parameter value given is associated with the time variable expressed in hours

** parameter value given is associated with the temperature variable expressed in °C

5.3.2 Practical application of the model

The model presented here could be used to predict the damage suffered by a specimen due to exposure to elevated temperature for a certain amount of time. The expected viability can be calculated directly from Equation 5.9 by substituting time (t) and temperature (T) variables with their corresponding values, provided that t≤18 hours and -20°C≤T≤37°C:

$$\upsilon = 100e^{(-0.02508t)e^{(0.0747T)}} \qquad (5.9)$$

where υ is the predicted specimen viability expressed in %.

Alternatively, the expected specimen viability can be determined graphically from Figure 5.4 by selecting a corresponding temperature curve and finding an intercept with a projected time value on the *x* axis. The projection of an intercept onto y axis will represent a predicted percentage of viable cells in the specimen.

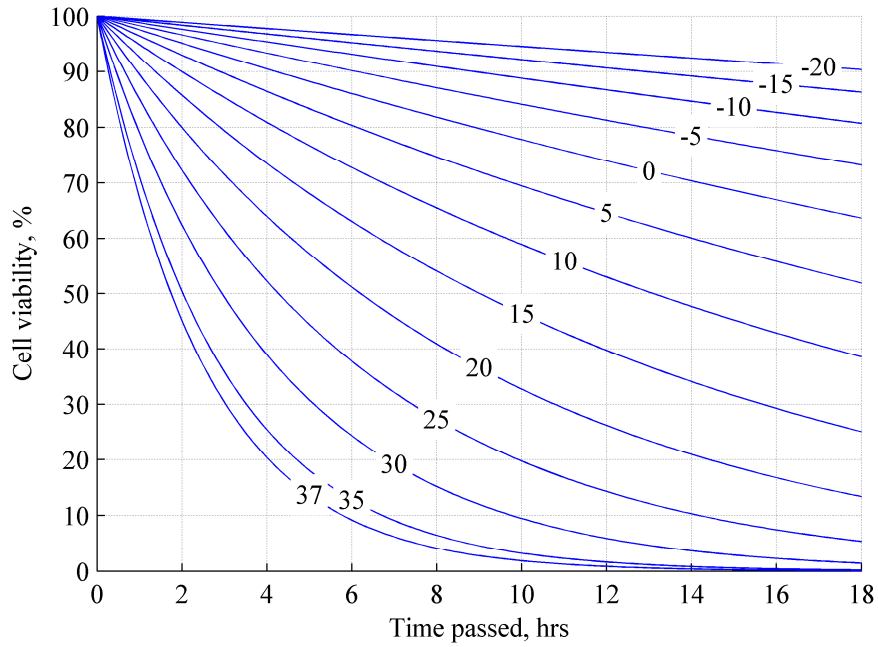

Figure 5.4: Cross-sectional representation of the rMSC viability model. Each section is drawn at fixed temperature (°C) and their corresponding values are labeled individually.

5.4 Discussion

This study investigated the effect of temperature elevation on the viability of cryopreserved rMSCs and has demonstrated that post-thaw viability can be significantly impaired due to this effect. Deterioration was slowest at -20°C, progressing rapidly as the temperatures approached 37°C. The observed effect of rapid degradation of cell viability in the region close to physiological temperatures is thought to be primarily a consequence of prolonged cell exposure to the cryopreservative solution containing DMSO. The toxicity of DMSO to cryobiology has been widely discussed. Arakawa et al. proposed a hypotheses that certain cryoprotectants (including DMSO) may interact hydrophobically with proteins and thus act as protein destabilisers or denaturants (107).

Based on the information gained from the experimental study, we were able to develop a parametric approximating model which relates the effect of temperature elevation with the survivability of cryopreserved rMSCs. Two approaches for the model parameter optimisation have been proposed which performed similarly, however one stage approach (here presented as Model 2) was considered a better realisation for the model parameter estimation. The optimal set of model parameters was identified and its statistical inference was validated employing cross-validation.

The primary benefit of this model is that it facilitates an estimation of rMSC membrane integrity response to the elevation of temperature and the consequent prolonged exposure to cryopreservative solution at high temperatures.

It is important to acknowledge several limitations associated with the proposed model. Firstly, the model was developed based on the observations obtained by the dye (specifically trypan-blue) exclusion test which, despite being a routine practice, is susceptible to higher measurement variance comparing to modern automated assays (155). It should also be noted that dye exclusion tests rely on cell membrane integrity as a sole indicator of cell viability. Other properties defining stem cell viability are measured by the capacity to proliferate and differentiate, thus function may be compromised even if the membrane, at least transitionally, remains intact. Secondly, alterations to the cryopreservation protocol, for example different solution compositions and freezing rates, will affect a number of variables including the phase diagram of the freezing solution, toxicity effects, water transport dynamics, likelihood of IIF etc. Furthermore, the thawing rate of cryopreserved cells may have a profound effect on post-preservation survival. Specifically, slow thawing contributes towards the secondary effect of IIF by allowing recrystallisation and

coalesce of intracellular ice, provided that there is IIF during freezing (82, 157). While in the present study the thawing rate was not a controlled parameter, it has been measured that specimens thawed at a rate of 8.4±3.2°C/min.

5.5 References

82. Gao D, Critser JK. Mechanisms of cryoinjury in living cells. ILAR. 2000;41(4):187-96.

107. Arakawa T, Carpenter JF, Kita YA, Crowe JH. The basis for toxicity of certain cryoprotectants: A hypothesis. Cryobiology. 1990;27(4):401-15.

143. Picard RR, Cook RD. Cross-Validation of Regression Models. Journal of the American Statistical Association. 1984;79:575-83.

153. Mylotte LA, Duffy AM, Murphy M, O'Brien T, Samali A, Barry F, et al. Metabolic flexibility permits mesenchymal stem cell survival in an ischemic environment. Stem Cells. 2008;26(5).

154. Freshney RI. Culture of animal cells: a manual of basic technique. 5 ed: Wiley; 2005. 672 p.

155. Brinkmann M, Lütkemeyer D, Gudermann F, Lehmann J. New technologies for automated cell counting based on optical image analysis 'The Cellscreen'. Cytotechnology. 2002;38:119-27.

156. Nelder JA, Mead R. A simplex-method for function minimization. Computer Journal. 1965;7(4):308-13.

157. Pegg DE. Principles of cryopreservation. In: Day JG, Stacey GN, editors. Cryopreservation and freeze-drying protocols. Totowa, NJ: Humana Press; 2007. p. 39-57.

Chapter 6 Application of Active Learning and Gaussian Process in Post-Cryopreservation Cell Membrane Integrity Experiments

6.1 Introduction

In this chapter we present a computer-intensive approach developed to assist in effective data sampling of severe temperature elevation (ranging from -40°C to 20°C) over a short term event (48 hours) on the post-cryopreservation viability of MSCs derived from human bone marrow (hMSC). In the previous study we selected a smooth parametric model consisting of two exponentials to approximate the process. While traditional parametric models have an advantage in ease of interpretability, for complex data sets simple parametric models may lack expressive power. Another consideration that emerged from the previous study was the limitation due to the data set size. Increasing the data set size substantially was not possible due to cost (monetary and time) concerns. In the previous study we used a simple approach by sampling at arbitrary selected locations ensuring that they were well distributed across the model space.

The new approach proposed in the current study utilises *active learning* methodology in combination with a *Gaussian process* data model to give the maximum return of information regarding the underlying process from the available sample set (158-161). Similarly to the previous study, we tailored our active learning algorithm to work with a *time series* data sampling strategy, as it is convenient for the proposed experiments. The algorithm iteratively uses the available data to inform on the *next best* sampling locations in a bounded temperature and time space as chosen for the investigation. We demonstrate the performance of this algorithm in this new application and develop a model of post-cryopreservation hMSC membrane integrity response to aforementioned temperature conditions.

6.2 Materials and methods

6.2.1 Experimental design

MSCs cryopreserved in 80 individual vials were dedicated for this investigation. Over a set of experiments, these vials with cells were exposed to various fixed level of temperatures (ranging from −40°C to 20°C) for the duration of the experiment using a controlled temperature chamber, and the cell membrane integrity response was observed over time. Henceforth, these time series observations will be referred to as *data vectors*, denoted S. A *data vector* contains counts of cells with an intact membrane (expressed in percentage) at a fixed temperature and k = 10 time points distributed along a 48 hour experiment time interval, i.e. $S = \{y_1; y_2; \dots; y_k\}$ where y_k denotes an observation at a particular time point. The available sample set enabled l = 8 such experiments to be completed. Table 6.1 summarises the composition of the data set which was to be collected in this work.

Table 6.1: Composition of the dataset

# of S, (l)	# of y in S_l, (k)	All observations, $y\{l,k\}$
8	10	80

An active learning method as outlined in Section 6.3, was employed for the selection of sampling locations (i.e. both the starting temperature and the set of times, S) with the aim of maximising the information return about the process from a limited size sample set. This was achieved through an iterative process as follows:

i. Three experiments were carried out with temperature levels set to −40°C, −20°C and 0°C (these values are subjectively thought to be interesting points); the corresponding vectors of observations (S_1, S_2 and S_3) composed the primary data set. The time intervals in (S_1, S_2 and S_3) were equally spaced along the 48 hour time interval.

ii. The data was processed by an active learning algorithm and the next vector of sampling points (with the highest expected return) was identified.

iii. A new experiment was then carried out sampling cell integrity at the locations identified and the data set was updated with a new vector of observations. The process was then repeated from step (ii).

6.2.2 Cell source

Bone marrow aspirates were obtained as described previously (162) from the iliac crest of normal donors. All procedures were performed with informed consent and approved by the Clinical Research Ethical Committee at University College Hospital, Galway. Donors selection criteria followed ethically approved guidelines: healthy males and non-pregnant females between the ages of 18 and 45 years old, tested negative for HIV, hepatitis B and hepatitis C. MSCs were isolated and expanded in culture as described previously by direct plating (55). Briefly, aspirates were washed with medium (DMEM-low glucose containing penicillin-streptomycin solution (both manufactured by Sigma-Aldrich, Ireland) at 100 U penicillin-G and 0.1 mg streptomycin/ml) and centrifuged. The precipitated cells were suspended in medium with 10% selected foetal bovine serum and plated at a final density of approximately 3.0×10^5 cells/cm^2. Serum was selected based on maintenance of MSC proliferation and multipotency in culture. Cells were seeded on T-175 flasks

(manufactured by Sarstedt, Ireland) and maintained at 37°C with 95% humidity and 5% CO^2 in the same medium. After 5 days, red blood cells were washed off with phosphate-buffered saline and fresh medium added. Colonies of adherent cells formed within 9 days. At the end of primary culture, adherent colonies were detached by treatment with 0.25% trypsin and 0.53 mm EDTA (manufactured by Sigma-Aldrich, Ireland). Cells were plated in hMSC medium (DMEM-LG; 10% FBS; 1% antibiotic) at 5.7×10^3 cells/cm^2. All MSC preparations were characterised for surface expression of CD14, CD34, CD45, CD73 (assay supplied by BD Pharmingen, UK) and CD105 (assay supplied by Serotec, UK) using a FACs ARIA sorter (manufactured by Becton Dickinson, UK). FACS analysis indicated the presence of a uniform population of cells negative for CD14, CD34, CD45 (<2%) and positive for CD73 and CD105 (>95%) (24). Cell multipotency was confirmed through adipogenic, osteogenic and chondrogenic assays. Cultures were passaged at 4-6 day intervals and expanded to passage 4 for experimentation.

6.2.3 Cryopreservation procedure

The cells were prepared for freezing following the conventional cryopreservation protocol with 10% DMSO and controlled rate freezing (163). Briefly, the freezing medium consisted of foetal bovine serum and 10% DMSO (v/v). Cell counts were obtained with the help of a heamocytometer and the cell density was adjusted to meet the target density of 1×10^6 cells/ml with freezing medium. The prepared cell suspension was then transferred to pre-labelled cryogenic tubes (0.5 ml/tube) and the samples were cooled at a controlled rate by transferring them to a cryogenic 1°C/min cooler (manufactured by NALGENE, Thermo Fisher Scientific, USA). The samples

were then transferred to a liquid-nitrogen container and stored in vapour phase until the day of experiment.

6.2.4 Thawing procedure

In the cases where cell suspension were solidified (this was observed at temperatures of -20°C and below) prior to the assessment, the samples were thawed in a 37°C water bath, gently agitating the vial until the suspension was mostly free of ice crystals. In all cases, the cells were resuspended in pre-warmed medium, pelleted by centrifugation and then resuspended in fresh media for membrane integrity assays.

6.2.5 Cytometric assay

Classical manual cell counting was used throughout the investigation using a heamacytometer and an inverted light microscope (manufactured by Olympus) at 10^3 magnification. Trypan-blue exclusion test was used throughout the study for MSC viability assessment (164). Briefly, cell suspension was stained with an equal volume of trypan-blue solution giving 0.2% (w/v) final dye concentration. The counting chamber of heamacytometer was filled with 10µl of stained cell suspension and counts of total cells (C_t) and stained cells (membrane-damaged necrotic cells which appear stained) (C_s) per multiples 0.1µl were obtained. The percentage of cells with an intact membrane was calculated according to the following formula:

$$p = (C_t D_t - C_s D_s)/C_t D_t \times 100 \qquad (6.1)$$

where p is the percentage of cells intact, D_t and D_s denote dilution factors for total and stained cell counts respectively. In all cases cytometric assays were performed in quadruplicate by the same investigator.

6.3 Active learning

Active learning is a recursive procedure in which an estimate of a process, based on current data, is used to inform on the best point to sample the function at next. The process is then sampled at that point and the process estimate is updated and so on recursively. Active learning is appropriate when the number of samples that can be taken is limited due to time or cost or, as in this case, both. Thus, it is important to maximise the information gained from each sample. Examples of active learning with GP may be found in (165-167). Active learning is implemented in several stages, each of which must be tailored to a particular application:

i. A model for the data which also specifies the confidence of the model; in this case we employ a 2-D hierarchical Gaussian Process model for regression (i.e. noisy measurements) as explained in Section 6.3.1,
ii. A function which takes the mean and variance estimates and converts these into a value representing the expected return if we were to sample at that point. This is known as the infill function (see Section 6.3.2). In this case the expected return is the improvement of the estimate of the entire function (aside: see (158) for an infill function which seeks instead a function minimum), and
iii. The maximum value of the infill function is estimated and used to select the location of the next sample. The infill function in this case is a bounded continuous 2-D function. The maximum of this function is found using the DIRECT algorithm (see Section 6.3.2).

6.3.1 Data model

The data model used is a 2-D *Gaussian Process* (GP) (159). A GP is defined as a process in which realisations from the process are jointly multivariate Normally distributed. It is a generalisation of a Gaussian probability distribution. A GP places a Gaussian prior on the space of functions and is fully specified by a mean function and a covariance function. Conveniently, the use of the finite number of points with a GP results in the same properties about the function at these finite number of points to those which might be observed if the entire function had been examined (168). Specifically, the data generated by the process at n sample points, $Y_{x_{1:n}}$ can be considered as drawn from a multivariate Gaussian distribution as:

$$Y_{x_{1:n}} \sim \mathcal{N}[\mu_x, C_{X,X}] \qquad (6.2)$$

where $\mathcal{N}$ denotes a Gaussian distribution, $x_{1:n}$, denotes n samples taken at points $x_1 \ldots x_n$, $\mu_x \in \Re^2$ is the mean of the process and $C_{X,X}$ is the covariance matrix. The covariance matrix depends on the separation of the data points and so is often referred to as covariance function.

In this paper, an isotropic covariance matrix is used, which assumes that the variation of the function is equal in all directions. However, before we can make that assumption, the data must be normalised prior to modelling. Given that the active region of interest for the function (i.e. [0,48] hours for time and [-40,20] °C for temperature) is known in advance, the data are normalised by mapping them into [0,1]×[0,1] prior to modelling. While this procedure is sub-optimal, it does reduce the number of parameters to be estimated by one by assuming that the diagonal elements of $C_{X,X}$ all have the same value. Given an isotropic covariance function it

now becomes more convenient to talk in terms of the correlation function which is related to the covariance function via[5]:

$$C_{X,X} = \sigma_x^2 R_{X,X} \qquad (6.3)$$

as σ_x^2, is the variance of the process and $R_{X,X} \in \Re^{n \times n}$ is the correlation function. The correlation function is defined by a kernel with the following properties:

$$R_{x,x} = R(0) = 1 \qquad (6.4)$$

the correlation function at a distance of zero (i.e. between a point x and itself) is one,

$$R_{x1,x2} = R(\| x_1 - x_2 \|) \qquad (6.5)$$

the correlation function is only a function of the separation of the sample points, where $\|\circ\|$ denotes Euclidean distance, and

$$R(h_1) < R(h_2) \text{ for } h_1 > h_2 > 0 \qquad (6.6)$$

the correlation function dies away as the distance increases; where h denotes a distance. This last condition is necessary in order for single function paths (i.e. a collection of samples taken from the GP) to be used for inference (159). A valid kernel function may be derived from any symmetric probability density function (pdf) (see (159) for details); in this application the Matern Kernel, derived from the t-distribution is used (see Figure 6.1) as it is a popular choice. The Matern kernel is defined as:

[5] Here is assumed that the overall process mean is zero; alternatively a non-zero mean may be subtracted from the data prior to modelling.

$$R(h,\theta,\nu) = \frac{1}{\Gamma(\nu)2^{\nu-1}}\left(\frac{2\sqrt{\nu}|h|}{\theta}\right)^{\nu} K_{\nu}\left(\frac{2\sqrt{\nu}|h|}{\theta}\right) \quad (6.7)$$

where K_{ν} is the modified Bessel function, θ and ν are parameters of the kernel with θ controlling the scale and ν the shape of the kernel.

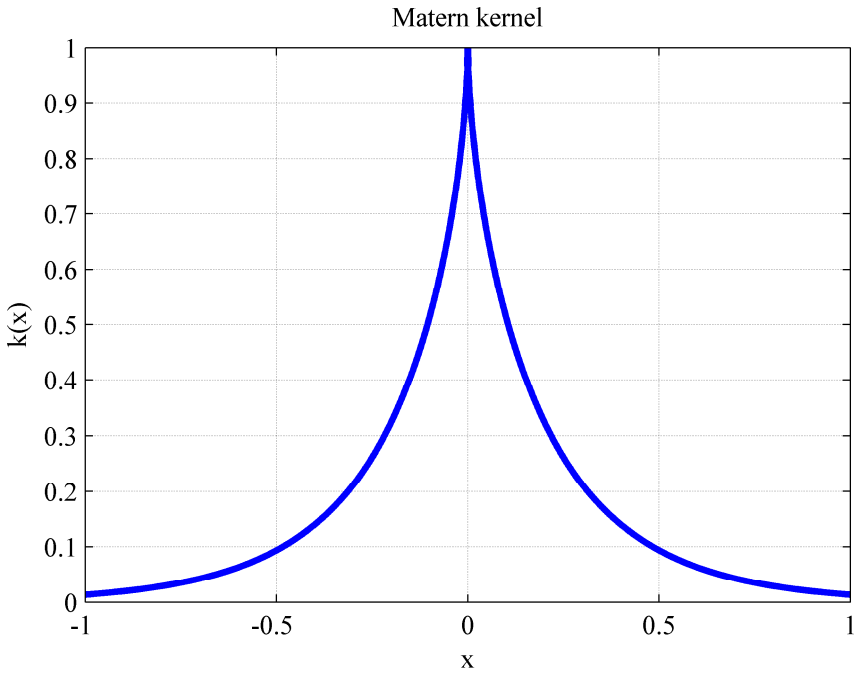

Figure 6.1: Matern kernel derived from the *t*-distribution with prior parameters θ= 0.3 and υ= 0.3.

Now, given a set of points at which samples have already been taken, $x_{1:n}$, and a set of locations (called evaluation points), x^*, at which we have not sampled, the relationship between the sampled and evaluation points may be expressed by partitioning Equation 6.2 in terms of the cross and auto-correlation matrices of the sampled and evaluation points as (159):

$$\begin{bmatrix} Y_{x_{1:n}} \\ Y_{x^*} \end{bmatrix} \sim \mathcal{N}\left[\begin{bmatrix} 1_n \\ 1_* \end{bmatrix}\mu_x, \sigma_x^2 \begin{bmatrix} R_{X,X} & R_{X,x^*} \\ R_{X,x^*}^T & R_{x^*,x^*} \end{bmatrix}\right] \quad (6.8)$$

where Y_{x^*} is the value of the process at x^*, 1_n and 1_* are appropriately dimensioned vectors of ones, $R_{X,X}$ is the auto-correlation between the known sample points, R_{X,x^*} is the cross-correlation between the sample and evaluation points and R_{x^*,x^*} is the auto-correlation of the evaluation points, ~ is used to denote *drawn from* and $\mathcal{N}$ denotes a Gaussian distribution.

The unknown parameters in the GP defined by Equation 6.8 are the process mean, the process variance and the shape parameters for the kernel; $\{\mu_x, \sigma_x^2, \theta, \nu\}$. These may be estimated iteratively using Bayesian congugate analysis and a hierarchical GP in which the parameters are organised in a hierarchy as:

$$[\mu_x, \sigma_x^2, \theta, \nu] = [\mu_x|\sigma_x^2] \times [\sigma_x^2] \times [\theta, \nu] \qquad (6.9)$$

where $[\circ]$ denotes distribution. It is thus assumed that the kernel parameters ν and θ (also referred to as *hyperparameters* for the GP model) are independent of the process mean and variance and may be estimated first followed by the next stage in the hierarchy; estimating the variance and then the process mean (conditional on the variance). Finally, estimates of the function at particular sample points may be made given the hyperparameters. Each stage is now explained further.

Given the current data points the kernel parameters are estimated by maximising the log likelihood function with respect to $[\theta, \nu]$. This function also known as the log marginal likelihood may be expressed as (168):

$$\log p(Y_{x_{1:n}}|x_{1:n}, \theta, \nu) = -\frac{1}{2} Z_{x_{1:n}}^T C^{*-1} Z_{x_{1:n}} - \frac{1}{2}\log|C^*| - \frac{n}{2}\log(2\pi) \qquad (6.10)$$

where $C^* = \sigma_x^2(R_{X,x^*} + \zeta_x)$, is the covariance matrix of the noisy data[6], $Z_{x_{1:n}} = Y_{x_{1:n}} - 1_n\hat{\mu}_x$ and ζ_x is the measurement noise covariance[7].

The process parameters are estimated using a congugate Bayesian approach in which the standard congugate Bayesian prior for a mean and (unknown) variance are used; specifically the mean has a normal prior; $\mu_x \sim \mathcal{N}(0, \sigma_x^2\delta^2)$ and the variance has a normal-inverse-Gamma prior; $\sigma_x \sim \mathrm{I}\mathcal{G}(\frac{a}{2}, \frac{b}{2})$. δ is our initial estimate of the variance of the mean, the variance is initially assumed to lie in the interval $[a, b]$.

An estimate of the function at the evaluation points may be constructed using least squares (see (159) for details). However, in the current application we are interested in estimating the value of Y_{x^*} given that the measurements are noisy. In the presence of measurement noise Equation 6.8 becomes (168):

$$\begin{bmatrix} Y_{x_{1:n}} \\ Y_{x^*} \end{bmatrix} \sim \mathcal{N}\left[\begin{bmatrix} 1_n \\ 1_* \end{bmatrix}\mu_x, \sigma_x^2\begin{bmatrix} R_{X,X} + \zeta_x & R_{X,x^*} \\ R_{X,x^*}^T & R_{x^*x^*} \end{bmatrix}\right] \tag{6.11}$$

and an expected value of the mean function at the evaluation points x^*, conditioned on the data, may be expressed as (168):

$$\hat{Y}_{x^*} = 1_*\hat{\mu}_x + R_{X,x^*}(R_x + \zeta)^{-1}(Y_{x_{1:n}} - 1_n\hat{\mu}_x) \tag{6.12}$$

An estimate of variance at the evaluation points, $\sigma^2(x^*)$, may be estimated via (168):

$$\hat{\sigma}^2(x^*) = \hat{\sigma}_x^2\left(R_{x^*} - R_{X,x^*}^T K R_{X,x^*} + \frac{\left(1 - 1_n^T K R_{X,x^*}\right)^2}{1_n^T K 1_n + \delta^{-2}}\right) \tag{6.13}$$

[6] It is assumed that the noise is heterogenous (169, 170); see Section 6.4.2 for the validation of this assumption.
[7] Unlike the process mean and variance the hyperparameters are point estimates.

where $K = \left(R_{X,X} + \zeta_x\right)^{-1}$ is used to simplify notation. The maximum a-posteriori estimates for the process parameters are (158):

$$\hat{\mu}_x = (1 - K + \delta^{-2})^{-1} 1_n^T K Y_{x_{1:n}} \qquad (6.14)$$

and

$$\hat{\sigma}_x^2 = \frac{\left(b + Y_{x_{1:n}}^T K Y_{x_{1:n}} - \left(1_n^T K 1_n + \delta^{-2}\right)\right)\hat{\mu}_x^2}{n+a+2}. \quad (6.15)$$

6.3.2 Infill function

The role of an infill function is to estimate the *expected return* from sampling at a particular point. In terms of approximating a function there are two commonly used infill functions; the entropy approach proposed by MacKay (171) and the squared error approach suggested by Cohn (172). The squared error approach is preferred here as simulations using the entropy approach tended to concentrate on the boundary of the search space (intuitively, a point in the interior of the search space may have samples to its right and left (in 1-D) and thus will be expected to have a lower variance than points on the boundary. Thus the bias is introduced in the infill function in (171). See (160) for a more in-depth discussion.). The squared error infill function is aimed at picking the next sampling point where the reduction in variance across the whole function is minimized. Specifically:

$$EI\{x^*\} = \sum_{x \in G} \hat{\sigma}^2(x|x^*) - \sum_{x \in G} \hat{\sigma}^2(x) \qquad (6.16)$$

where $\hat{\sigma}^2(x)$ is the current estimate of the variance at point x, $\hat{\sigma}^2(x|x^*)$ is the estimated variance at point x in the function *if a sample was taken at* x^*, G is a grid of points in the range of the function at which the variance reduction is estimated. Note that in order to estimate $\hat{\sigma}^2(x|x^*)$ several samples are drawn from the current distribution around x^*.

At this point a complication is introduced into the algorithm, due to the nature of the experiments. The data consists of a 2-D range for $x \in \Re^2$; the fixed temperature at which the experiment is carried out and the time passed. Defining the fixed temperature as x_1 and the time passed as x_2, an experiment consists of a set of k readings as $\left\{\{x_1, x_2^1\}\{x_1, x_2^2\} \ldots \{x_1, x_2^k\}\right\}$. Thus, a *vector* of readings is made at a fixed temperature as opposed to the typical situation in which a single measurement is made. In addition, the time between the readings is also constrained by the fact that it takes a set (significant) amount of time, τ say, to make the assessment (this value was set to 1 hour to allow sufficient time). Thus the optimum point at which to select the next *sample vector* consists of first selecting the best vector given a fixed temperature, *subject* to the constraint that there must be at least τ minutes between each sample. Then the best temperature point is determined:

$$x_{opt}^* = \underset{x_1}{argmax} \underset{\{x_2^1,\ldots,x_2^k | x_1 : x_2^{i+1} - x_2^i \geq \tau \ \forall i > 1\}}{argmax} EI\{S\} \qquad (6.17)$$

where $S = \left\{\{x_1, x_2^1\}\{x_1, x_2^2\} \ldots \{x_1, x_2^k\}\right\}$ is used for notational purposes. The inner optimisation is calculated using the constrained optimisation function in Matlab. The outer optimisation is a 1-D optimisation problem which consists of determining the

optimum temperature given the best vectors for each. The DIRECT algorithm (173) is used for this purpose.

Figure 6.2 shows an example of this algorithm when tested on a synthetic data set. The algorithm begins by taking some random samples of the function at 6 points. Then 4 rounds of vector samples have already been calculated (i.e. this figure is taken on the 5^{th} iteration). These four vector samples are well distributed across the function and away from the boundaries as expected. The dots represent the optimised vectors at each temperature level. It is satisfying to note how these points avoid those already sampled (thus maximising the returned information) and that the minimum distance between these points is preserved. The infill function is shown on the X-Z plane and reaches a maximum around 0.23. This will be the set temperature for the next vector of samples which will be taken at the times indicated on the X-Y plane.

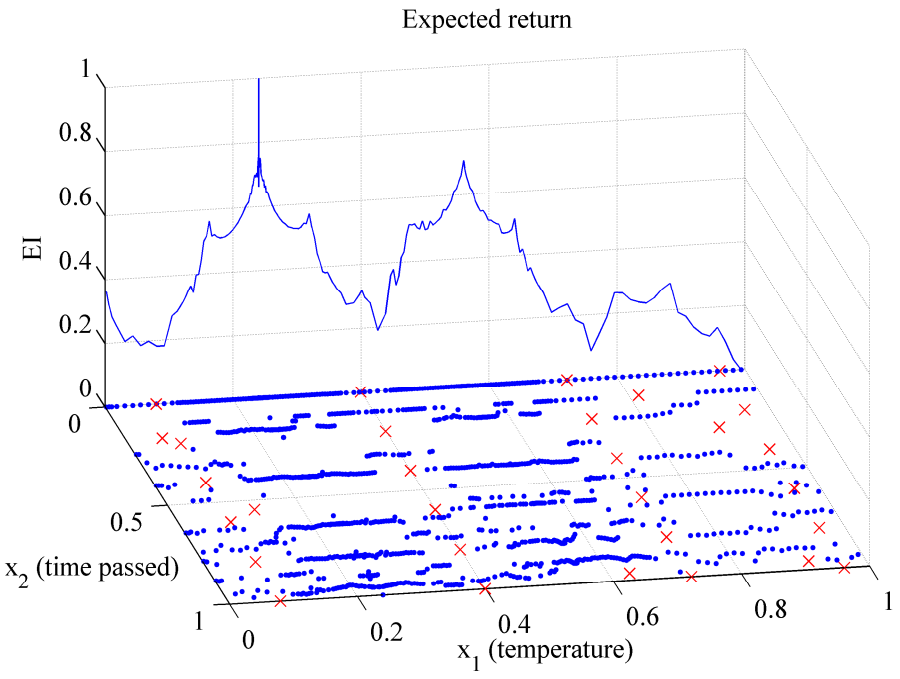

Figure 6.2: The infill function and location points for a synthetic example. The X-Y plane represents the points at which the function has already been sampled (represented by 'x') and those at which the constrained optimisation proposes to sample (represented by '.'). The Y-Z plane shows the expected return if a vector of samples is taken at that temperature level.

6.4 Results

6.4.1 Data sampling with active learning

Using the active learning technique from the last section we have conducted the following experiments: in the first instance, three vector samples (S_1, S_2 and S_3) of the response function were taken at arbitrary selected locations, namely x_1 = -40°C, -20°C and 0°C with time points $\left(x_2^1, \ldots, x_2^k\right)$ distributed evenly along the time axis.

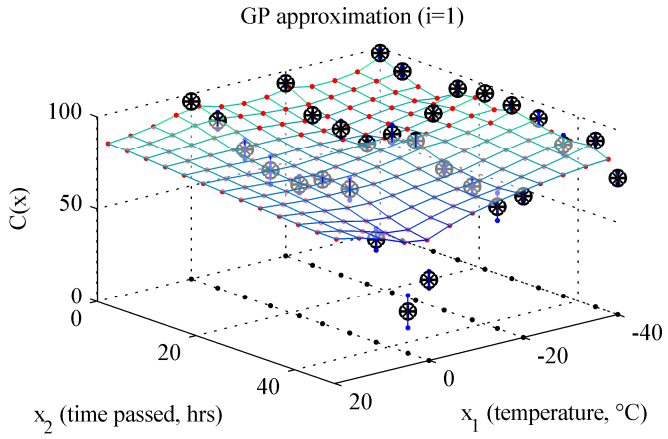

Figure 6.3: Gaussian process model mean estimate based on the initial sample vectors.

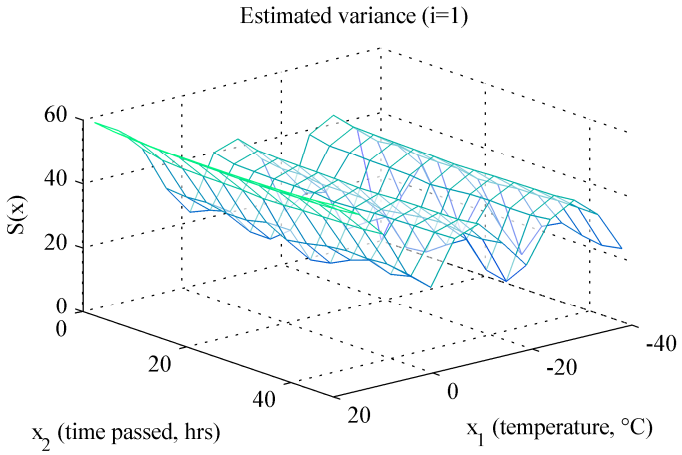

Figure 6.4: An estimate of the Gaussian process variance.

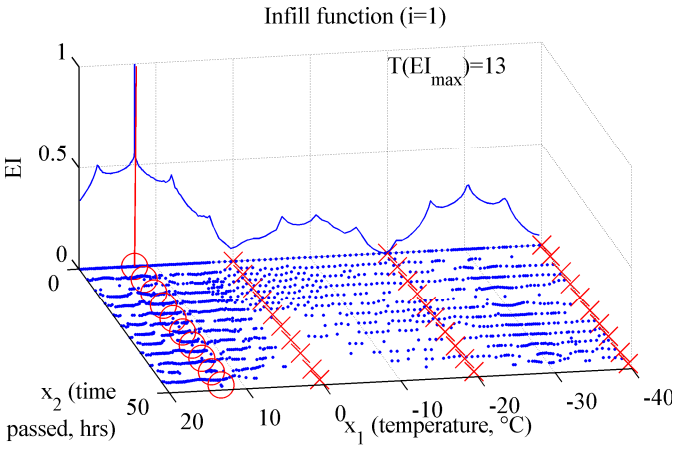

Figure 6.5: The infill function (shown on the X-Z plane) and the location points of the candidate sample vectors (shown as dots on the X-Y plane). The highest peak of the infill function (x^*_{max}) is the optimal sampling location for the next sample vector.

Figure 6.3 shows the Gaussian process model mean estimate based on the current data (3 sample vectors). Figure 6.4 shows the corresponding estimate of process variance. Figure 6.5 shows the infill function on the X-Z plane and the location points of the candidate sample vectors represented by dots on the X-Y plane. The highest peak of the infill function (x^*_{max}) is the optimal sampling location for the next sample vector; these optimal location points are represented by circles on the X-Y plane. In the first iteration (i = 1) the primary data set is used to model the process and calculate the infill function. The infill function peaks at x_1 = 13 (see Figure 6.5) which is in the (so far) least explored area of the search space. Note how the estimated variance is highest on the boundary x_1 = 20 (see Figure 6.4) as it is the most distant point from the current observations and only has them to its one side; nevertheless it is important to note that the algorithm selects a point which is located away from the boundary whereby a reduction of variance across the entire function is achieved rather than only in a localised area of the function.

For the second iteration (i=2), the data set was extended with a new vector of observations (S_4) and used to model the process and calculate a new infill function. This new infill function has two distinct peaks (at x_1=-30 and x_1=-11) which point to the least explored areas of the search space. In this case these peaks correspond to the highest estimated variance locations as they both are located away from the boundaries of the search space. The higher expected return location at x_1 = -30 was sampled first while the other peak location at x_1 = -11 was sampled after the third iteration.

A minimum region of the response function becomes evident from the Gaussian model on the fourth iteration, occurring around x_1=-10; by this stage the data set has

extended to six sample vectors (60 observation points). The new infill function has multiple peaks spread across the search space with the maximum at x_1=3. This peak again does not match the location of the highest estimated variance which appears on the boundary of the search space.

The Gaussian process model mean and variance estimates in the last active learning iteration (i=5) are shown in Figures 6.6 and 6.7 respectively. The new infill function shown in Figure 6.8 has a highest peak at x_1=18; this location is close to the boundary point at x_1=20 which has the highest estimated variance of the function (see Figure 6.7); however, this boundary location is again avoided and a point in the interior of the search space is selected.

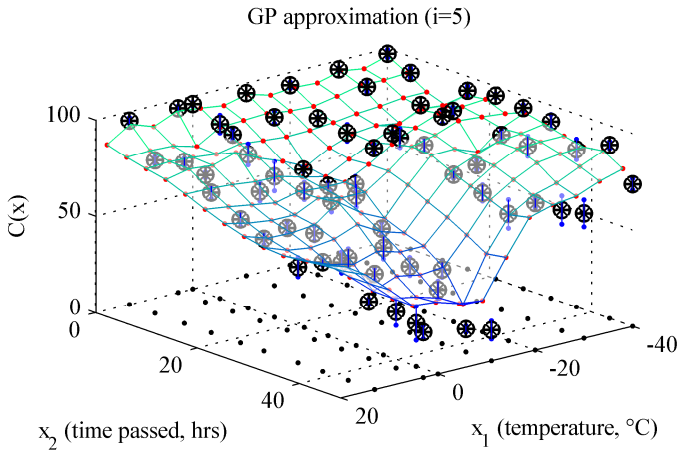

Figure 6.6: Gaussian process model mean estimate in the last active learning iteration (i=5).

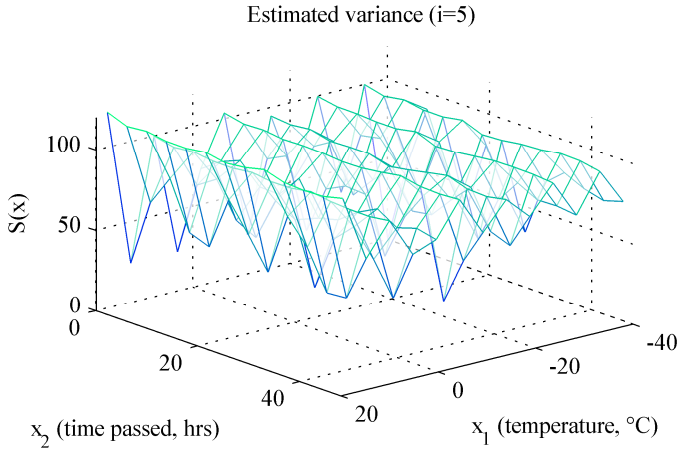

Figure 6.7: An estimate of the Gaussian process variance. Note, that the highest variance is on the boundary at $x_1 = 20$.

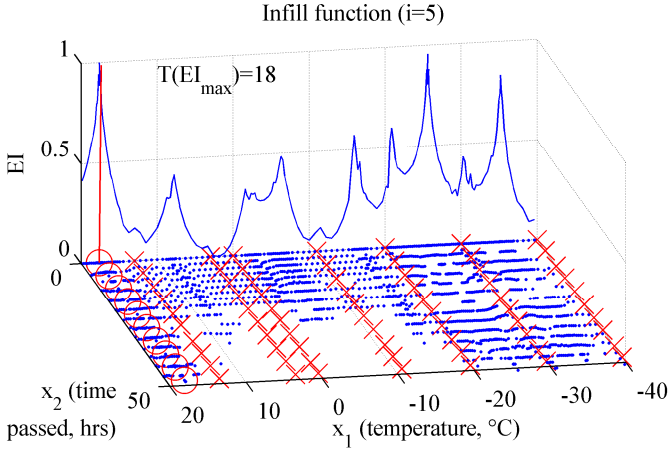

Figure 6.8: The new infill function peaks at $x_1 = 18$ avoiding the boundary of the search space despite the highest variance associated with this location.

6.4.2 Measurement variance

In Section 6.3.1 we made an *a priori* assumption of *heterogeneous* noise (i.e. noise has *uneven* distribution across the sampling space) associated with the observations from the experiments. In order to verify this assumption, we examine the distribution of variance ($\sigma^2(x)$) associated with the test points across the sampling space; the variance is established from n=4 repeated assays of MSC membrane integrity at each of the test locations. Specifically, a simple average is taken of these four measurements and used as an input to the active learning algorithm; the measurement noise variance is estimated using the standard error of the four measurements. Figure 6.9 illustrates an approximate distribution of the observation variance across the sampling space. From the figure it can be seen that the variance has rather uneven distribution across the sampling space; a large area of low variance is seen towards the lower half of (x_1, x_2) while higher variance regions appear towards the higher half of either x_1 or x_2. However, there are some isolated regions which do not fall within this trend, therefore the justification of the overall trend is somewhat ambiguous from the current data set.

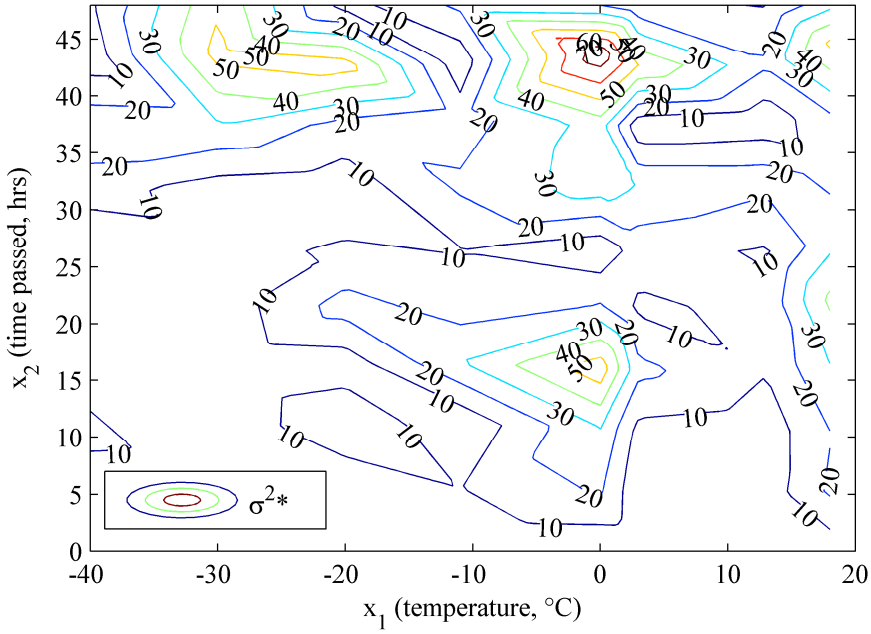

Figure 6.9: Approximate distribution of variance $\sigma^{2*}(x)$, associated with the MSC membrane integrity assays at the test points across the sampling space. This approximation was generated from the linear interpolation between the observed variance values, $\sigma^{*}(x)$, from the repeated measurements n=4 at each of the test locations. The variance appears to be unevenly distributed across the sampling space hence indicating heterogenous nature of associated noise.

The hypothesis of *homogeneity* may be tested via the ANalysis Of VAriance (ANOVA). Specifically *Levene's test* (174) or the *Brown-Forsythe test* (175) for homogeneity. The two tests are very similar except that Levene's test uses the *mean* while Brown-Forsythe test uses the *median*, hence the later is more robust for abnormality of the data.

A null hypothesis for these two tests may be constructed as:

$$H0: \sigma_{x_{1,1}}^2 = \sigma_{x_{1,2}}^2 = \cdots = \sigma_{x_{l,k}}^2 \qquad (6.18)$$

then an alternative hypothesis (for heterogeneity of variance) can be expressed as:

$$H1: \sigma^2_{x_{g,h}} \neq \sigma^2_{x_{i,j}} \qquad (6.19)$$

for at least one pair of $(x_{g,h}; x_{i,j})$.

Table 6.2: Summary of ANOVA statistics

Test	Significance	Power	Result (0-accept, 1-reject)
Levene's	5%	<0.001	1
Brown-Forsythe	5%	0.103	0

It is found by Levene's test that the null hypothesis is violated; the opposite result however is found by Brown-Forsythe test which indicates that the null hypothesis holds. Under further examination of the data it was found that several test points of highest variance had one observation which was an outlier with respect to the other three observations, hence robust Brown-Forsythe test accounted for lower variance on these points. From these tests we conclude that the actual nature of noise remains elusive from the current data set.

6.4.3 The advantage of the active learning strategy

The potential gains made from using active learning are difficult to assess in this experiment; only one set of experiments are possible due to the monetary cost and time involved. However, a Monte Carlo simulation based approach is possible. For a very smooth function a grid may be close to optimal, conversely, for a function with large gradients, active learning should provide a better result. Active learning does

not directly target high variance (here meaning fast changes in the underlying function), rather it aims to reduce uncertainty about the function. The variance in the Gaussian process posterior is an estimate of uncertainty about the function, caused by noise in observations and by lack of samples. In areas of fast change it can be more difficult to tell the difference between noise and real changes, so with limited samples there may be more uncertainty left in such areas, which active learning can then target. That is the potential gains depend on the unknown underlying function. Given the data from the actual experiments an *empirical function* is constructed by means of a thin plate spline[8]. This empirical function is then used as a benchmark to compare the performance of three different schemes. The first is active learning, the second is a uniform grid and the third is random sampling. Homogeneous Gaussian noise is added to the samples using the standard error of the actual samples. 100 runs are produced for the grid and random approaches while 20 runs are used for the active learning approach (due to computational complexity). The metric for comparison is the Sum Squared Deviation (SSD) between the empirical function and the estimates based on a GP using the samples (i.e. collected via grid, random or active learning)[9]. Figure 6.10 shows the distribution of the deviations (over different runs) from all three approaches. The first thing to notice is that the random approach leads to significantly higher deviations and so forms a baseline. Secondly, the active learning and grid approaches both produce similar results. However, the distribution for the grid approach has a much larger right hand side tail due to the presence of a second mode. This occurs as the grid approach tends to react badly to the presence of noise around the -10°C dip in the function. In contrast, the active learning SSD

[8] Specifically the tpaps function in Matlab is used; the choice of model effects the results and so they are only indicative. We did not use a GP to avoid a self-fulfilling prophecy. The regularisation parameter for the thin-plate spline is chosen uniformly at random from [0,0.6] each time a simulation is run to allow for variation in the smoothness of the function.

[9] The SSD is estimated numerically using a very fine grid.

distribution is more concentrated around the mean showing that experiments based on this approach are more consistent in their performance. Finally, the average SSD for active learning is 899 while that for the grid is 920 and so active learning can be expected to give a better result.

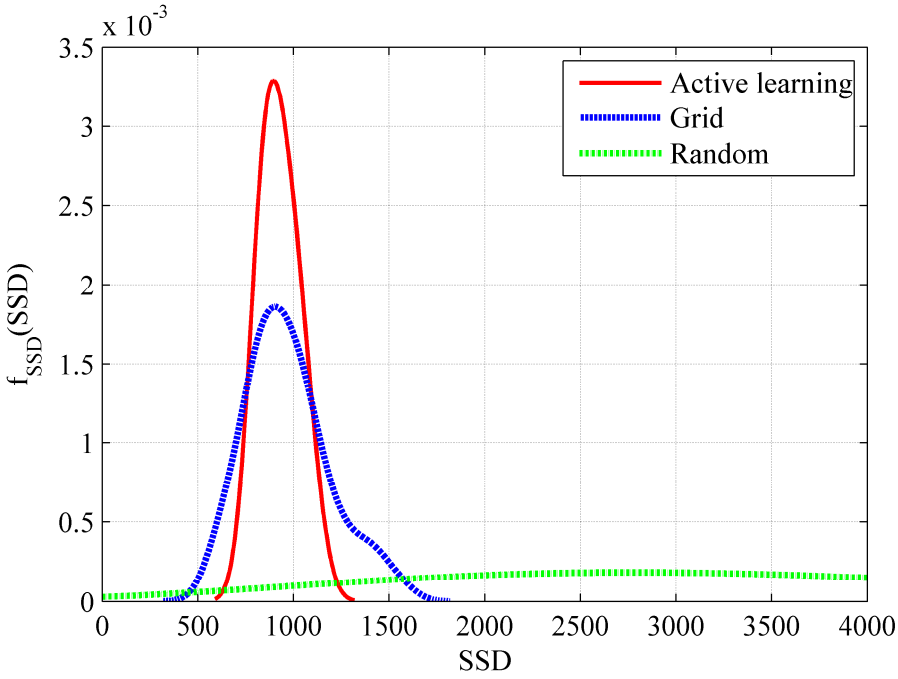

Figure 6.10: The distribution of the deviations from the active learning, equally spaced grid and random sampling approaches obtained from the Monte Carlo simulations.

6.5 Discussion of results

The Gaussian approximation of the response function from the complete data set $S_1, \ldots, S_8$ is represented in Figures 6.11 and 6.12. From this approximation (clearly seen in the cross-sectional plot of the response model mean represented in Figure 6.13) it is evident that the fastest response of MSC integrity decay occurs in the

temperature region around -10°C, while it is much slower towards either of the boundaries of the investigated temperature range.

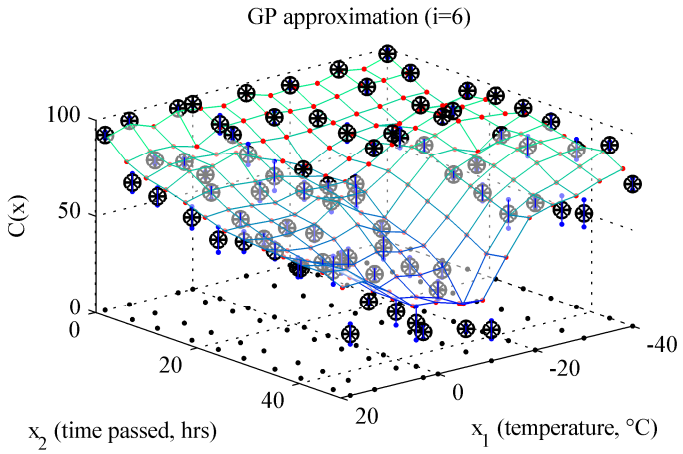

Figure 6.11: Gaussian process model mean estimate based on the complete data set.

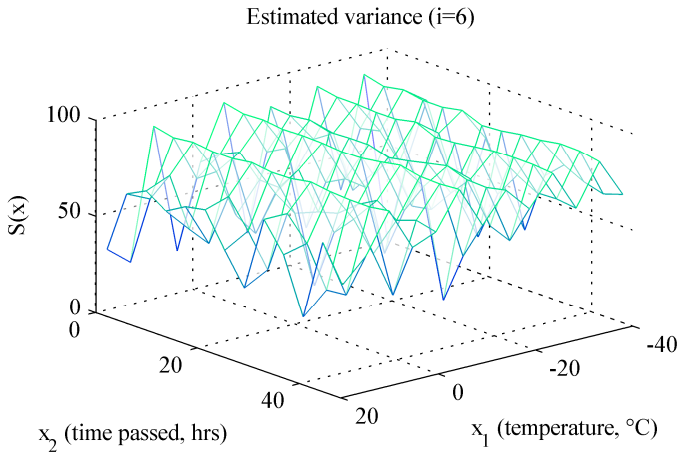

Figure 6.12: An associated estimate of the Gaussian process variance.

This phenomenon is credibly related to the nucleation of ice and change in hydraulic permeability properties of the cellular membrane. The principles of water flux with regard to cell freezing was described in Mazur's "Two-Factor Hypothesis" (176). The lower the temperature, the lower the hydraulic membrane permeability, thus minimising cell death due to severe dehydration. On the other hand, high water

content at low temperatures is suspect to cell death because of intracellular crystallisation. Specifically, the severity of the temperature region around -10°C may be associated with the effect elaborated by Gao and Critser (82). These authors emphasised the temperature zone between ~0°C and -15°C as having the highest lethality due to the effect of ice crystallisation in the extra-cellular solution (but not intracellular) hence super-cooled water flows out of the cells and freezes externally. Due to this effect cells may experience severe volume shrinkage and extended exposure to high solute concentrations in the cytoplasm. Cell volume shrinkage and concentrated solute exposure were previously reported as factors causing cryoinjury to the cell membrane (95).

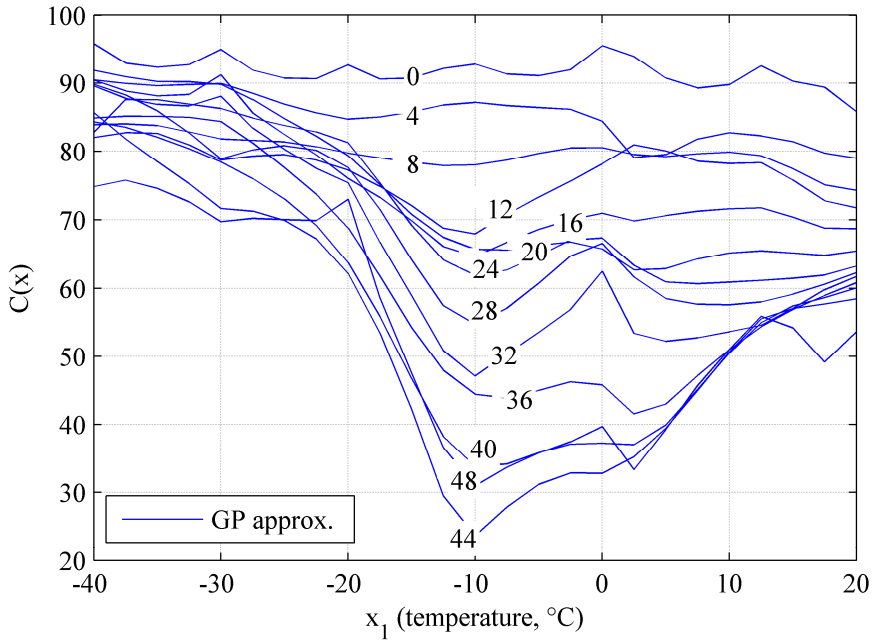

Figure 6.13: Cross-sectional representation of the Gaussian approximation from the whole data set. These sections were drawn at 4 hour intervals; their corresponding time points (hours passed) are labeled individually.

At lower temperatures (<-10°C) the magnitude of the cellular integrity decay effect drops quickly as most of the solution (including intracellular) remain solidified. However, there is some solution which is not fully solidified because these temperatures are above eutectic, consequently cells still experience damage due to multiple factors as discussed in Section 6.2. A similar trend of slower response is observed as the temperature increases above -10°C. At these temperatures ice crystals gradually diminish and this process is quicker at higher temperatures, therefore it takes less time to traverse through the most lethal region. Nevertheless, it is evident that at temperatures >-10°C, cells still experience higher overall damage comparing to the range <-10°C because of the traverse through this lethal region.

In contrast to the experimental results presented in Chapter 5 the current study covers a much longer time interval i.e. 48 hours compared to 18 hours in the previous study. Hence it is not unexpected that we observe behaviour in this longer time span which was not observed in the shorter duration. This would offer an explanation why the previous study did not highlight this lethal region around -10°C. Note from Figure 6.13 that this lethal region becomes more apparent after 24 hours into the study.

6.6 Conclusions

In this chapter we presented a computer-intensive approach which was designed to identify the best sampling locations in the post-cryopreservation cell integrity experiments investigating their response over a range of temperature excursion conditions. We proposed the use of an active learning methodology described in Section 6.3 in order to gain the maximum return of information from the size-limited

experimental sample set. We used a 2D (comprising bounded temperature and time space) hierarchical *Gaussian process* data model (see Section 6.3.1) for regression (noisy measurements) to enable process approximation from the prior data set. The *infill function* (see Section 6.3.2) was used to get a measure of expected information return from sampling at a particular location.

The performance of this algorithm was demonstrated over the experimental study on post-cryopreservation MSCs integrity response to severe temperature elevation (in a range from -40°C to 20°C) over a short term event (48 hours). This algorithm was used to identify the best temperature and time points for sampling in five experiments. The algorithm showed excellent performance by selecting the locations which appeared to be sensible and required no manual adjustment. It was satisfying to observe that the algorithm avoided the locations which had already been sampled (hence maximising return of information) while simultaneously maintaining the constraint of the minimum time interval between the experiments (giving enough time needed for sample assessment).

Finally, we tested the distribution of noise associated with the data set to verify our *a priori* assumption of heterogeneity. We used two tests for this purpose and found contradicting results. Thus the tests revealed no clear result and homogeneity was opted for being the simpler case.

Judging from the Gaussian approximation of the response function we conclude that cryopreserved MSC from human bone marrow experience highest membrane integrity damage in the temperature region around -10°C (lethal region), while it is much slower towards either of the boundaries of the investigated temperature range.

Cell survival rate improves greatly at temperatures of -20°C and below; e.g. at -40°C even after 48 hours approximately 75% MSC survival was observed. A similar trend was observed at temperatures above -10°C where cell survival rate greatly improves, possibly because it takes less time to traverse through the lethal region.

Future work in the area includes the possible use of multi-step ahead prediction in which the next sample to be taken is done so in consideration of the total number of samples to be taken. That is, given say N samples the optimum location would be approximately at intervals of $1/N$ for a smooth function; thus the optimum depends on the number of samples left to be taken.

6.7 References

24. Dominici M, Le Blanc K, Mueller I, Slaper-Cortenbach I, Marini FC, Krause DS, et al. Minimal criteria for defining multipotent mesenchymal stromal cells. The International Society for Cellular Therapy position statement. Cytotherapy. 2006;8(4):315-7.

55. Murphy JM, Fink DJ, Hunziker EB, Barry FP. Stem cell therapy in a caprine model of osteoarthritis. Arthritis and Rheumatism. 2003;48(12):3464-74.

82. Gao D, Critser JK. Mechanisms of cryoinjury in living cells. ILAR. 2000;41(4):187-96.

95. Lovelock J. The denaturation of lipid-protein complexes as a cause of damage by freezing. Proceedings of the Royal Society of London Series B - Biological Sciences. 1957;147:427-33.

158. Martinez-Cantin R, de Freitas N, Doucet A, Castellanos J. Active Policy Learning for Robot Planning and Exploration under Uncertainty. Proceedings of Robotics: Science and Systems. Atlanta, GA, USA2007.

159. Santner TJ, Williams B, Notz W. The Design and Analysis of Computer Experiments: Springer-Verlag; 2003. 283 p.

160. Gramacy RB. Bayesian treed Gaussian process models, PhD thesis: UC Santa Cruz; 2005.

161. Seo S, Wallat M, Graepel T, Obermayer K, editors. Gaussian process regression: active data selection and test point rejection. International Joint Conference on Neural Networks IJCNN; 2000.

162. O'Cearbhaill ED, Punchard MA, Murphy M, Barry FP, McHugh PE, Barron V. Response of mesenchymal stem cells to the biomechanical environment of the endothelium on a flexible tubular silicone substrate. Biomaterials. 2008;29(11):1610-9.

163. Harrison MA, I. F. Rae. General techniques of cell culture: Cambridge university press; 1997.

164. Butler M. Cell counting and viability measurements. Animal cell biotechnology: methods and protocols. NJ: Humana press; 1999. p. 131-44.

165. Krause A, Singh A, Guestrin C. Near-Optimal Sensor Placements in Gaussian Processes: Theory, Efficient Algorithms and Empirical Studies. J Mach Learn Res. 2008;9:235-84.

166. Osborne MA, Rogers A, Ramchurn S, Roberts SJ, Jennings NR. Towards Real-Time Information Processing of Sensor Network Data using Computationally Efficient Multi-output Gaussian Processes. International Conference on Information Processing in Sensor Networks (IPSN 2008)2008.

167. Osborne MA. Bayesian Gaussian Processes for sequential prediction, optimisation and quadrature: University of Oxford; 2010.

168. Rasmussen CE, Williams CKI. Gaussian Processes for Machine Learning: MIT Press; 2006.

169. Goldberg PW, Williams CKI, Bishop CM. Regression with Input-dependent Noise: A Gaussian Process Treatment. NIPS1997.

170. Kersting K, Plagemann C, Pfaff P, Burgard W. Most Likely Heteroscedastic Gaussian Process Regression. Proceedings of the 24th Annual International Conference on Machine Learning (ICML 07). Corvallis, OR, USA2007. p. 393 -400.

171. MacKay DJC. Information-based objective functions for active data selection. Neural Computation. 1992;4:589–603.

172. Cohn DA. Neural network exploration using optimal experimental design. NIPS1996. p. 679–86.

173. Finkel DE. The DIRECT Optimization algorithm user guide: North Carolina State University; 2003.

174. Lavene H. Robust test for equalaity of variances. Contributions to probability and statistics. Standford, CA: Standford university press; 1960. p. 278-92.

175. Brown MB, Forsythe AB. Robust tests for equality of variance. American statistical association. 1974;69:364-7.

176. Mazur P. The role of intracellular freezing in the death of cells cooled at supraoptimal rates. Cryobiology. 1977;14(3):251-72.

Chapter 7 Discussion and Conclusions

Cryopreservation plays an important role in stem cell research and clinical translation of regenerative therapies. Efficient cryopreservation dictates the rate at which recovered stem cells proliferate and differentiate to facilitate the expansion and production of the cell line of choice. At transient sub-physiological temperatures cell survival is governed by a large number of factors before the stabilised state of complete biophysical and biochemical process suppression can be reached. Maintenance of the ultra-low temperature is vital to ensure continuation of the stabilised condition. Nevertheless, uncontrolled elevated temperatures cannot always be avoided in applied stem cell preservation. In this thesis we investigated the influence of elevated temperatures on cryopreservation of Mesenchymal Stem Cells (MSCs). The main contributions of this thesis are:

- It was found that conventional stem cell transportation practice may cause considerable temperature elevations. Dynamic activities related to shipment transportation were determined to be the root cause of this effect. This new information may help to develop improved protocols for the transportation of stem cell specimens.
- An approximating model was developed relating the elevated temperature conditions and the viability of cryopreserved rMSCs. This model provides new information and can be used to predict the damage to the specimen if it was exposed to a specific elevated temperature for a certain amount of time.
- A novel application of active learning was employed to increase the information return from the experiments investigating the effects of elevated temperatures on the viability of cryopreserved hMSCs. To our knowledge, such methodology has never been applied for similar investigation in the field of cryobiology.

7.1 Temperature elevation during transportation with dry ice

In Chapter 3 a study investigating temperature variations during transportation of stem cell specimens using conventional practice in which dry ice is utilised to maintain ultra-low temperature was presented. It was found that considerable temperature elevations are common during transportation. In four shipments out of five, the specimens experienced temperature fluctuations exceeding the eutectic point of the conventional cryopreservative solution. As reported previously, the eutectic temperature of the freezing solution containing 10% DMSO is approximately -70°C and the temperature has to be maintained below this critical point in order for the solution to be completely solidified and to prevent injury from the high solute concentration as well as from the growth of ice crystals. We suggested that dynamic transportation activities were the root cause of the temperature fluctuations. The analysis of barometric and accelerometer data recorded during transportation of the shipments revealed the predominant presence of dynamic activities in the time window around the temperature fluctuations. The results also suggested that ground transportation by vehicle and manual handling activities were the most frequent around the time of these fluctuations, while transportation by air was the least frequent. It was further suggested that changes in the container orientation is the primary cause for the observed thermal fluctuations. It was observed that change of orientation occurred around the time of temperature fluctuations, especially in the case of large fluctuations. It was concluded that introduction of the movement of dry ice pellets is a likely cause of the observed fluctuations; specifically, due to the movement, the samples may become partially exposed to the warmer gas-filled part of the container therefore causing a temperature elevation. The opposite effect, when the specimens become covered

under a layer of dry ice can explain the observed drops of temperature. These results raise some concerns of possible negative consequences for the specimens during transportation with dry ice under normal conditions. In fact, even larger temperature elevations can occur in the case of prolonged transportation. An experiment carried out under static conditions using an equivalent storage procedure as used for the shipments, showed a rise in the internal temperature of the shipping container after approximately 4 days as the amount of dry ice becomes scarce. The results obtained from these shipment studies provide a focus for the subsequent research presented in this thesis which investigates the effects of such uncontrolled elevation conditions ranging from -20°C to 37°C and from -40°C to 20°C.

7.2 The effects of temperature elevation on cryopreserved rMSCs

Chapter 5 presented a study focused on the development of a mathematical model which predicts the effects of temperature elevation on conventionally cryopreserved rMSCs. The range of temperatures examined in the investigation was from -20°C to 37°C. During this investigation, cryopreserved rat MSCs were exposed to fixed levels of temperature elevation and the cell viability was assessed by trypan-blue exclusion test at various time points. In order to maintain precise temperature during the experiments, the system presented in Chapter 4 was utilised. Under inspection of the collected data set, a trend resembling an exponential decay of viability in respect to both, increasing temperature and exposure time, was observed. The rapid damage observed at temperatures close to normothermic range may be explained by the cytotoxicity of DMSO present in the cryopreservative solution. At sub-zero temperatures the observed damage may be associated with the “solution effects” and ice crystallisation. According to the observed trends, a multiple regression model

(for noisy measurements) composed of two exponentials was selected to approximate the underlying relationship. While the proposed model provided good generalisation properties for the experimental data as revealed by cross-validation and most of the residuals were distributed normally, an additional mode was observed in the tails of the distribution. It was concluded that larger data sets are needed in order to determine if this was a genuinely different mode or a result of experimental error. In the former case an approximating model of higher expressive power may be needed for optimal approximation. The presented model could be used by the practitioners to estimate the damage to the cells if specimens have been exposed to specific temperature for a certain interval of time.

7.3 Application of active learning for the investigation of temperature elevation effects on cryopreserved hMSCs

A larger scale study investigating the effects of elevated temperatures ranging from -40°C to 20°C on conventionally cryopreserved human MSCs was presented in Chapter 6. A similar experimental approach was used as in the previous study. Specifically, cryopreserved cells were exposed to various levels of temperature elevation and their viability was assessed as the time passed using trypan-blue test. In order to help maximise the return of information from the experiments we developed and utilised a novel computer-intensive algorithm to help identify the optimal locations (temperatures and time points) at which to sample data from the experiments. This sampling technique uses an active learning strategy in combination with a Gaussian process data model whereby the sampling locations for the next experiment are determined based on the information available from the current data set. Once the new experiment is carried out at the identified sampling

locations, the current data set is extended with this new information. This extended data set is then used for the identification of the new best sampling locations, and so on iteratively. The model developed using this active learning strategy has revealed the minimum region (indicating the most severe damage to the cells) at around -10°C. This phenomena was previously described for cell freezing and was referred to as the "lethal region". Similar effects related to the phase change of water may be associated with the death of cells is this most harmful region revealed by the presented model. It was concluded that hMSCs experience the most severe damage at temperatures around -10°C and the effect becomes less damaging at either end of the investigated temperature range.

Appendix

846 IEEE/ACM TRANSACTIONS ON COMPUTATIONAL BIOLOGY AND BIOINFORMATICS, VOL. 9, NO. 3, MAY/JUNE 2012

On the Application of Active Learning and Gaussian Processes in Postcryopreservation Cell Membrane Integrity Experiments

Mindaugas Norkus, Damien Fay, Mary J. Murphy, Frank Barry, Gearóid ÓLaighin, and Liam Kilmartin

Abstract—Biological cell cryopreservation permits storage of specimens for future use. *Stem cell* cryostorage in particular is fast becoming a broadly spread practice due to their potential for use in regenerative medicine. For the optimal cryopreservation process, ultralow temperatures are needed. However, elevated temperatures are often unavoidable in a typical sample handling cycle which in turn negatively affects the postcryopreservation integrity of cells. In this paper, we present an application of active learning using an underlying *Gaussian Process* (GP) model in an experimental study on postcryopreservation membrane integrity response to a range of elevated temperature conditions. We tailored this technique for the current investigation and developed an algorithm which enabled identification of the sampling locations for the experiments in order to obtain the highest information return about the process from a limited size sample set. We applied this algorithm in the experimental study investigating the effects of severe temperature elevation (ranging from -40 to $20^{\circ}\mathrm{C}$) over a short term event (48 hours) on the postcryopreservation membrane integrity of Mesenchymal Stem Cells (MSCs) derived from human bone marrow. The algorithm showed excellent performance by selecting the locations which maximized the reduction of variance of the process response estimate. An approximating GP model developed from this experimental data shows that the elevated temperatures during cryopreservation have an imminent detrimental effect on cell integrity.

Index Terms—Active learning, Gaussian process, postcryopreservation cell integrity, stem cells, temperature elevation.

1 Introduction

Biological cells can be stored for extended periods of time at ultralow temperatures (typically in or above *liquid nitrogen*)—this process in known as *cryopreservation*. It plays an important role in modern medicine, including the newly developing branch of *regenerative* medicine. This branch in particular requires large stocks of *stem cells* (seen by many as the primary tool for future therapies in regenerative medicine) available on demand, either for research or therapeutic applications. Accordingly, it is becoming a widespread practice to harvest stem cells from patients during the early phases of treatment or even from healthy individuals with no immediate intention of performing cell transplantation. It has been shown that stem cells retain their viability (integrity and function) after years of storage at cryogenic temperatures (vapor or liquid phase of liquid nitrogen). For example, a study by Spurr et al. has reported that haematopoietic stem cells from bone marrow and peripheral blood maintain cellular integrity and engraftment properties after over a decade of cryostorage [1]. A different study by Kotobuki et al. has shown that bone marrow-derived human MSCs retain cellular integrity and osteogenic potential after more than 3 years of cryostorage [2]. However, in reality, exposure to elevated temperatures is often unavoidable in the typical sample handling cycle. This may be due to the design of the cryostorage system whereby adding or removing samples is associated with imminent ambient temperature exposure of other samples located in the same storage area. Another typical situation is transportation in *dry ice* shipper units where temperatures above $-80^{\circ}\mathrm{C}$ may be experienced for extended periods (e.g., overseas transportation may take several days). At elevated temperatures cells can no longer be effectively protected and various damaging effects occur which cause injury to the cells (known as *cryoinjury*). This in turn affects postcryopreservation integrity and function of cells. The fundamentals of the physiochemical processes associated with the cryopreservation and cryoinjury of living cells have been extensively studied (detailed reviews can be found in [3], [4]). Despite a solid body of research available on fundamental cryobiology, modeling of the effects related to temperature elevations during the cryopreservation process is still limited due to a large array of factors involved. Comparative studies between various temperatures have been carried out which clearly demonstrate that

- *M. Norkus, G. ÓLaighin, and L. Kilmartin are with the Electrical & Electronic Engineering, School of Engineering and Informatics, National University of Ireland Galway, University Road, Galway, Ireland, and with the Bioelectronics Research Cluster, National Centre for Biomedical Engineering Science, National University of Ireland Galway, University Road, Galway, Ireland.*
  E-mail: {m.norkus1, gearoid.olaighin, liam.kilmartin}@nuigalway.ie.
- *D. Fay is with the Computer Laboratory, University of Cambridge, 15 JJ Thompson Avenue, Cambridge, United Kingdom.*
  E-mail: damien_fay@yahoo.co.uk.
- *M.J. Murphy and F. Barry are with the Regenerative Medicine Institute, National Centre for Biomedical Engineering Science, National University of Ireland Galway, University Road, Galway, Ireland.*
  E-mail: {mary.murphy, frank.barry}@nuigalway.ie.

Manuscript received 10 Feb. 2011; revised 29 Oct. 2011; accepted 6 Nov. 2011; published online 5 Dec. 2011.
For information on obtaining reprints of this article, please send e-mail to: tcbb@computer.org, and reference IEEECS Log Number TCBB-2011-02-0032.
Digital Object Identifier no. 10.1109/TCBB.2011.155.

THE EFFECT OF TEMPERATURE ELEVATION ON CRYOPRESERVED MESENCHYMAL STEM CELLS

M. Norkus[1,2,*], L. Kilmartin[1,2], D. Fay[3], M. J. Murphy[4], G. ÓLaighin[1,2] and F. Barry[4]

[1]School of Engineering and Informatics, National University of Ireland Galway, University Road, Galway, Ireland.

[2]Bioelectronics Research Cluster, National Centre for Biomedical Engineering Science, National University of Ireland Galway, University Road, Galway, Ireland.

[3]Computer Laboratory, Cambridge University, 15 JJ Thompson Ave, Cambridge, United Kingdom.

[4]Regenerative Medicine Institute, National Centre for Biomedical Engineering Science, National University of Ireland Galway, University Road, Galway, Ireland.

*Corresponding author e-mail: m.norkus1@nuigalway.ie

Abstract

Background: Cryopreservation is of particular importance in stem cell research and regenerative medicine as it permits long term stabilisation of biological cells. Cells retain their regenerative capacity after years of storage at cryogenic temperatures. However, elevation of temperature may occur due to variety of reasons, for example in the event of equipment malfunction or during delays in transportation. To date, a limited amount research has been carried out to examine the effects of temperature elevation on stem cell survival during cryopreservation. Methods: Mesenchymal Stem Cells (MSCs) obtained from 8-12 week Sprague Dawley male rats were cryopreserved according to the standard procedures. Under experimental conditions, cryopreserved specimens were exposed to elevated temperatures ranging from -20°C to 37°C and cellular membrane integrity assessed via trypan-blue exclusion at various time points. Results: An approximating model of multiple regression was fitted to the experimental data and optimisation of model parameters was carried out. This model provides an approximation of cell viability in response to elevated temperature conditions. Discussion: The results demonstrate that elevation of temperature has a dramatic effect, even over short periods of time, on the viability of cryopreserved specimens. The model presented here could be used to predict the damage suffered by a specimen due to exposure to elevated temperature over a defined period of time.

Keywords: Cell viability, cryopreservation, mesenchymal stem cells, temperature elevation